

Development of Novel Bimetallic Nickel-Cobalt Catalysts for Hydrodeoxygenation of Bio-oil producing a Co-feed for a Standard Refinery Unit



Dissertation
zur
Erlangung des akademischen Grades
doctor rerum naturalium (Dr. rer. nat.)
der Mathematisch Naturwissenschaftlichen Fakultät
der Universität Rostock

vorgelegt von
M.Sc. Thuan Minh Huynh
geboren am 19.05.1981 in Binh Dinh, Vietnam
Rostock: 27.08.2015

Name: Thuan Minh Huynh

Submission date: 28th August 2015

Defense date: 24th November 2015

Defense place: Hörsaal 001, Institut für Chemie, Universität Rostock

Dissertation title: Development of Novel Bimetallic Nickel-Cobalt Catalysts for Hydrodeoxygenation of Bio-oil producing a Co-feed for a Standard Refinery Unit.

Referees:

1. PD Dr. habil. Andreas Martin
Leibniz Institute for Catalysis
University of Rostock
Albert Einstein Str. 29a
18059, Rostock
Germany

2. Prof. Dr. Thomas Willner
HAW Hamburg - Campus Bergedorf
Lohbrügger Kirchstraße 65
21033 Hamburg
Germany

Declaration

I declare that the work presented in this thesis entitled “Development of Novel Bimetallic Nickel-Cobalt Catalysts for Hydrodeoxygenation of Bio-oil producing a Co-feed for a Standard Refinery Unit” is original and carried out by myself to obtain the doctoral degree at Leibniz Institute for Catalysis e.V., Rostock, Germany, under the guidance of my supervisors PD Dr. habil. Andreas Martin (Head of Department of Heterogeneous Catalytic Processes) and Dr.-Ing. Udo Armbruster (Group leader). I further declare that this thesis has not been submitted, either wholly or in part, to any academic institutions for the award of any other degree or qualifications.

Rostock, 27.08.2015

Thuan Minh Huynh

Acknowledgements

I would say the present work could not be completed without the supports from numerous people who I am greatly indebted.

First and foremost, I would like to express my sincerest gratitude and appreciation to my supervisor, **PD Dr. habil. Andreas Martin**, who has given me the opportunity to work the department and has supported me throughout my doctoral work with his patience, encouragement, valuable advice and the financial support.

I am deeply thankful to my co-supervisor, **Dr. Ing. Udo Armbruster**, for his tremendous support and valuable discussion. I am greatly indebted to him for teaching me how to solve the problems with the experimental set-up and detailed revisions, which truly improve the thesis.

I would like to express my acknowledgements to Dr. D.-L. Hoang, Dr. M. Schneider, Dr. J. Radnik, Dr. M.-M. Pohl, Mr. R. Eckelt, Dr. H. Atia, Mrs. A. Lehmann, Ms. A. Simmula and other analytical staffs of LIKAT for their help in characterization of my samples and valuable discussion.

Special thanks to my colleagues in the Heterogeneous Catalytic Processes Department for unconditional support during my study. Mrs. Evert for her help to solve some problem with experimental set-up; Christine for help with German language, Hoan, Sumeet, Quan, Markus, Anna, Katharina, Diego, Emily, Fernando, Andres for sharing valuable information not only in research but also in culture and social life. Thanks to other friends in LIKAT and in Rostock who have made my stay more fruitful.

I would like to thank the leaders of Vietnam Petroleum Institute (VPI): Dr. N.A. Duc, Dr. P.M.Q. Binh, Dr. N.H. Luong, Dr. D.T. Tung, Mr. T.V. Loc and Mr. N.T. Nhon (CLJOC) for teaching me during initial working days at VPI, encouraging and giving me an opportunity to study abroad. Special thanks to Tri and Sura for their help to operate the MAT set-up and colleagues in Biofuels Department, Catalysis Research Department for their help during working at VPI.

I gratefully acknowledge for Vietnam Oil and Gas Group for supporting the research project and the financial.

Last but not least, I owe my deepest gratitude to my parents for raising, loving and supporting me all my life; to my brothers, my sisters and their families for everything they have done for me from childhood until now; to my beloved wife, Lan Anh for always being on my side, supporting and encouraging me to achieve my goals.

Thanks again to all of you, who have made my stay in Rostock more enjoyable with a wonderful memory that I would never forget.

Abstract

The conversion of biomass to renewable liquid fuels has received considerable attention for partly replacing conventional fuels and for environmental concern. Converting biomass to so-called bio-oils via fast pyrolysis or hydrothermal liquefaction helps to increase volumetric and energy density and also to reduce transportation costs. However, the direct use of bio-oil for combustion engine/turbine has some implications because of different properties of bio-oil compared with conventional fossil fuels. More than 200 compounds in bio-oils are known, having various types of functional groups with specific chemistry. Upgrading of bio-oil via hydrodeoxygenation (HDO) is thus necessary to improve its properties and to make it suitable for further use.

Several catalyst systems have been applied for bio-oil HDO, e.g. conventional hydrodesulfurization ($\text{CoMoS}_2/\text{Al}_2\text{O}_3$, $\text{NiMoS}_2/\text{Al}_2\text{O}_3$) and hydrotreating catalysts (supported noble metals - Pt, Pd, Ru, Rh etc.), and supported non-noble metals (Ni, Co, Cu, Fe, etc.). Finding out suitable catalysts for this process is, however, challenging up to now. Various possible reasons have been expressed such as loss of sulfur, loss of active sites, unstable supports, high coke formation, high costs and so on which stem from the highly reactive, highly functionalized oxygenates and a large amount of water (15-30 wt%) in the original bio-oil. To overcome these drawbacks, the aim of this study is to develop novel non-sulfided, non-noble bimetallic Ni based catalysts for mild HDO of bio-oil under hydrothermal conditions.

At the start of my work, monometallic Ni, Cu and Co reference catalysts and two catalyst series (Ni-Cu/HZSM-5 and Ni-Co/HZSM-5) with different metal ratios were prepared by incipient wetness (co)impregnation method and deeply characterized by various techniques (ICP, N_2 physisorption, XRD, XPS, py-IR, TEM, TPR, TPO). The catalytic activity was first checked in batch runs (autoclave) using phenol as a model compound for bio-oil. The activity tests revealed that Ni/HZSM-5 showed significantly higher activity compared to both Cu/HZSM-5 and Co/HZSM-5 reference catalysts. The substitution of any fraction of Cu to Ni/HZSM-5 significantly reduced the catalytic activity, whereas the addition of Co preserved high activity. This result can be explained with the solid state properties of these catalysts. Both Cu and Co form alloys with Ni; however, Cu caused a loss of active sites and tended to segregate at the surface whereas Co made the Ni particles smaller and strongly stabilized the active Ni sites, thus Ni dispersion increased. Regarding the selectivity to saturated hydrocarbons, Ni-Co/HZSM-5 showed better performance than Ni/HZSM-5 at comparable conversion. Moreover, coke formation over Ni-Co/HZSM-5 was strongly decreased compared to Ni/HZSM-5. The further tests on

Ni and Ni-Co catalyst series on other acidic supports such as HBeta, HY and ZrO₂ showed the same trend.

The advantages of the bimetallic catalysts over the corresponding monometallic catalysts were subsequently evaluated in a continuous fixed bed reactor with phenol. Similar to batch runs, the HZSM-5 support showed higher activity compared to other support material. Remarkably, bimetallic catalyst 10Ni10Co/HZSM-5 is steadily stable after 24 h on-stream, and selectivity toward deoxygenated products is slightly decreasing after 24 h on-stream at complete conversion. In contrast, 21Ni/HZSM-5 shows a relative drop in both the phenol conversion and deoxygenated products selectivity due to high coke formation and fast agglomeration of Ni active sites compared to bimetallic catalyst as proved by the characterization result of spent catalysts. The well-balanced combination of Ni-Co alloys and acidic properties (redox as well as acid base) bring 10Ni10Co/HZSM-5 as a superior catalyst for promoting all essential individual steps within a reaction network.

The transfer from model reaction to the conversion of bio-oil seems to be complicated due to the above mentioned complexity of the feed and the analytical evaluation of this reaction are also challenging. The activity tests with wood derived bio-oil obtained from fast pyrolysis process at various reaction conditions and with different supports in a batch reactor showed that the bimetallic catalyst with HZSM-5 support was significantly more active in terms of degree of deoxygenation and oil yield as compared to the other catalysts, further confirming the result from the model reaction. This catalyst obviously provides a well-balanced mixture of metal sites for activation of hydrogen and acid sites for cracking and dehydration steps, this helps to significantly reduce the molar O: C ratio and also increase the molar H: C ratio in the upgraded bio-oil (UBO).

Finally, the co-processing of such UBO with a conventional feedstock (atmospheric distillation residue) using a commercial catalyst in an ASTM certified lab-scale fluid catalytic cracking (FCC) unit was successful. Compared to 100% conventional feed, the yields toward the desired light cycle oil, gasoline and gas fractions obtained from a co-feed (a mixture of UBO up to 20 wt%) at a similar conversion were slightly increased owing to the reduction of the heavy cycle oil yield. The significant change in structure and composition during HDO with the 10Ni10Co/HZSM-5 catalyst make UBO suitable as a co-feed in FCC unit, indicating that an overall successful solution to convert pyrolysis oil into fuels requires an effective HDO process and the subsequent tuning of the FCC process. In sum, these finding provide valuable data on upgrading of bio-oil and the integration of UBO into a standard refinery unit and demonstrate a potential route for conversion of biomass to renewable liquid fuels.

Zusammenfassung

Die Umwandlung von Biomasse in erneuerbare flüssige Treibstoffe hat eine enorme Beachtung gefunden, denn sie bietet die Möglichkeit, konventionelle Treibstoffe zumindest teilweise zu ersetzen und zudem umweltrelevante Anliegen zu berücksichtigen. Die Biomasseumwandlung in sogenannte Bio-Öle mittels Pyrolyse (fast pyrolysis) oder hydrothormaler Verflüssigung hilft bei der Erhöhung der Energiedichte und der volumetrischen Dichte und reduziert die Transportkosten. Allerdings ist der direkte Einsatz von Bio-Ölen in Verbrennungsmaschinen nicht möglich, denn diese Bio-Öle unterscheiden sich zu stark in ihren Eigenschaften im Vergleich zu fossilen Brennstoffen. Bisher sind mehr als 200 Verbindungen bekannt, die in den Bio-Ölen enthalten sind und aufgrund ihrer verschiedenen funktionellen Gruppen die chemischen Eigenschaften bestimmen. Ein Schlüsselschritt zur Verbesserung der Eigenschaften ist die Bioölaufbereitung (engl. Upgrading of bio-oil) mit Hilfe der hydrothermalen Deoxygenierung (HDO).

Eine effektive Deoxygenierung ist nur mit Hilfe von Katalysatoren möglich. Es wurden bereits viele verschiedene Katalysatorsysteme für die HDO von Bio-Ölen angewandt, z. B. kommerzielle Katalysatoren für die Hydrodesulfurierung (HDS) wie $\text{CoMoS}_2/\text{Al}_2\text{O}_3$ oder $\text{NiMoS}_2/\text{Al}_2\text{O}_3$ sowie Katalysatoren für das Hydrotreating in Raffinerien (diese enthalten meistens Edelmetalle wie Pt, Pd, Ru oder Rh), aber auch Katalysatoren mit unedlen Metallen wie Ni, Co, Cu oder Fe, welche auf bestimmten Trägermaterialien zur Oberflächenvergrößerung aufgebracht sind. Doch die Suche nach geeigneten Katalysatoren für den genannten Prozess bleibt bis heute eine herausfordernde Aufgabe. Als mögliche Ursachen sind der Verlust von Schwefel oder von aktiven Zentren des Katalysators, instabile Trägermaterialien, die Bildung von Koks und auch hohe Kosten bekannt. Diese sind zurückzuführen auf die hohe Reaktivität der stark funktionalisierten Oxygenate und auf den hohen Wassergehalt (15-30 Gew.-%) im ursprünglichen Bio-Öl. Um dieses Hindernis zu überwinden, war das Ziel dieser Arbeit die Entwicklung eines edelmetallfreien und schwefelfreien Nickel-basierten bimetallicen Katalysators für die HDO von Bio-Ölen unter milden hydrothermalen Reaktionsbedingungen.

Zu Beginn dieser Arbeit wurden zwei Katalysatorserien (Ni-Cu/HZSM-5 und Ni-Co/HZSM-5) mit unterschiedlichen Metallbeladungen mittels Imprägnierung (incipient wetness impregnation) hergestellt. Zudem wurden monometallische Nickel-, Kupfer- und Kobalt-Referenzkatalysatoren unter denselben Bedingungen präpariert. Alle diese Katalysatoren wurden umfangreich physikalisch-chemisch mit Hilfe verschiedener Analysetechniken wie ICP, N_2 Physisorption, XRD, XPS, py-IR, TEM, TPR und TPO charakterisiert. Zunächst wurde die Effektivität der Katalysatoren mit Hilfe einer

Modelltestreaktion - der Hydrodeoxygenierung von Phenol - in Batch-Experimenten bestimmt. Die Aktivitätstests offenbarten, dass der Katalysator Ni/HZSM-5 eine signifikant höhere Aktivität besitzt im Vergleich zu den anderen beiden Katalysatorsystemen Cu/HZSM-5 und Co/HZSM-5. Die Substitution beliebiger Ni-Mengen durch Kupfer im Katalysator Ni/HZSM-5 verschlechterte dessen Aktivität jedoch erheblich, hingegen blieb die Aktivität beim Austausch mit Kobalt erhalten. Dieses Ergebnis ist auf die Festkörpereigenschaften der Katalysatoren zurückführbar. Beide Metalle Kupfer und Kobalt bilden mit Nickel Legierungen, aber Kupfer verursacht einen Verlust von aktiven Zentren des Katalysators und neigt dazu, sich an der Metallpartikeloberfläche anzureichern. Kobalt hingegen ist ursächlich für die Bildung von kleineren Nickelpartikeln in der Legierung und stabilisiert diese aktiven Nickelzentren, so dass eine hohe Dispersität von Nickel auf dem Träger erreicht wird. Hinsichtlich der Selektivität für gesättigte Kohlenwasserstoffe in der HDO-Reaktion zeigt Ni-Co/HZSM-5 bessere Leistungen als Ni/HZSM-5 unter vergleichbaren Bedingungen. Ferner wurde mit Ni-Co/HZSM-5 weniger Koks gebildet als mit Ni/HZSM-5. Weitere Untersuchungen mit Nickel und Nickel-Kobalt auf anderen Trägermaterialien wie H-Beta, H-Y und ZrO_2 zeigten den gleichen Trend.

Diese Vorteile der bimetallicen Katalysatoren wurden nachfolgend in einem kontinuierlichen Festbettreaktor mit Phenol als Reaktand evaluiert. Dabei zeigte das Trägermaterial HZSM-5 ebenfalls höhere Aktivität im Vergleich mit den anderen untersuchten Trägermaterialien. Bemerkenswerterweise arbeitete der bimetallic Katalysator 10Ni10Co/HZSM-5 nach 24 Stunden Laufzeit nahezu stabil und nur eine geringfügige Verschlechterung der Selektivität für deoxygenierte Produkte bei vollständigem Phenol-Umsatz war während dieser Zeit nachweisbar. Im Gegensatz dazu zeigte der monometallic Katalysator (21Ni/HZSM-5) einen merklichen Abfall von Phenolumsatz und Selektivität für deoxygenierte Produkte. Laut Charakterisierung der gebrauchten Katalysatoren resultieren die schlechteren Katalysatorleistungen von 21Ni/HZSM-5 aus der hohen Koksbildung und der schnellen Agglomeration der Nickelpartikel im Vergleich zu 10Ni10Co/HZSM-5. Die ausgewogene Kombination von Nickel-Kobalt-Legierung und aciden Eigenschaften des Trägers macht 10Ni10Co/HZSM-5 zu einem überlegenen Katalysator für alle essentiellen Teilschritte innerhalb des Reaktionsnetzwerkes.

Der Übergang von der Modellreaktion zur Umsetzung von Bio-Öl ist schwierig wegen der bereits genannten Komplexität des Bio-Öls sowie der Herausforderungen für die analytische Erfassung der Reaktion. Die Aktivitätstests mit Bio-Öl, welches im vorliegenden Fall aus Holz via Fast Pyrolysis erhalten wurde, zeigten, dass die

bimetallischen Katalysatoren auf HZSM-5 hinsichtlich Deoxygenierungsgrad und Produktausbeute im Vergleich zu den anderen Katalysatoren sehr aktiv sind. Dies bestätigten die Ergebnisse aus der Untersuchung der Modellreaktion. Der Katalysator 10Ni10Co/HZSM-5 besitzt offensichtlich eine ausgewogene Mischung von Metallzentren für die Aktivierung von Wasserstoff und von aciden Zentren für Deoxygenierung sowie Wasserabspaltung. Damit hilft der Katalysator, das molare O: C-Verhältnis signifikant zu erniedrigen und gleichzeitig das molare H: C-Verhältnis im aufbereiteten Bio-Öl (UBO) zu erhöhen.

Abschließend wurde in dieser Arbeit die gemeinsame Umsetzung (co-processing) von UBO mit konventionellem Rohmaterial (atmosphärischer Rückstand) an einem kommerziellen ASTM-zertifizierten FCC-Katalysator (fluid catalytic cracking) erfolgreich durchgeführt. Das co-processing (mit bis zu 20 Gew.-% UBO) lieferte ebenso wie der Test mit 100 % konventionellem Rohmaterial vollständigen Umsatz. Zudem zeigte der Co-Prozess einen leichten Anstieg in der Ausbeute von Gasöl (Light cycle oil), Benzin und Gasfraktion, einhergehend mit einem geringeren Anfall an Schweröl (Heavy cycle oil). Die erhebliche Änderung der Struktur und Zusammensetzung des UBO während der HDO mit dem Katalysator 10Ni10Co/HZSM-5 machen UBO zu einem geeigneten Zusatz (co-feed) in FCC-Anlagen. Die Ergebnisse zeigen, dass ein erfolgreicher Lösungsansatz für die Gewinnung von Kraftstoffen aus Pyrolyseöl eine effektive HDO-Stufe und eine anschließende Justierung des FCC-Prozesses erfordert. Zusammenfassend liefern diese Ergebnisse wertvolle Daten zur Aufbereitung von Bio-Ölen und die Einspeisung von UBO in eine standardisierte Raffinerieanlage. Sie demonstrieren somit ein mögliches Vorgehen in der Umwandlung von Biomasse zu erneuerbaren flüssigen Treibstoffen.

List of Abbreviations, Acronyms and Symbols

ASTM	American Society for Testing and Materials
AAS	Atomic Adsorption Spectroscopy
BET	Brunauer – Emmet – Teller model
BJH	Barret – Joyner – Halenda model
BAS	Brønsted Acid Sites
CHNS	Carbon, Hydrogen, Nitrogen, Sulfur
CTO	Catalyst to Oil
¹³ C-NMR	Nuclear Magnetic Resonance of ¹³ C
°C	Degree Celsius
DCM	Dichloromethane
DOD	Degree of Deoxygenation
EDXS	Energy Dispersive X-ray Spectroscopy
FCC	Fluid Catalytic Cracking
FID	Flame Ionization Detector
FP	Fast Pyrolysis
GC	Gas Chromatography
GC-MS	Gas Chromatography Mass Spectrometry
HAADF	High Angle Annular Dark Field
HCO	Heavy Cycle Oil
HDO	Hydrodeoxygenation
HDS	Hydrodesulfurization
HDN	Hydrodenitrogenation
HHV	Higher Heating Value
HPTT	High Pressure Thermal Treatment
ICP-OES	Inductive Coupled Plasma Optical Electron Spectroscopy
py-IR	Infrared Spectroscopy of Adsorbed Pyridine

K	Kelvin
LAS	Lewis Acid Sites
LCO	Light Cycle Oil
LF	Liquefaction
LHSV	Liquid Hourly Space Velocity
NH ₃ -TPD	Temperature Programmed Desorption of Ammonia
nm	nanometer
RT	Room Temperature
PIONA	Paraffin, Iso-paraffin, Olefin, Naphthene, Aromatic
SR-SCT-MAT	Single Receiver Short Contact Time Micro Activity Test
SIMDIST	Simulated Distillation
TCD	Thermal Conductivity Detector
TOF	Turnover Frequency
TPO	Temperature Programmed Oxidation
TPR	Temperature Programmed Reduction
TEM	Transmission Electron Microscopy
UBO	Upgraded Bio-Oil
VGO	Vacuum Gas Oil
WHSV	Weight Hourly Space Velocity
XRD	X-ray Diffraction
XPS	X-ray Photoelectron Spectroscopy

Table of contents

Chapter 1 Introduction and Objectives	1
1.1 Overview of conversion of biomass to liquid fuels.....	2
1.2 Properties of biomass derived bio-oil and the role of bio-oil upgrading	3
1.3 HDO of bio-oil and its model compounds.....	7
1.3.1 Model compounds.....	7
1.3.2 Bio-oil.....	10
1.4 Catalysts for HDO of bio-oil and its model compounds	15
1.5 Objectives of the thesis	17
Chapter 2 Experimental Procedures	19
2.1. Catalyst preparation	20
2.1.1 Preparation of monometallic and bimetallic catalysts	20
2.1.2 Preparation of unsupported catalysts	20
2.1.3 Equilibrated catalyst.....	20
2.2. Catalyst characterization	20
2.2.1 Chemical analysis	20
2.2.2 Nitrogen physisorption	21
2.2.3 X-ray powder diffraction (XRD)	22
2.2.4 X-ray photoelectron spectroscopy (XPS)	23
2.2.5 Temperature programmed methods.....	23
2.2.6 Fourier transform infrared spectroscopy of absorbed pyridine (py-IR)	24
2.2.7 Transmission electron microscopy (TEM)	24
2.3. Experimental setup.....	25
2.3.1 HDO of phenol in a batch reactor	25
2.3.2 HDO of phenol in a fixed bed down-flow reactor	26
2.3.3 HDO of bio-oil in a batch reactor	27
2.3.4 Catalytic cracking of UBO together with conventional feed	29
Chapter 3 Hydrodeoxygenation of Phenol as a Model Compound for Bio-oil in a Batch Reactor	31
3.1 Characterization of fresh and pre-reduced catalysts	32
3.1.1 Elemental analysis and N ₂ physisorption.....	32
3.1.2 X-ray diffraction (XRD).....	33
3.1.3 Temperature programmed reduction (TPR)	34
3.1.4 X-ray photoelectron spectroscopy (XPS)	37

3.1.5 Infrared spectroscopy of absorbed pyridine (Py-IR).....	38
3.1.6 Transmission electron microscopy (TEM).....	39
3.2 Effect of second metal on catalytic performance of bimetallic catalysts.....	41
3.2.1 Feedstock and products analysis.....	41
3.2.2 Catalyst performance in HDO of phenol and intermediates	42
3.3 More insight into effect of reaction conditions.....	50
3.4 Effect of support nature on bimetallic Ni-Co catalysts	52
3.5 Summary and conclusions	55
Chapter 4 Hydrodeoxygenation of Phenol in a Continuous Fixed Bed Reactor	57
4.1 Effect of supports on bimetallic catalysts.....	58
4.1.1 Performance of supported bimetallic Ni-Co catalysts.....	58
4.1.2 Spent catalyst characterization results.....	59
4.2. Effect of various reaction conditions.....	64
4.2.1 Temperature.....	64
4.2.2 Pressure.....	65
4.2.3 WHSV	67
4.2.4 Long term evaluation of 10Ni10Co/HZSM-5 and 21Ni/HZSM-5	67
4.3. Proposed reaction pathways	70
4.4. Summary and conclusions	72
Chapter 5 Hydrodeoxygenation of Bio-oil in a Batch Reactor	73
5.1 Feedstock	74
5.2 Effect of the catalyst supports on bio-oil HDO	74
5.3 Characterization of spent catalysts	77
5.4 Effect of reaction conditions on bio-oil HDO over 10Ni10Co/HZSM-5	80
5.4.1 Effect of reaction temperature	82
5.4.2 Effect of reaction time.....	83
5.4.3 Effect of pressure	83
5.4.4 Effect of catalyst amount	84
5.4.5 Chemical analysis.....	84
5.5 Summary and conclusions	85
Chapter 6 Co-processing of Upgraded Bio-oil with Conventional Feed in a FCC unit	87
6.1 Feedstocks and catalyst.....	88
6.2 Catalytic cracking.....	89
6.3 Summary and conclusions	93
Chapter 7 Conclusions and Outlook	95

7.1 The role of second metal in bimetallic catalysts for bio-oil HDO.....	96
7.2 The effect of supports in bimetallic catalysts.....	96
7.3 Performance of Ni-based catalysts in HDO of phenol.....	97
7.4 HDO of bio-oil and subsequent co-processing in a standard refinery unit.....	98
7.5 Outlook.....	99
8. References	101

Chapter 1

Introduction and Objectives

This chapter begins with general information about the potential use of the renewable sources as an attractive option for partly replacing petroleum liquid fuels. Then, the literature review provides the information on state of the art of upgrading of bio-oil for liquid fuels, including catalyst development, processing and application of upgraded bio-oil. Based on the advantages and disadvantage of previous studies, the objectives of this thesis are ultimately given.



1.1 Overview of conversion of biomass to liquid fuels

The basement of the presently consumed energy is significantly depending on the fossil fuels including oil, coal and natural gas. According to British Petroleum statistical review of world energy, 86% of the energy consumed worldwide in 2014, particularly 86% and 81% of energy consumed in the US and Germany, respectively, are from those sources [1]. Nevertheless, due to the increasing of energy demand, the growing environmental concerns and the limited availability of petroleum reserves, the search for renewable and sustainable resources is needed to serve as alternatives to close future gaps in the supply of transportation fuels as well as of feedstock for chemical industry [2, 3]. A significant increase in use of renewables for energy supply and production of chemicals has been achieved within the last two decades. Particularly the use of biofuels has been established around the world such as bioethanol and biodiesel used for blending of up to 10 vol% in conventional gasoline or diesel fuel. In fact, bioethanol is mainly produced from sugarcane (e.g. Brazil) and corn (e.g. US), whereas biodiesel is manufactured via trans-esterification of edible oils (e.g. rape seed oil in Germany, palm oil in Malaysia) with alcohol (mainly methanol). However, there is still an intensive debate because the use of edible oils and seeds for the biofuels might compete with the food value chain, affecting material availability and prices. The access to biofuels from biomass resources, therefore, has been considered as an attractive option due to the availability, renewability and CO₂ neutrality of the feed. To promote the implementation of renewable energy, the governments of many countries have set ambitious goals and set the mandatory legislation for partly replacing fossil fuels, e.g. the European Union (EU) Renewable Energy Directive sets a target for the EU to consume 20% of its final energy from renewable sources by 2020 or the U.S Department of Energy sets a target to expect use 20% of transportation fuel from biomass [4].

Regarding the technology platforms, there are several general pathways for conversion of biomass to liquid fuels (see Figure 1.1) that can be simply separated based on primary processes such as hydrolysis-fermentation (biochemical route), gasification and fast pyrolysis (FP)/hydrothermal liquefaction (LF) (thermal-chemical routes) [5]. In the latter case, biomass can be converted to mainly liquid oil (so called bio-oil) in the absence of oxygen. Fundamentally FP is the thermal decomposition process in which biomass is rapidly heated in the absence of oxygen in a typical temperature range (450 – 550 °C) with short residence time (1-2 s) at atmospheric pressure or lower [6-8]. It is noted that intermediate and slow pyrolysis at lower temperature (< 400 °C) favor char production compared to FP. On the other side, hydrothermal LF is carried out in mostly hot liquid

water with or without catalysts under lower temperature (300-400 °C), but higher pressure (120-200 bar) compared to FP technology [9-11].

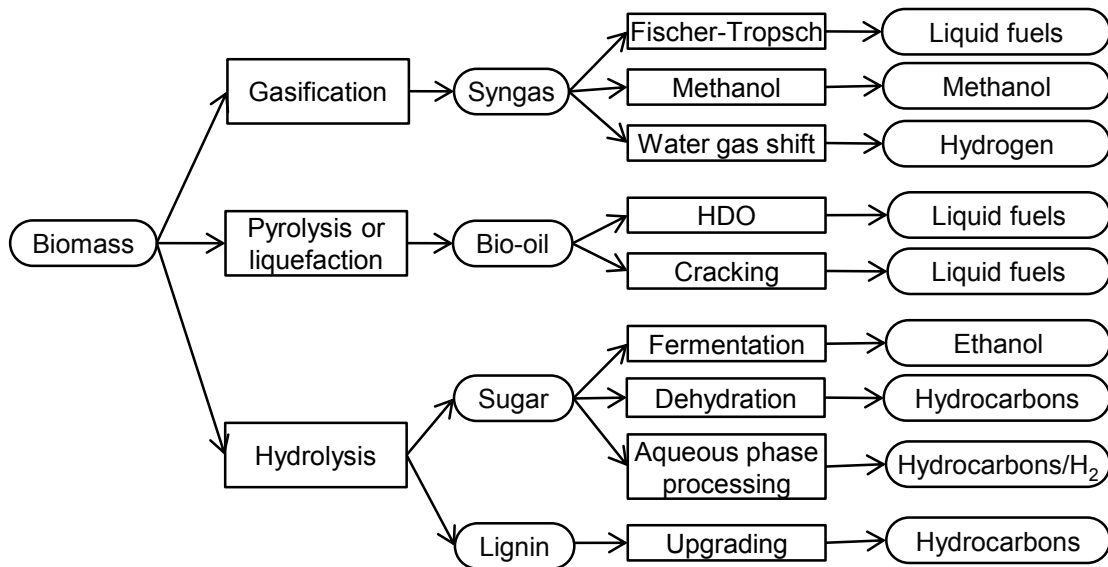


Figure 1.1. General pathways of converting biomass to liquid fuels [5].

In the following sections, this chapter will provide a comprehensive review on FP/LF of biomass to bio-oil and deoxygenation of bio-oil and then the focus is put on the catalyst development for hydrodeoxygenation (HDO) of bio-oil and its model compounds. Based on the review, some advantages and disadvantages of previous studies are discussed and then the objective of this work is finally given.

1.2 Properties of biomass derived bio-oil and the role of bio-oil upgrading

The second generation biomass is referred to the ligno-cellulosic biomass and includes a variety of materials such as woods, agricultural residues and lignin residues, which are available around the world. Cellulose, hemicellulose and lignin are three main classes of such raw materials in portions of approximately 35-45%, 25-35% and 15-25%, respectively, depending on the specific biomass. Therefore, these materials possess oxygen contents varying in a range of 35-45 wt%, causing one serious drawback for production of fuels from such biomass compared to those from conventional feed. Besides that, biomass has low volumetric and energy densities, resulting in high cost for collecting and transportation. As a result, converting biomass to liquid form seems to be a good option dealing with these characteristics.

Hydrothermal processes have been developed in 1920s with a concept of oil production from biomass in hot water using alkali as catalyst. Following, several other

concepts have been proposed such as hydro-pyrolysis (LF of biomass with high pressure hydrogen and a heterogeneous catalyst), solvolysis (high pressure process used organic solvent like ethylene glycol, alcohol or phenols), but they face some technical problems as well as the high capital and operating costs. The great efforts have been focused in hot water and entitled hydrothermal upgrading (HTU), which was developed by Shell and is currently being commercialized by e.g. Shell and BTG [12]. One of the advantages of LF is the direct processing of wet biomass without pre-drying; however, the process proceeds under high pressure which results in some technical difficulties and an increase of capital cost.

FP technology appeared as a promising method which has been first developed in the later 1970s for converting biomass to mainly liquid product (up to 80% liquid yield calculated on dry feed) [6]. Several aspects of this technology have been studied, especially in reactor process design. In fact, four main reactor technologies have been developed and are currently available for commercialization, involving fluidized bed (Dynamotive – 8,000 kg/h), circulating fluidized bed or transported bed (Ensyn – 4,000 kg/h, VTT – 20 kg/h), ablative pyrolyser (PYTEC – 250 kg/h, NREL, Aston University – 20 kg/h), rotating cone (BTG – 2,000 kg/h), in addition some currently developing reactors such as vacuum pyrolyser (Laval University/Pyrovac) and Entrained flow (Georgia Tech Research Institute) [13]. A state of the art for FP has been recently reviewed in detail elsewhere [6-8].

Figure 1.2 shows a typical concept of FP technology. In this, biomass firstly is dried, typically reaching less than 10% water, and then it must be ground to specific particle size depending on type of reactor. Normally, the rate of particle heating is the rate-limiting step, thus small biomass particle sizes of less than 2-3 mm are needed to achieve fast heat transfer. The ground biomass is fed to a reactor which is designed to run at high temperature and rapid heat transfer rates ($200 - 10^4$ K/s) which can be achieved by hot preheated fluidizing gases, heated reactor walls, hot sand and/or combination thereof [14]. With the specific design, biomass is fast decomposed to the condensate and non-condensate gases and char, which is removed typically by a cyclone system. The gases flow/pass through the condenser and the liquid (or bio-oil) is formed by rapid quench and collected in a separator. Much efforts focused on the char separation to remove as much as possible formed char because it causes some problems in downstream processing and acts as catalyst for cracking of gases, affecting the quality of formed bio-oil. The by-product char can be used within the process to provide heat by combustion or it can be separated and sold.

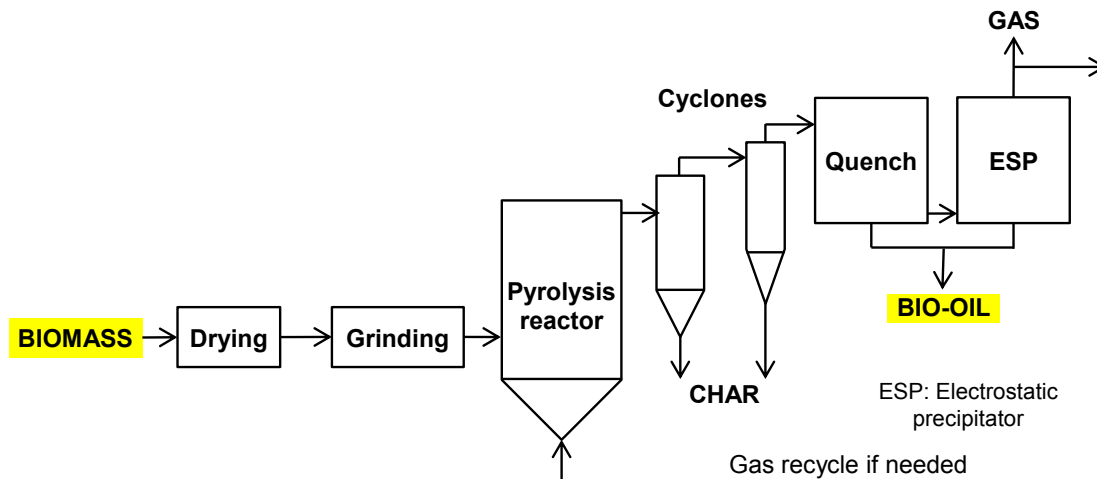


Figure 1.2. A scheme of FP process [6].

With respect to the quality, Table 1.1 lists the typical properties of FP oil and LF oil obtained from woody biomass compared to the fossil heavy fuel oil [12]. Obviously, FP oil has a higher oxygen content, water content and roughly half of high heating value (HHV) compared to the heavy fuel oil. LF oil is different from FP oil, e.g. much more viscous and less dense, and has a higher HHV owing to its more hydrophobic nature with less dissolved water [9, 15, 16]. It is also noted that the properties of bio-oils are different from the respective biomass feedstock (wood, agricultural residues, algae etc.) due to the fraction of the main components (cellulose, hemicellulose and lignin) [9, 17].

Table 1.1. Typical properties of wood based bio-oil from FP, LF compared to heavy fuel oil [12]

Properties	FP oil	LF oil	Heavy fuel oil
Water content (wt%)	15-30	5.1	0.1
pH	2.5	-	-
Specific gravity ^[a]	1.2	1.1	0.94
Elemental composition (wt%)			
Carbon	54-58	73	85
Hydrogen	5.5-7.0	8	11
Oxygen	35-40	16	1.0
Nitrogen	0-0.2	-	0.3
Ash	0-0.2	-	0.1
HHV (MJ/kg)	16-19	34	40
^[a] ratio of the density of the substance to the density of water			

It should be emphasized that FP or LF of any biomass toward bio-oil can be seen as a primary step of deoxygenation despite the oxygen content in bio-oil is still relatively high

(15-30% on dry basis). Bio-oil reveals a general sum formula of $\text{CH}_{1.4}\text{O}_{0.4}$, whereas conventional liquid fuel or hydrocarbons show a sum formula close to CH_2 [18]. Remarkably, more than 200 oxygenate compounds in bio-oils are known, having various types of functional groups (e.g. acids, alcohols, phenols, sugars, aldehydes, ketones and esters etc.) with specific chemistry. The detection of all oxygenates in the bio-oil is challenging up to now and their concentrations are connected with the nature of biomass feed and the process conditions [9, 19]. Figure 1.3 illustrates the structure of the three main components of biomass and variety of common detected monomer oxygenates with various functional groups in bio-oil; in addition, phenolic dimers are represented largely in bio-oil, especially in lignin derived bio-oil [12].

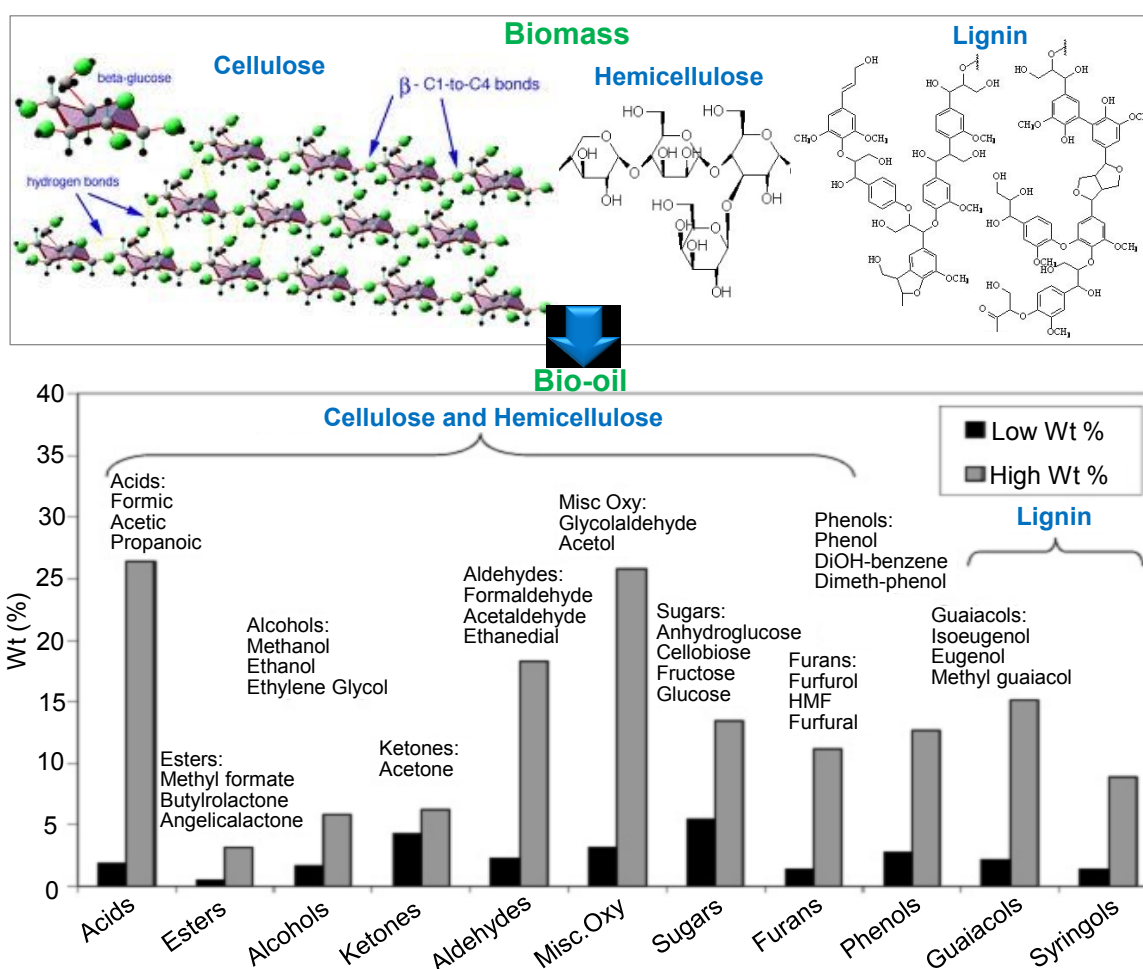


Figure 1.3. Main components of biomass and typical chemical composition of bio-oil [12].

The high oxygenates content in bio-oil causes some negative characteristics such as high viscosity, low volatility, immiscibility with conventional fuels, corrosion and instability during long-time storage. The biggest challenge of bio-oil is that the quality is far away

from conventional liquid fuels. It is necessary therefore to further reduce the oxygen content to improve the quality via upgrading and ultimately make it suitable for further uses as a chemical feedstock or a fuel component. In this respect, two main routes have been intensively investigated for deoxygenation of bio-oil: catalytic cracking and catalytic hydrotreating/HDO. In the first case, the oxygen is removed via several reactions such as decarboxylation, decarbonylation and dehydration using cracking catalysts (e.g. zeolites, silica-alumina) at atmospheric pressure or lower pressure without external hydrogen source, thus the resulting oil has lower HHV and molar H: C ratio. On the other side, HDO appears as an interesting route, which is performed under high hydrogen pressure and at moderate or high temperature in presence of a heterogeneous catalyst. The oxygen is generally eliminated as water, leading to a high liquid product yield compared to the catalytic cracking. HDO normally plays a minor role compared to hydrodesulfurization (HDS) or hydrodenitrogenation (HDN) in standard refineries because of the very low oxygen content in conventional feed although the technologies and respective processes are similar. However, HDO has evolved quickly into a major technology platform due to the increasing demand for alternative and renewable liquid fuels, especially from biomass resources. In light of that, HDO was selected as primary bio-oil deoxygenation for detailed study in this thesis.

1.3 HDO of bio-oil and its model compounds

1.3.1 Model compounds

As mentioned above, bio-oil is a complex mixture with high functionalities, thus the analysis and evaluation of bio-oil are very difficult, requiring more elaborated analysis techniques and still remaining a challenge up to now. As a result, more attention has been put on studies of individual model compounds to get more insight into the chemistry before switching to bio-oil. Among the above named functional groups, the oxygen elimination from phenols and aromatic ethers will be difficult compared to that from alcohols and aliphatic ethers with respect to the thermal stability, which can be seen via the bond dissociation energies shown in Table 1.2 [20].

Table 1.2. Bond dissociation energies [20].

Groups	Bond dissociation energy (kJ/mol)
RO-R	339
R-OH	285
Ar-OR	422
Ar-OH	468

On one hand, the reactivity of different functional groups in bio-oil under hydroprocessing conditions follows the order aldehydes, ketones < aliphatic ether < aliphatic alcohols < carboxylic groups < phenolic ethers < phenols < diphenyl ether < dibenzofuran, as e.g. reported by Elliott [21]. As a consequence, the hydroprocessing of aldehydes and ketones can take place at low temperature (< 200 °C), whereas carboxylic acids, phenolic ethers and phenols might need 300 °C or more. Additionally, considerable concentrations of phenols and substituted phenols have been found in bio-oil obtained from lignin [22, 23]. As a result, the phenolic compounds (phenol, catechol, anisole, guaiacol) have significantly attracted more attention as model compounds compared to other groups like furanes, acids, aldehydes, ketones and alcohols. Substituted phenols like guaiacol are readily transformed to phenol or catechol [24-26], but the conversion of phenol to the oxygen-free compounds is difficult. Therefore, phenol seems to be a refractory probe model compound for understanding of fundamental chemistry of catalytic HDO reaction.

Regarding the reaction pathway, there are two general routes to eliminate oxygen from phenol, either the direct deoxygenation of phenol to benzene (DDO route) or the hydrogenation of the aromatic ring followed by dehydration for oxygen removal (HYD route) [27-29] (see Figure 1.4). The latter pathway involves several steps such as phenol hydrogenation to cyclohexanone, which is further hydrogenated to cyclohexanol. Subsequently, cyclohexanol may dehydrate to form cyclohexene and finally be hydrogenated to cyclohexane. Types of catalysts and reaction conditions (temperature, pressure, solvent properties, etc.) mainly influence the observed reaction steps.

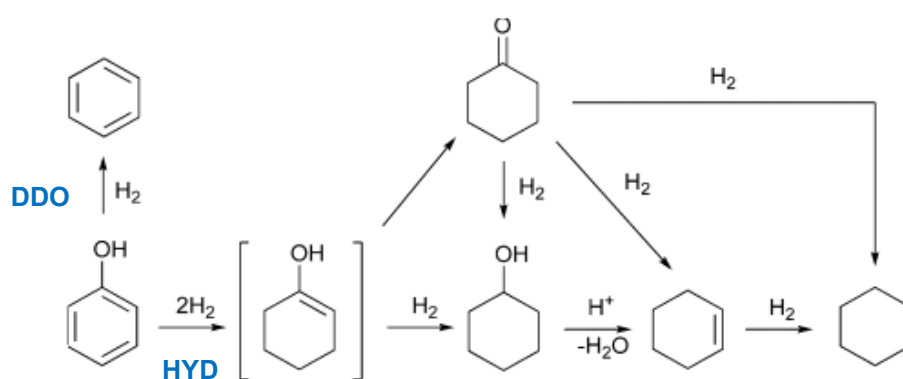


Figure 1.4. Proposed reaction pathways of phenol HDO over supported Pt catalysts [28].

Depending on types of catalysts, several reaction mechanisms have been proposed [29-34]. Romero et al. [30] proposed the mechanism of 2-ethylphenol HDO over Ni-MoS₂, Co-MoS₂ catalysts in gas phase (340 °C, 70 bar) as shown in Figure 1.5. Sulphur vacancy

sites are considered as active sites which are generated due to the weak bond between molybdenum and sulphur. The oxygen of the oxygenates can be adsorbed on these sites of a MoS_2 slab edge and then might occur the direct C-O bond cleavage with the elimination of water as a by-product (DDO route). On the other side, the aromatic ring can be adsorbed on at least two neighboring vacancies, thus total hydrogenation toward 2-ethylcyclohexanol is possible which is further dehydrated over acid sites of alumina before the subsequent hydrogenation to 2-ethylcyclohexane (HYD route).

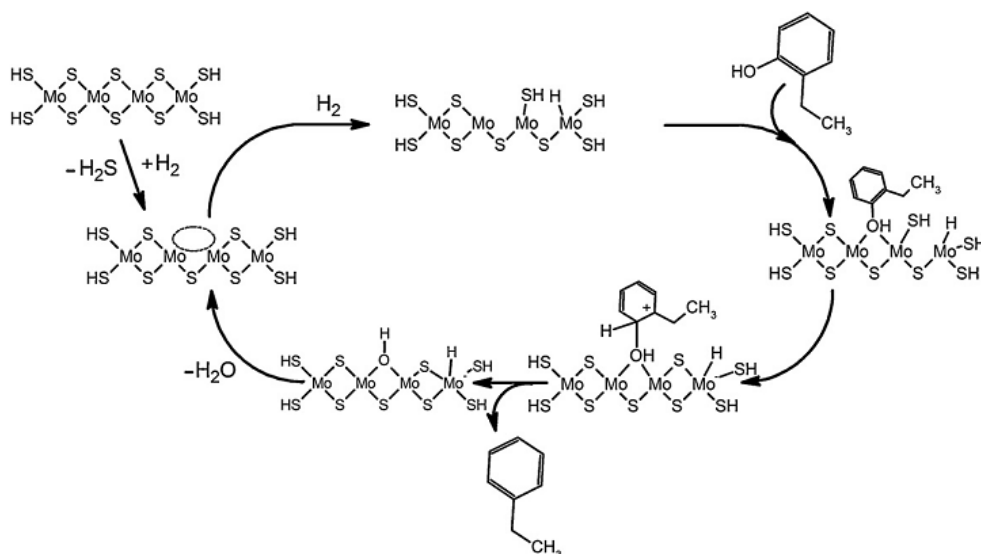


Figure 1.5. Proposed mechanism of HDO of 2-ethylphenol on a $\text{Co-MoS}_2/\text{Al}_2\text{O}_3$ catalyst [30].

Another HDO reaction mechanism has been proposed for metal catalysts or supported metal catalyst systems (see Figure 1.6) [31-33, 35, 36]. The combination of transition metals and the different supports (e.g. oxophilic metals (MoO_3 , Cr_2O_3 , WO_3 , ZrO_2 , Al_2O_3) or zeolites HZSM-5, HBeta, HY etc.) enables alternative pathways. In the case of former supports, the oxophilic metal acts as Lewis acid site, where the oxygen electron pair of oxygenate compounds can be adsorbed, whereas the hydrogen molecule is adsorbed and activated on the transition metal. The activated hydrogen is next transferred to the adsorbed molecule and water is finally obtained [31, 32].

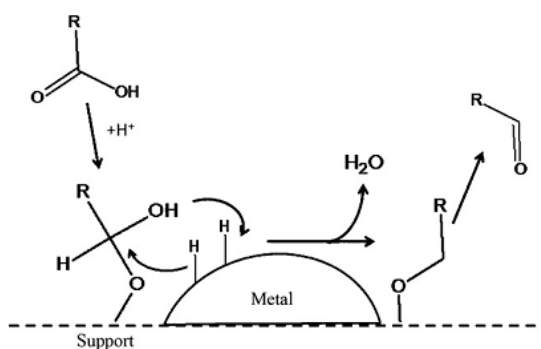


Figure 1.6. HDO mechanism over transition metal catalysts.

Few kinetic studies on HDO of phenol as a model compound on different catalysts, e.g. Co-MoS₂/Al₂O₃ [29], bifunctional catalyst (Pd/C, Ru/C, Rh/C or Ni catalysts combined with several aqueous acids (e.g. H₃PO₄, CH₃COOH and Nafion solution)), or solid acid (HZSM-5, Nafion/SiO₂, ZrO₂) [36, 37]. In this context, Zhao et al. [37] found that the dehydration of cyclohexanol to cyclohexene (step 3 in Figure 1.7) is the rate-determining step in the reaction sequence in the phenol HDO over Pd/C and aqueous H₃PO₄ under mild conditions (200 °C, 50 bar of H₂) (see Figure 1.7 and Table 1.3); however, the same authors found that the hydrogenation of phenol (step 1) was rate determining over Ni/HZSM-5 at the same conditions [38]. On the other side, Mortensen et al. [36] reported that hydrogenation of phenol to cyclohexanone (step 1) and dehydration of cyclohexanol (step 3) are slower compared to the other steps (hydrogenation of cyclohexanone to cyclohexanol (step 2), hydrogenation of cyclohexene to cyclohexane (step 4)). These results indicate that the nature of catalyst system (metal site or acid site) and reaction conditions play an important role in the catalytic performance.

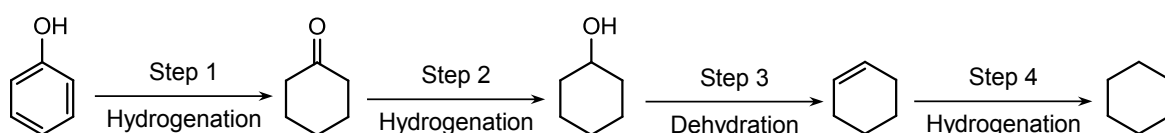


Figure 1.7. Reaction sequence of phenol HDO to cyclohexane on bifunctional catalysts

Table 1.3. Turnover frequencies (TOFs) for steps 1-4 in Figure 1.7 in phenol HDO to cyclohexane

TOF (h ⁻¹)	Pd/C and H ₃ PO ₄ 200 °C, 50 bar H ₂ at RT [37]	Ni/HZSM-5 200 °C, 50 bar H ₂ at RT [38]	Ni/ZrO ₂ 275 °C, 100 bar [36]
TOF1	6210	398	360
TOF2	1.2 × 10 ⁴	2443	2484
TOF3	15	7428	108
TOF4	> 9 × 10 ⁶	> 5.5 × 10 ⁵	> 1.4 × 10 ⁴

More insights into the HDO of model compounds regarding the other functional groups (guaiacols, short chain carboxylic acids, furans, alcohols) in bio-oil have been given in our book chapter [39] and relevant reviews [40-43].

1.3.2 Bio-oil

The upgrading of bio-oil has started several decades ago. The first study began in 1979 with the first pilot scale plant for LF of woody biomass started. To take the advantage of hydroprocessing technology of the conventional refinery, the same catalysts and conditions were applied for bio-oil hydrotreatment. With the LF oil, the upgraded product

was analysed using the standard petroleum tests showing that the oxygen content can be reduced to near zero [44]. Nonetheless, this is a really difficult task for the FP oil due to the reactivity and the different properties of such original oils. The application of the same catalysts and approaches seems to be insufficient because the catalysts appear to be unstable due to the high levels of formed char/coke, causing reactor plugging. Several hydrotreatment concepts for FP oil such as two-stage, nonisothermal and low severity hydrotreatment over the conventional catalysts were also proposed [45-49]. However, the known sulfided hydrotreating catalysts seem to be insufficient and unstable owing to the same reasons. It should be noted that those catalysts need continuous sulfur supply for activation and to keep the activity, but the bio-oil possesses very low sulfur content compared to fossil crude oil. Additionally, the conventional support Al_2O_3 is unstable at the hydrotreating conditions with the FP oil, thus requiring the development of stable and active non-sulfided catalysts and advanced processing concepts [21].

Various supported noble metal catalysts (e.g. Ru/C, Ru/ Al_2O_3 , Ru/ TiO_2 , Pt/C, Pd/C) were intensively used for this process in batch reactors [50, 51]. According to the van Krevelen plot, which displays molar O: C and molar H: C ratios as a measure of fuel quality and is connected to the degree of deoxygenation (DOD) [50], a lower molar O: C ratio (correlates with high DOD) could be achieved with a suitable catalyst by deep HDO treatment (using severe conditions: 200 bar and 350 °C, Figure 1.8). The authors suggested that Ru/C is one promising catalyst for bio-oil HDO with regard to oil yield, DOD and hydrogen consumption. Nevertheless, a loss of activity during catalytic cycles was observed, probably due to high coke deposition and a decrease in pore volume and metal dispersion of the catalyst.

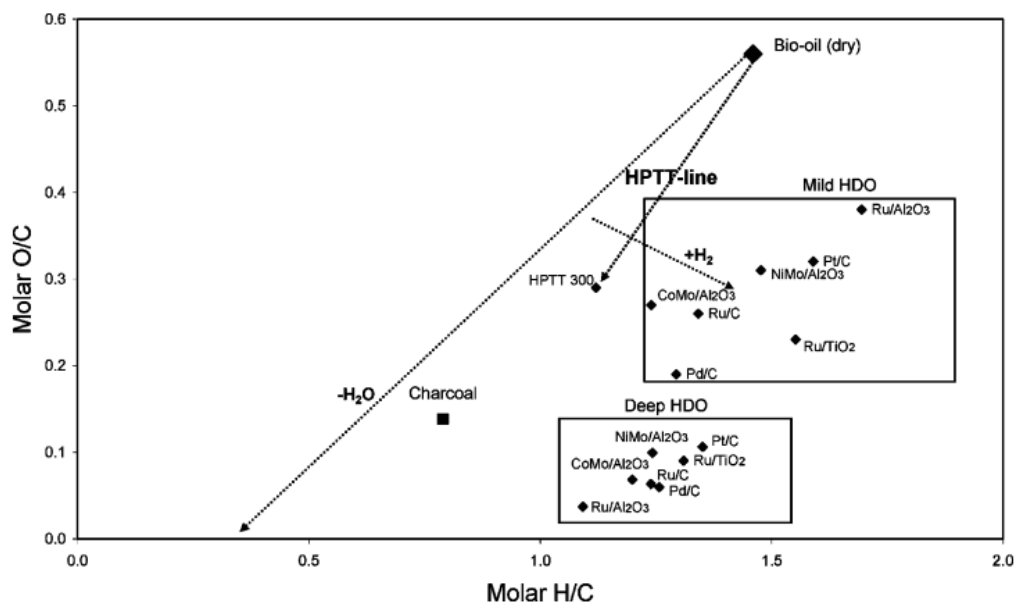


Figure 1.8. van Krevelen plot for the elemental composition of the mild and deep HDO oils [50].

Elliott et al. [52, 53] studied the HDO of wood and bagasse FP oils in a continuous flow reactor with noble metal catalysts (Ru/C, Pd/C). At 340 °C and 138 bar over Pd/C catalyst, the oxygen content of the hydrotreated bio-oil dropped from 34 to 20 wt% at LHSV = 0.7 h⁻¹ and to 10 wt% at LHSV = 0.25 h⁻¹ with an oil yield of 62% based on dry feed [53]. However, plugging of catalyst bed and pressure drop were observed during 10-100 h on-stream depending on the reaction conditions. The tests with several bio-oils from other feedstocks (corn stover, oak, poplar) indicated that the effect of feed is negligible in terms of oil yield and hydrogen consumption.

Various parallel and/or consecutive reactions, namely hydrogenolysis, hydrogenation, dehydration, decarbonylation, decarboxylation, cracking, hydrocracking, polymerization, methanation are relevant in the hydrotreatment of bio-oil, as e.g. recently reported by the group of H.J. Heeres (see Figure 1.9) [51, 54, 55].

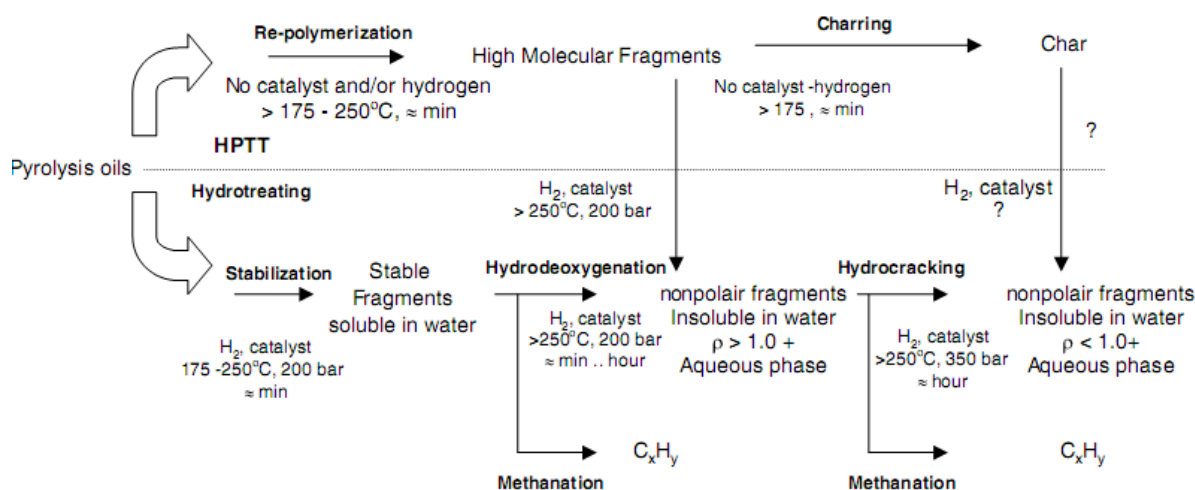


Figure 1.9. Proposed reaction pathways in hydrotreatment of FP oil [51, 54, 55].

Notably, in the absence of catalyst (referred to HPTT - high pressure and temperature treatment), thermal reactions including mainly re-polymerization reactions and less decarboxylation and decarbonylation took place, leading to a phase separation and different oxygen content in both organic and aqueous phases. The authors observed that the oxygen content of organic phase was reduced from 40 to 25 wt% whereas the aqueous phase contained 15-30 wt% (both on dry feed basis). In the presence of catalyst (Ru/C), the HDO, catalytic decarbonylation, decarboxylation and methanation together with the named thermal reactions occurred. Depending on the reaction conditions, two or three phases are obtained. Under mild conditions (175-250 °C), HDO reaction runs to a lesser extent and only two liquid phases are noticed, whereas the formation of two organic phases with different composition together with an aqueous phase are observed at

extreme conditions (350 °C, 200 bar). Additionally, the repolymerized compounds and char formed by the parallel non-catalytic HPTT reaction are also hydrotreated to form products in the liquid and/or gas phase.

It is well known that the unsaturated double bonds containing oxygenates, particularly carbonyl compounds (aldehyde, ketone) and olefins are highly reactive and responsible for the chemical instability of bio-oil, which in turn points to a stabilization step via hydrogenation playing an important role. Therefore, two-stage HDO processes have been widely investigated (e.g. [53-57]). Elliott et al. [56] reported a two-stage hydrotreating process for FP oil obtained from pine sawdust feed. The first stage was catalyzed by Ru/C at 175 °C or 250 °C, the other one by sulfided CoMo/C at 400 °C. The resulting product oils had oxygen contents of 0.2-2.7 wt% and 35-45 wt% yield (dry basis); however, a pressure drop and plugging of the catalyst bed were noticed due to char formation.

It should be noted that bio-oils are acidic and possess high water content (15-30 wt%), causing corrosion of vessels and pipework for direct use in fuels or chemicals, thus aqueous phase processing appears as an alternative approach. Vispute et al. [58, 59] reported the HDO of wood derived bio-oil or its fractions via an integrated catalytic processing. The feed is firstly stabilized by low temperature hydrogenation using Ru/C at 125 °C and 100 bar H₂, which is followed by upgrading over ZSM-5 zeolite towards high yields of olefins, aromatics and light alkanes. Moreover, the authors stated that the yield of named products was further increased due to lower coke formation (only 12.6%) by combining an additional hydrogenation stage using Pt/C at 250 °C and 100 bar after first hydrogenation step (using Ru/C), running without plugging during 5 days on operation [59].

Hot compressed and supercritical water has received considerable attention owing to its properties different from ambient water [60, 61]. In this regard, Duan and Savage reported hydrotreatment of bio-oil, obtained from algae via non-catalytic LF, in supercritical water with Pt/C, Mo₂C and HZSM-5 catalysts [62-64]. The authors reported that several factors affected the quality and quantity of product oil among which the temperature (430 °C) appeared to be the best for producing an oil in high yield with high molar H: C ratio and HHV (42-43 MJ/kg). Zhao et al. [65] reported that a bifunctional catalyst (Ni/HZSM-5) could be effective to convert the n-hexane-extracted crude bio-oil to C₅-C₉ paraffins, naphthenes and aromatics in presence of a considerable amount of water in a batch reactor. HDO of bio-oil has been reviewed in references [9, 21, 40].

Hydrogen consumption in HDO reaction is an important aspect because it is decisive for the DOD, the HHV and the operating costs of the process. Venderbosch et al. [54] reported that the hydrogen consumption is increasing non-linearly with the DOD. In fact,

roughly 300 Nm³ of hydrogen might be consumed per ton of FP oil at a degree of oxygen removal of 70%, which is significantly lower than the complete deoxygenation requires (approximately 600 Nm³/t in extrapolation). The reactivity of the oxygenates in bio-oil could be the reason for this observation: the highly reactive components (ketones, aldehydes) are easily converted with low hydrogen consumption, whereas the more complex molecules (phenols, guaiacols, dimers) are recalcitrant to deoxygenation and thus an initial hydrogenation/saturation proceeds before oxygen elimination, causing the hydrogen consumption to exceed the stoichiometric prediction [20]. The DOD is in relation with the oil yield, that means full removal of oxygen would lead to rather low product yields; for instance, the oil yield drops from 55% to 30% when the DOD increases from 78% to 100% [66]. Mercader et al. found that the hydrogen consumption correlates with HHV of product oil at ca. 22 Ni(H₂)/MJ [67]. One strategic question for researchers is therefore which extent of deoxygenation should be pushed.

As summarized above, the total removal of oxygenates from bio-oil for direct use in transportation fuels is very challenging. High energy input and severe reaction conditions are required to reach complete conversion and DOD. Furthermore, high investment costs for a standalone plant to convert bio-oil to new biofuels are also needed. Otherwise, the co-feeding of bio-oil with conventional feed in standard refinery units has been discussed as promising strategy owing to the utilization of the existing infrastructures for processing, transport and distribution of liquid fuel as well as the guarantee of product quality [68-72]. Following the above considerations, the upgrading of bio-oil under mild conditions might be a feasible option to just partly reduce oxygenates and more importantly to stabilize the bio-oil in order to provide a suitable co-feed for further processing in existing refinery units.

Fluid catalytic cracking (FCC) unit appears as best choice because it transforms high molecular weight compounds to more valuable products, namely gasoline, liquefied petroleum gas (LPG), olefins, and light cycle oil (LCO) for fuels or starting material for petrochemical industry. Moreover, FCC is flexible for changing feedstock and product specifications depending on market demands. Some researchers proposed a direct use of bio-oil by catalytic cracking in a standard refinery; however, several cumbersome issues are observed such as fast polymerization and significant amount of coke formation, which lead to an irreversible catalyst deactivation. Thus, direct use of an untreated bio-oil in standard refinery unit is not considered as a straightforward option.

Several attempts have been reported for co-processing various oxygenated model compounds for bio-oil in a lab-scale FCC unit in order to get more insight into co-feeding of such bio-oil into real FCC unit, e.g., by Corma et al. [73], Domine et al. [74], and Graça et al. [75, 76]. The latter authors reported that the maximum amount of 10 wt% of

oxygenated compounds (referred to gas-oil) can be fed to a FCC unit without major problem. Few reports on co-feeding of HDO products of bio-oil into a FCC unit have been presented. For example, Mercader et al. [77] observed that the mixed feed led to a lower conversion than that obtained with a conventional feed (vacuum distillation residue – Long residue) and in order to obtain an equivalent conversion, a slightly higher catalyst to oil (CTO) mass ratio was required. Depending on the nature of different bio-oils treated at 60 wt% conversion, CTO ratios were required in the range of 3.4-4.3 (g/g) for the co-feeding of 20 wt% treated oils compared to 3.1 (g/g) for 100% Long residue. The authors also reported that the required CTO ratio was significantly higher (in the range of 12-20 g/g) than in cracking of 100% undiluted treated oil at same conversion. On the other hand, Fagassy et al. [78] showed that the conversion achieved in co-processing of hydrotreated bio-oil with vacuum gas oil (VGO) is higher than that obtained from pure VGO feed experiment. Another study by Samolada et al. [67] on co-feeding of hydrotreated bio-oil and an aromatic feedstock (15/85 wt/wt) using two commercial FCC catalysts (ReUSY₁, ReUSY₂) showed that the conversion of these mixtures is slightly lower than that of the ordinary VGO. The limited crackability of the aromatic feedstock seemed to be the primary reason rather than the reactivity of the co-feed. In sum, the overall conversion in co-processing of hydrotreated bio-oil with a conventional feedstock in the FCC unit depends on the nature of conventional feeds, FCC catalysts and reaction conditions [68, 79].

On the other side, Mercader et al. reported the co-processing test of 80 wt% of straight run gas oil + 10 wt% of HDO oils + 10 wt% of isopropanol (to reduce viscosity) in a lab-scale HDS reactor and concluded that this way of co-processing is possible but a competition between HDS and HDO is observed and the degree of HDS is reduced [80, 81].

As a result, co-processing of biomass-derived resources together with a conventional feed in a standard refinery unit (e.g. FCC unit) is considered as a realistic scenario to increase the fraction of bio-based fuel components in the short term. Therefore, this scheme was selected in this thesis.

1.4 Catalysts for HDO of bio-oil and its model compounds

As partly shown above, variety of catalysts have been developed and tested for HDO of bio-oil and its model compounds. Table 1.4 provides a summary of the tested catalysts for bio-oil and its model compound in relevant studies, followed by a discussion about advantages and disadvantages of these catalysts.

Table 1.4. Summary on the tested catalysts for bio-oil and its model compounds

Catalysts	Feedstock	Reaction conditions ^[a]	Reference
Oxides or sulphides (Mo/Al ₂ O ₃ , CoMo/Al ₂ O ₃ / NiMo/Al ₂ O ₃)	2-ethylphenol, bio-oil	FBR (340 °C, 70 bar) BR (250 - 350 °C, 100 bar)	[30, 50, 82-84]
Pt/MZ-5 (Pt supported on mesoporous zeolite)	dibenzofuran, cresol, guaiacol, bio-oil	FBR (200 °C, 40 bar, LHSV =2-6 h ⁻¹); BR (200 °C,40 bar)	[85]
Pt/C, Pt/ZrO ₂ , Pt/TiO ₂ , Pt/CeO ₂	4-propylphenol, guaiacol and syringol	BR (280 °C, 40 bar)	[86]
Pt/SiO ₂ -Al ₂ O ₃	sorbitol, isosorbite, 1,2-hexandediol.	FBR (245 °C, 29.3 bar, WHSV = 0.73 h ⁻¹)	[87]
Ru/C, Ru/TiO ₂ , Ru/Al ₂ O ₃ , Pt/C, Pd/C	FP oil	BR (250 - 350 °C, 100 bar)	[50]
Pt/Al ₂ O ₃ , Pt/SiO ₂ , Pt/ZSM-5, Pt/HBeta, Pt/HY, Ga/HBeta	phenol, anisole aqueous phenolics,	FBR (200 °C, 40 bar, WHSV = 20 h ⁻¹); BR (200-300 °C, 40 bar RT)	[28, 88-92]
Pd/C, Pt/C, Ru/C, Rh/C combined HZSM-5 or aqueous H ₃ PO ₄	phenolic model compounds (monomers or dimers)	BR (200 - 250 °C, 50 bar at RT)	[37, 93, 94]
Ru and Rh /(Al ₂ O ₃ , SiO ₂ -Al ₂ O ₃ , ZrO ₂)	guaiacol	BR (250 °C, 40 bar RT)	[95]
Ni/ZrO ₂ , Fe/SiO ₂ , Co/SiO ₂ , Cu/SiO ₂ , copper chromite	phenol, furfural	BR (275 °C, 100 bar RT) FBR (300 °C, 1 bar)	[36, 96-98]
Ni/HZSM-5-Al ₂ O ₃ , Ni/HZSM-5	model compounds, fraction of hexane- extracted bio-oil	BR (250 °C, 50 bar)	[27, 65]
Ni-Pt/γ-Al ₂ O ₃ , Co-Pt/γ-Al ₂ O ₃	m-cresol	FBR (260 °C, 1 bar)	[99]
Pd-Fe/C	guaiacol, m-cresol	FBR (300 °C, 1 bar)	[100, 101]
Ni-Cu/δ-Al ₂ O ₃	anisole, bio-oil	FBR (300 °C, 10 bar) BR (150-350 °C, 100 bar)	[102]
Ni-Cu/ZrO ₂ -SiO ₂ -La ₂ O ₃ , Ni-Fe/γ-Al ₂ O ₃	guaiacol, m-cresol, furfuryl alcohol	FBR (300 °C, 1 bar) BR (280-320 °C, 174 bar)	[26, 103, 104]
MoO ₃ /TiO ₂ , Mo ₂ C/TiO ₂ , Mo ₂ N/TiO ₂ , MoP/TiO ₂	phenol	FBR (350 °C, 25 bar, WHSV = 0.27 h ⁻¹)	[105]
Pd/C, Pt/C, Mo ₂ C, HZSM-5	LF oil	BR (400-530 °C , 340 bar)	[62-64]

^[a] FBR: Fixed bed reactor, BR: batch reactor.

For HDO catalyst development, two kinds of catalysts, namely HDS and hydrotreatment catalysts that have been used in refinery for a long time, were first investigated. However, HDS catalysts (binary sulfides of CoMo or NiMo/ γ -Al₂O₃) are quickly deactivated due to loss of sulfur, coke deposition and the support is unstable in the presence of the abundant amount of water in bio-oil [30, 50, 82-84]. Meanwhile, hydrotreatment catalysts (e.g. supported noble metal catalysts with Pt, Pd, Ru, Rh etc.) show higher activity than conventional HDS catalysts [28, 50, 86-92, 95]. Such precious metal catalysts are, however, more expensive than HDS catalysts and their resources are limited, thus further progress is needed to realize economic alternative formulations.

Various supported non-noble monometallic catalysts (such as Fe/SiO₂, Co/SiO₂, copper chromite, and Ni based catalyst) have been already used in HDO studies [27, 36, 38, 96-98]. Although Ni-based catalysts showed higher activity than others, coke deposition, deactivation of Ni catalysts due to sintering and Ni leaching into water are still a problem for bio-oil HDO [27, 38]. Few groups also reported on bimetallic catalysts for HDO of model compound and bio-oil due to their properties being different compared to the corresponding monometallic catalysts [106]. In this respect, Ardiyanti et al. [102] stated that bimetallic Ni-Cu/ δ -Al₂O₃ catalysts improve product properties of upgraded FP oil. Bykova et al. [26] proposed that bimetallic catalyst (36.5%Ni2.3%Cu/ZrO₂-SiO₂-La₂O₃) was most promising for HDO of guaiacol. Do et al. [99] observed that bimetallic catalysts (Ni-Pt/ γ -Al₂O₃ and Co-Pt/ γ -Al₂O₃) show high conversion and change the product selectivity compared to monometallic catalysts (Pt/ γ -Al₂O₃) in HDO of meta-cresol. Other groups also reported on the HDO of model compounds (e.g. meta-cresol, guaiacol) or bio-oil with bimetallic catalysts such as Pt-Fe/C, Ni-Fe/SiO₂, Ni-Fe/Al₂O₃. Nevertheless, the precious metal catalysts rule out the application and the hydrothermal stability of supports should be taken into account [83, 84, 107]. To increase the catalyst efficiency, the use of a hydrothermally stable, high surface area support is beneficial. Additionally, the combination of metallic and acidic sites in catalysts with suitable acid-base properties seems to be essential as they can promote all the elementary steps in the preferred deoxygenation pathways. More importantly, the material should be resistant to coking and heteroatoms in biomass (S, N, P, K...) in order to increase the catalyst lifetime.

1.5 Objectives of the thesis

Thus, the main objective of this work was to develop bimetallic catalysts using non-sulfided, non-noble metals with high hydrothermal stability for aqueous phase HDO of bio-oil from FP process to overcome the indicated drawbacks (deactivation, coke formation and cost) under mild conditions to produce a co-feed for FCC unit. In order to achieve this

goal, it was planned to use non-noble Ni, which is more active in hydrogenation. Cu and Co were used as modifiers because Cu can help to reduce nickel oxide at lower temperature and to increase activity, whereas Co might decrease particle size and increase metal dispersion. Zeolite (HZSM-5) was selected as starting support due to its exceptional performance in dehydration reaction. Zeolites are also widely used as a catalyst and support in the oil refining and petroleum industry owing to their outstanding properties such as well-defined structure and high acidity, i.e. number and strength of acidic sites. Figure 1.10 provides an overview of the approach and strategy in this study.

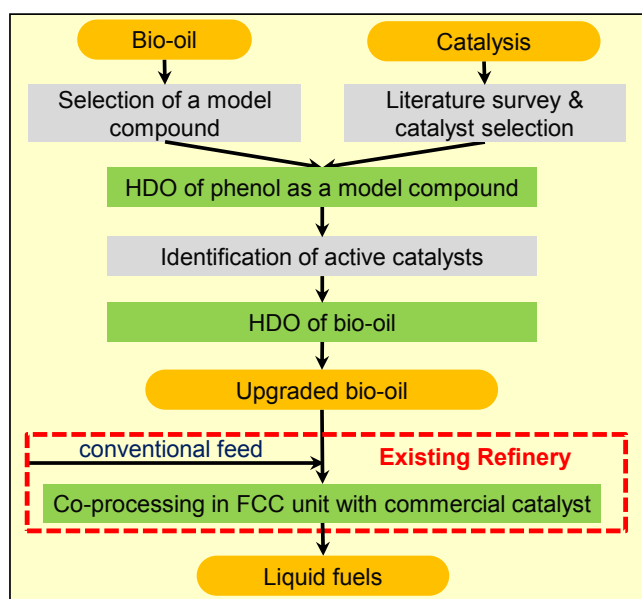


Figure 1.10. Overall approach and working scheme in this thesis

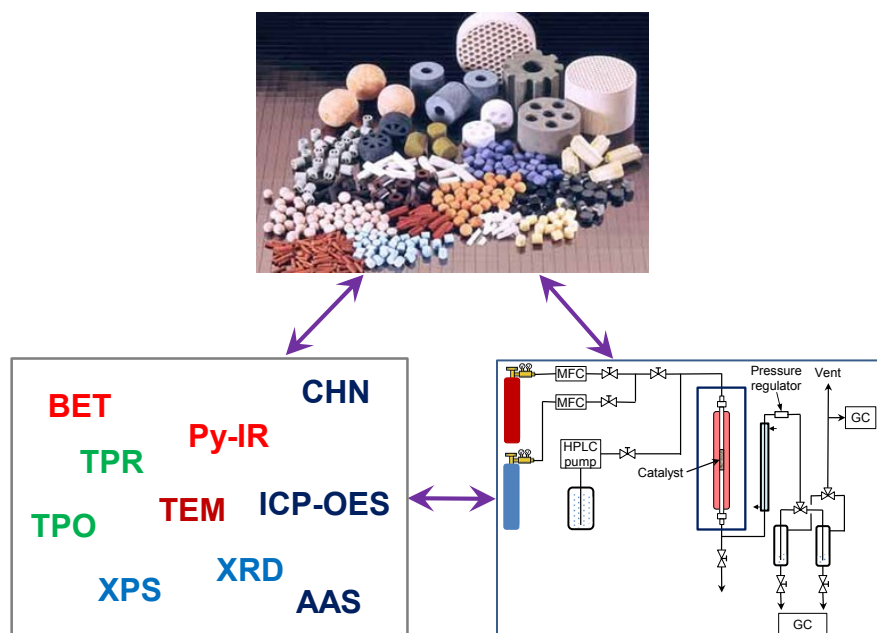
To understand the chemistry of HDO reaction and for catalyst screening purpose, phenol was selected as a model compound for bio-oil. Catalysts were evaluated to gain insight into effect of secondary metals in bimetallic catalysts, the reaction network and to identify the crucial features (metal sites and acid sites) to provide a highly selective catalyst. This had to be done in batch autoclaves as well as a continuous fixed bed reactor at high H_2 pressure. Following that, the best-performing catalysts should be used for upgrading of a wood-based bio-oil obtained from FP process in autoclave. Larger amounts of thereby upgraded bio-oil should be tested in co-processing with conventional feed with a commercial catalyst in a regular FCC unit using an ASTM certified test setup to finally demonstrate the potential of converting bio-oils into regular fuels.

To evaluate and explain the obtained catalytic performance, the prepared heterogeneous catalysts and spent catalysts had to be characterized by various physico-chemical techniques like N_2 physisorption, ICP-OES, AAS, BET, XRD, XPS, TPR, TPO, TEM, py-IR and CHN analyzer.

Chapter 2

Experimental Procedures

Chapter 2 explains the detailed procedures for the preparation of monometallic and bimetallic catalysts using impregnation method. The principle and applications of the different methods for catalyst characterization are illustrated. Finally, the experimental set-ups for batch autoclaves, a continuous fixed bed reactor and a short contact time-micro activity test together with product analysis and evaluation of catalytic performance are described.



2.1. Catalyst preparation

2.1.1 Preparation of monometallic and bimetallic catalysts

All the monometallic catalysts used in this work were prepared by incipient wetness impregnation method and bimetallic catalysts were prepared by co-impregnation method. HZSM-5 (PZ-2/25H with $\text{SiO}_2/\text{Al}_2\text{O}_3 = 34$, Zeochem AG), HBeta (PB/H – Zeochem AG), $\text{NH}_4\text{-Y}$ (CBV712 - Zeolyst) and ZrO_2 (Saint Gobain) were used as supports. The $\text{NH}_4\text{-Y}$ was calcined at 550 °C for 4 h to get the HY form before impregnation, whereas the others were calcined in air at 450 °C for 2 h to remove physisorbed water. $\text{Ni}(\text{NO}_3)_2 \cdot 6\text{H}_2\text{O}$ (Merck), $\text{Cu}(\text{NO}_3)_2 \cdot 3\text{H}_2\text{O}$ (Merck) and $\text{Co}(\text{NO}_3)_2 \cdot 6\text{H}_2\text{O}$ (Fluka) were used as Ni, Cu and Co precursors, respectively.

In the typical synthesis, the calculated amounts of precursor (or mixture of two precursors for bimetallic catalysts) were dissolved in known amount of deionized water, and then impregnated onto support under stirring for 16 h at room temperature (RT). A rotary evaporator was used to remove water. The samples were ground and dried at 110 °C overnight and then calcined in air at 550 °C for 4 h with a heating ramp of 10 K/min to get the calcined catalyst (or precursor). Prior to the reaction test, the calcined catalyst powder was pre-reduced in a tubular quartz reactor from RT to desired temperature (depending on the catalyst) at a heating rate of 10 K/min under a hydrogen flow of 100 ml/min. The final temperature was maintained for 4 h. After cooling to RT, the reduced sample was transferred to the autoclave or the continuous fixed bed reactor.

2.1.2 Preparation of unsupported catalysts

Pure nickel and nickel-cobalt alloy were also prepared using the same above procedure without impregnation onto supports.

2.1.3 Equilibrated catalyst

To evaluate the effect of the co-feeding of upgraded bio-oil with conventional feed into a FCC unit, an equilibrium catalyst from a commercial refinery in Vietnam was used. Its physicochemical properties are given in Table 6.1, chapter 6.

2.2. Catalyst characterization

2.2.1 Chemical analysis

The metal (Ni, Co, Cu, Al) and Si contents of the samples were determined by inductively coupled plasma-optical emission spectroscopy (ICP-OES, 715-ES, Varian) and atomic

adsorption spectroscopy (AAS, Analyst 300, Perkin Elmer), respectively. In principle, the atoms or ions of the samples are excited electronically in argon plasma at temperature to 8000 °C and emit electromagnetic radiation at wavelengths characteristic of a specific element. The spectrometer is used to collect the light which is then resolved into a spectrum. The quantitative analysis was done by standard calibration. Approximately 10 mg of the sample were digested with 8 ml of aqua regia and 2 ml of hydrofluoric acid. The solution was filled up to 100 ml and analyzed with ICP-OES or AAS.

The elemental compositions (C, H, N, S) can be rapidly determined by CHNS analyzer via a combustion process. The combustion products (e.g. CO₂, H₂O, NO₂...) were further purged by carrier gas He through a glass column packed with an oxidation catalysts (e.g. WO₃) and a copper reducer to remove the excess oxygen and reduce the nitrogen oxides to N₂. The gases (CO₂, H₂O, N₂, and SO₂) are passed through absorbent traps and then quantified by thermal conductivity detector (TCD).

Elemental analysis of deposits on spent catalyst was carried out using a Truespace CHNS analyzer (Leco Instrument, Ltd.).

2.2.2 Nitrogen physisorption

Whenever a gas (adsorbate) is brought into contact with the surface of a solid (adsorbent), the gas will adsorb on the surface and cover the entire adsorbent to form a thin layer. If the number of gas is raised, the formation of multilayers is forced, accompanied by capillary condensation. Regarding the adsorption gases, N₂ physisorption (at -196 °C) is generally considered to be the most suitable method for determining the surface area of non-porous and porous materials.

The Brunauer, Emmett and Teller (BET) theory is generally accepted for evaluation of surface area in spite of its theoretical limitation (e.g. an oversimplified model of physisorption). The BET equation is basically expressed in the following form:

$$\frac{P}{V(P_0-P)} = \frac{1}{V_m C} + \left[\frac{C-1}{V_m C} \right] \left(\frac{P}{P_0} \right) \quad (\text{Eq. 2.1})$$

Where P₀ and P are the saturation vapor pressure and equilibrium pressure of adsorbate at its boiling point, V is the volume of adsorbed gas and V_m is the monolayer volume of the adsorbate. C is the BET constant, which is related to the heat of adsorption of adsorbate in the first and subsequent layers.

V_m and C in the equation (2.1) can be easily estimated from the slope and intercept of the linear BET plot of P/V(P-P₀) versus P/P₀. Consequently, the specific BET surface (S_{BET}, m²/g) can be calculated in the following equation:

$$S_{\text{BET}} = \frac{V_m \times N_A \times A_m}{21214 \times W} \quad (\text{Eq. 2.2})$$

Where V_m is the monolayer volume (ml) at standard temperature and pressure conditions (STP: 1 bar, 0 °C), N_A is the Avogadro constant, A_m is the mean cross sectional area filled by adsorbate molecule (e.g. 0.162 nm² for nitrogen) and W is the weight of the sample (g).

In this study, N₂ physisorption measurements were carried out on a Micromeritics ASAP 2010 apparatus. Before measurements, the samples were degassed at 200 °C in vacuum for 4 h.

2.2.3 X-ray powder diffraction (XRD)

XRD is the most common used analytical technique for elucidation of phase composition in heterogeneous catalyst. In principle, as X-rays interact with atomic planes of a crystalline sample, each plane creates a specific reflection with the incident rays. All the reflected waves from planes interfere and in case of positive interference they form a diffraction, which occurs only when the wavelength of electromagnetic radiation (λ), the diffraction angle θ (the angle between the incident ray and the scattering planes) and the lattice spacing between the planes in the atomic lattice (d) satisfy Bragg's Law (Eq. 2.3).

$$n \lambda = 2 d \sin \theta \quad (\text{Eq. 2.3})$$

Here n is the order of a detectable reflection ($n = 1, 2, 3, \dots$). Therefore, as λ is known and θ is measured, the value of n/d follows, and the value of spacing of the set of reflecting planes is determined. By putting the information on various sets of reflecting planes, obtained with X-ray spectrometer, the crystal structure of sample can be determined. The crystallite size of a phase can be estimated using the Scherrer equation (Eq. 2.4) by the analysis of line broadening of the peak shape of one or more diffraction lines:

$$D_B = \frac{K \lambda}{\beta \cos \theta} \quad (\text{Eq. 2.4})$$

Where D_B is mean crystallite diameter, K is Scherrer's constant, λ is the wavelength and β is full width at half maximum.

XRD measurements in this study were carried out with a theta/theta diffractometer (X'Pert Pro from Panalytical, Almelo, Netherlands) with CuK α radiation ($\lambda = 1.5418 \text{ \AA}$, 40 kV, 40 mA) and a X'Celerator RTMS Detector. The samples were scanned in the 2θ range of 5 to 65-80°. The phase analysis was carried out with the program suite WinXPOW by STOE&CIE, including the powder diffraction file (PDF) data based on the ICDD (International Centre of Diffraction Data).

2.2.4 X-ray photoelectron spectroscopy (XPS)

XPS is a useful technique for determining composition in the near surface region (in the top 1-10 nm layer). Electrons of each element have characteristic binding energies. X-ray photons generated by an X-ray source excite a sample, causing the emission of core electrons. These electrons are detected and counted for the given specific binding energies, which then form the spectra. The numbers of detected electrons are thus related to the number of the specific element and can be used for quantification of composition. As the energy of the X-rays with a particular wavelength is known (E_{photon}), the electron binding energy (E_{binding}) of each of the emitted electrons can be determined by using the following equation.

$$E_{\text{binding}} = E_{\text{photon}} - E_{\text{kinetic}} - \phi \quad (\text{Eq. 2.5})$$

Where E_{kinetic} is the kinetic energy of the emitted electron measured by the instrument and ϕ is the work function of the spectrometer.

XPS measurements were carried out with a VG ESCALAB 220iXL instrument with monochromatic Al K(alpha) radiation ($E = 1486.6$ eV). The binding energies were referenced to C1s at 284.8 eV. The areas of the peak were determined after background subtraction and fitting with Gaussian-Lorentzian curves. From these peak areas, the amount of each component in the near-surface region can be calculated by division by the element-specific Scofield factor and the transmission function of the spectrometer.

2.2.5 Temperature programmed methods

Temperature programmed reduction (TPR) experiments were performed to investigate the reducibility of catalyst as well as to determine the optimum temperature to reduce the metal oxide completely. TPR experiments were carried out in a home-made setup described in detail elsewhere [108, 109]. The calcined catalyst samples were powdered and placed into the reactor and heated in a nitrogen flow at 300 °C for 30 min before the TPR experiment. Optimum sample weights were estimated according to the equation by Monti and Baiker [110]. After cooling the sample in nitrogen flow to 50 °C, the TPR was carried out in 5.03% hydrogen in argon at a flow rate of 50 ml/min (temperature program: hold at 50 °C for 20 min, increase to 650 °C at 10 K/min, hold at 650 °C for 40 min). Hydrogen consumed was monitored by a calibrated TCD (GOW-MAC Instruments).

Temperature programmed oxidation (TPO) measurement was done using a Micromeritics Autochem II 2910 instrument connected with an online Quadrupol mass spectrometer (Balzers Omnistar). The spent catalysts (60 mg) were loaded into an U-

shaped quartz reactor and pretreated at 200 °C for 60 min in He flow (50 ml/min) for the removal of adsorbed water, then cooled to RT. The samples were then heated from RT to 580 °C in a flow of 5% O₂/He (50 ml/min) with a temperature ramp of 10 K/min.

2.2.6 Fourier transform infrared spectroscopy of adsorbed pyridine (py-IR)

For acidity characterization by means of IR technique, pyridine was used as probe molecule. Py-IR provides the discrimination of Brønsted and Lewis acid sites, which NH₃-temperature programmed desorption method does not show. Fundamentally this method is based on the adsorption of pyridine onto two types of acid sites, and by means of well-known assignments of vibrational modes associated with pyridinium ions formed at Brønsted sites and with coordination complexes at Lewis sites, quantification is possible. The Brønsted and Lewis acid site concentrations were calculated based on the molar extinction coefficient and the intensities of the bands at 1544 cm⁻¹ and 1448 cm⁻¹ in the spectra recorded at 150 °C, respectively, according to literature [111].

The measurements were carried out in transmission mode on a Bruker Tensor 27 spectrometer equipped with a heatable and evacuable homemade reaction cell with CaF₂ windows connected to a gas-dosing and evacuation system. The sample powders were pressed into self-supporting wafers with a diameter of 20 mm and a weight of 50 mg. Before pyridine adsorption, the samples were pretreated by heating in 5% H₂/He to 400 °C for 10 min, subsequent cooling to RT and evacuation (around 0.02 mbar). Pyridine was adsorbed at RT until saturation. Then the reaction cell was evacuated for removing physisorbed pyridine. The desorption of pyridine was followed by heating the sample in vacuum up to 300 °C and recording spectra every 50 K.

2.2.7 Transmission electron microscopy (TEM)

Transmission electron microscopy (TEM) was employed to gain more information on metal sites, their dispersion and particle size on the catalysts. This is the most powerful microscope for catalyst characterization. This method utilizes highly energetic electrons transmitted through a very thin sample (< 50 nm) to image and analyze the structure of materials and can provide the morphologic and crystallographic information from micron sizes to atomic scale. In this study, the measurements were performed at 200 kV on a JEM-ARM200F (JEOL) which is aberration-corrected by a CESCOR (CEOS) for the scanning transmission (STEM) applications. The microscope is equipped with a JED-2300 (JEOL) energy-dispersive X-ray-spectrometer (EDXS) for chemical analysis. High-angle annular dark field (HAADF) combined with EDXS imaging was operated with a spot size of 0.16 nm and a 40 μm condenser aperture. The HAADF mode operated with a spot size

of 0.13 nm and a 40 μm condenser aperture. For the bright field STEM images, annular bright field (BF) with beam stopper and a 3 mm BF aperture was used. The sample was ground and deposited on a holey carbon supported Cu grid and transferred to the microscope.

2.3. Experimental setup

2.3.1 HDO of phenol in a batch reactor

In a typical test, phenol (0.5 g, 5.3 mmol), H_2O (10 g), and catalyst (0.025 g) were loaded into an autoclave (Parr Instruments, 25 ml volume, see Figure A1 in Appendix A). The reactor was flushed with argon and then with H_2 to remove air. Then, the autoclave was pressurized with H_2 to 50 bar at RT and heated to 250 $^\circ\text{C}$. The start time was recorded when the required reaction temperature was reached and then stirring speed was set to 650 rpm. After reaction, the autoclave was cooled to RT and the gas was analyzed by gas chromatography (GC, HP 5890) online from autoclave via a transfer line. This GC was equipped with both FID (Poraplot Q column, 25 m \times 0.53 mm \times 0.20 μm) and TCD (HP PLOT Molesieve column, 25 m \times 0.53 mm) using Ar as a carrier gas. The liquid products (organic and aqueous phase) were analyzed by another gas chromatograph (Shimadzu GC 17A) with autosampler and FID (CP-FFAP column, 25 m \times 0.32 mm) using He as carrier gas. Mesitylene and 1,4-dioxane were used as the internal standards for quantification of organic and aqueous phase, respectively. Pure components were used for peak identification and calibration.

Conversion and selectivity (product distribution) were calculated basing on the number of carbon moles defined as follows. Carbon balances were calculated from detected products in gas and liquid phase and reached more than 90% in this work. Missing carbon was due to mostly deposits on the surface of catalysts, some unknown minor peaks in chromatograms and work-up procedure (e.g. extraction step). The mass balances were determined based on weight of liquid product and achieved more than 95% for all experiments.

$$\text{Conversion (\%)} = \frac{\text{moles of phenol consumed}}{\text{moles of initial phenol}} \times 100 \quad (\text{Eq. 2.6})$$

$$\text{Selectivity (\%)} = \frac{\text{moles of C atoms in each product}}{\text{total moles of C atoms in the products}} \times 100 \quad (\text{Eq. 2.7})$$

2.3.2 HDO of phenol in a fixed bed down-flow reactor

The setup consisted of a stainless steel tubular reactor (i.d. = 5 mm, l = 310 mm, V = 7 ml) that was heated by an electric heating coil. Reactor temperature was controlled by using a thermocouple installed in the heating coil. In addition, a movable thermocouple was placed in a guiding tube inside the reactor to measure the temperature of the catalyst bed. The reactor was placed in a heating box (set to 150 °C) to avoid undesired condensation (see Figure 2.1).

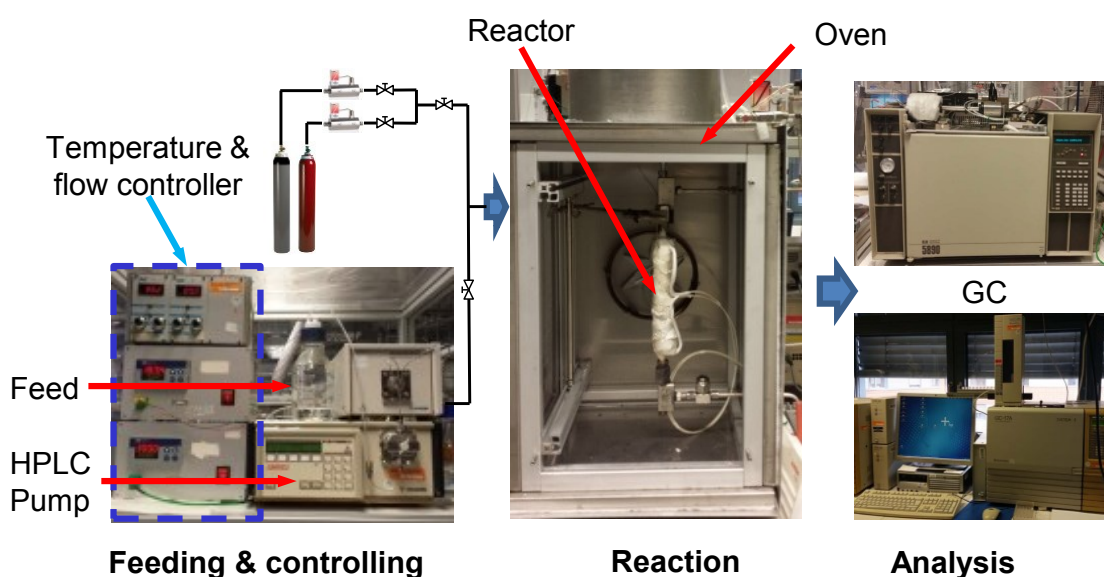


Figure 2.1. Experimental set-up of the continuous flow reactor

The feed was pumped by a HPLC pump (Gilson). The nitrogen and hydrogen were fed from commercial cylinders (Air Liquide). The outlet of reactor was connected with a countercurrent water cooler. A back pressure regulation was used to release the reaction pressure to ambient and then the gas and liquid were separated in a separator system (two separators with a 3-way valve) that was placed in iced water to avoid any vaporization of the products.

The HDO reaction was carried out in the above setup with both liquid and gas moving downward. In a typical experiment, the catalyst with particle size of 180-250 μm (0.3-0.5 g) was diluted with silicon dioxide (100-160 μm , Supelco) to get a volume of reaction zone of 2 ml that was placed between two silicon dioxide zones (100-160 μm) and glass wool plugs at both sides. Prior to each run, the pre-reduced catalyst was pretreated again at 450 °C in H_2 flow of 100 ml/min for 30 min and then cooled to RT in N_2 at 50 ml/min. Then, the feed solution (3 wt% phenol in water, flowrate = 0.5 ml/min) was pumped to the reactor up to the desired pressure, which was controlled by a back pressure regulator,

and then H₂ was subsequently fed into the reactor and the catalyst bed was heated to the reaction temperature. The system was run at least 2 h to achieve steady-state operation. Thus, the standard test program for each catalyst consisted of 3 h for stabilization and subsequently 8 h or more on-stream at the desired temperature. The sample was collected over 15 min in a separator in which toluene was preloaded as absorbent. The aqueous phase and toluene phase were analyzed by an offline GC, whereas the gas was analyzed online by another GC. The details of both GCs are described in the previous section 2.3.1. According to the GC result, hydrogen and small traces of toluene and cyclohexane were found in the gas phase, thus in this study only the liquid phase was taken into account for calculation of conversion and selectivity. The carbon balances of all experiments were more than 93% and the mass balances were better than 95%.

The conversion and selectivity (product distribution) were calculated based on number of carbon moles on-stream in the following equations:

$$\text{Conversion (\%)} = \frac{\text{moles on stream of phenol consumed}}{\text{moles on stream of phenol fed}} \times 100 \quad (\text{Eq. 2.8})$$

$$\text{Selectivity (\%)} = \frac{\text{moles on stream of C atoms in each product}}{\text{total moles on stream of C atoms in the products}} \times 100 \quad (\text{Eq. 2.9})$$

2.3.3 HDO of bio-oil in a batch reactor

2.3.3.1 Experimental procedure

In a typical test, 5 g of bio-oil, 25 g of H₂O and 0.5 g of catalyst were loaded into an autoclave (Parr Instruments, 100 ml volume, see Figure A1). The autoclave was flushed with N₂ and then with H₂ to remove air. Then, the reactor was pressurized with H₂ to 50 bar at RT. Subsequently, the autoclave was heated to desired temperature. The start time was recorded when the temperature reached 150 °C and then stirring speed was set to 650 rpm. After completing the reaction, the autoclave was cooled to RT, part of the gas phase was collected with a syringe and analyzed by a GC.

After gas phase analysis, the autoclave was released to atmospheric pressure. Dichloromethane (DCM) was used to recover and to extract the oil phase (two times). All of the DCM extracts were combined and then the DCM was evaporated under a vacuum of 27 kPa at RT for 45 min. The obtained oil phase is denoted as an upgraded bio-oil (UBO). The catalyst was recovered by filtering off and rinsing with acetone before drying and weighing. The amounts of oil phase, aqueous phase, char and gas phase were determined experimentally and the yields toward the different products (wt% on wet basis)

was calculated by dividing by the amount of bio-oil loaded into the autoclave. The coke deposition on spent catalyst was also analyzed using a CHN analyser (Leco-CS600).

2.3.3.2 Feedstock and product analysis and catalytic evaluation

Bio-oil was produced by FP of wood supplied by the PYTEC GmbH. Some typical properties of bio-oil are presented in Table 5.1 in Chapter 4. The following paragraphs explain the methods for the feed and product analysis as well as the catalytic evaluation.

The gas phase was analyzed by a GC (Agilent 7890), which was equipped with both FID and TCD using Ar as a carrier gas. The TCD channel was configured with three columns (0.5M Haysep Q 80/100 mesh, 6 Ft Hayesep Q 80/100 mesh, 6 Ft Molecular Sieve 5A 60/80 mesh) to analyze H₂, CO₂, CO, O₂, N₂ and light hydrocarbon as CH₄. The FID channel was configured with two columns (123-1015 (cut) 2 m × 0.32 mm × 5 μm DB-1, 19091P-S12 25 m × 0.32 mm × 8 μm HP-AL/S) to analyze hydrocarbons (C₁-C₅). The oven temperature was kept at 60 °C for 2 min, then increased to 190 °C at 20 K/min, and held for 2 min. A reference gas was used for peak identification and calibration. The amounts of individual formed gases (except H₂) were calculated based on total gas volume at STP (0 °C, 1 bar), concentration (mol-%) and molecular weight and summed up to the gas phase amount (Eq. 2.10).

$$W_{\text{gas phase}} = \sum W_{\text{the formed gases}} \quad (\text{Eq. 2.10})$$

To identify volatile compounds in the bio-oil and the liquid products (aqueous phase and DCM phase), a GC-MS (Agilent 7890 GC coupled with a mass spectrometer 5970C) equipped with a DB-1701 column (60 m × 0.25 mm × 0.25 μm) was used. Temperature program: 40 °C (10 min hold), 4 K/min to 280 °C (20 min hold). To protect filament, solvent delay was set to 6.5 min.

Water content of the original bio-oil and the UBO was measured by Karl-Fischer-titration (MKS-520 Mettler Toledo) according to ASTM E203. Measuring pH of the bio-oil was carried out on an UB-10 pH/mV/Temp (Denver Instrument) according to ASTM E70.

Elemental compositions (C, H, N) of the original bio-oil and UBO were carried out on a CHN/CHNS Vario Macro analyzer according to ASTM D5291-10. The dry elemental compositions were calculated by subtracting the contribution of H and O originating from water and then the oxygen content was calculated by difference. These results were used for calculating the DOD and the HHV using Dulong's formula [112].

$$\text{DOD (\%)} = \frac{\%O (\text{bio-oil}) - \%O (\text{UBO})}{\%O (\text{bio-oil})} \times 100 \% \quad (\text{Eq. 2.11})$$

$$\text{HHV (MJ/kg)} = \left[338.2 \times \%C + 1442.8 \times \left(\%H - \frac{\%O}{8} \right) \right] \times 0.001 \quad (\text{Eq. 2.12})$$

To get more insight into the nature of bio-oil and UBO, ^{13}C -NMR technique was used. The NMR spectra were recorded on a 500 MHz-spectrometer (Avance III 500 Bruker) at 125 MHz. The sample (10 mg) was dissolved in CDCl_3 and filled up to 0.6 ml.

The coke formation was evaluated by LECO CS-600 analyzer.

2.3.4 Catalytic cracking of UBO together with conventional feed

2.3.4.1 Feedstock, catalyst and experimental procedure

To demonstrate the efficiency of the co-feeding of UBO into the FCC unit, a conventional feed and a typical equilibrated FCC catalyst from a commercial refinery in Vietnam were used. The properties of conventional feed and the equilibrated catalysts are listed in Table 5.1 (chapter 5) and Table 6.1 (chapter 6), respectively. The FCC reaction was performed in a fully automated Single Receiver - Short Contact Time - Micro Activity Test (SR-SCT-MAT) supplied by GRACE Davison. This setup consists of three main parts: oil injection, reaction (an annular gap fixed bed reactor covered by a three-zone furnace) and product collection (glass receiver) (see Figure 2.2).

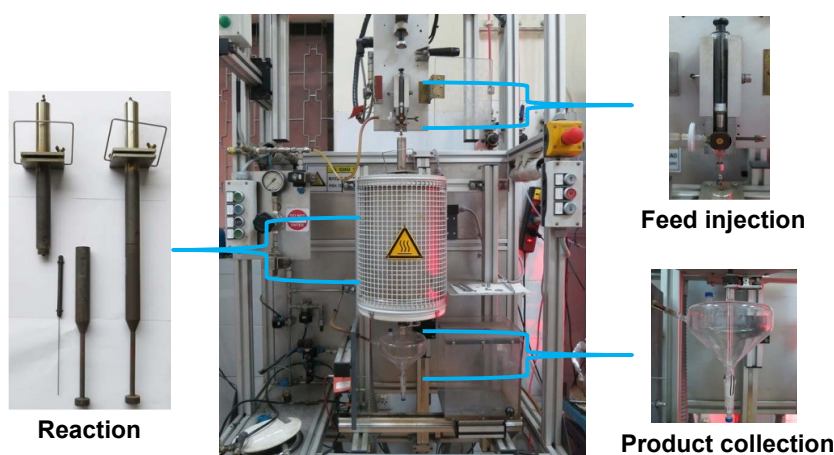


Figure 2.2. Experimental set-up of SR-SCT-MAT unit

Prior to a run, the equilibrated catalyst was calcined in air at $540\text{ }^{\circ}\text{C}$ over 3 h. The catalyst was diluted with glass beads before being fed into the reactor, and the CTO mass ratio was varied by keeping a constant feed and changing the catalyst weight. Before reaction, the catalyst was preheated at the reaction temperature for 1 h in a N_2 flow of 40 ml/min. Normally 1.75 g of oil (either the conventional feed or a mixture of UBO and the

conventional feed) were fed into a syringe in the oil injection part. The system automatically performed pressure drop measurement and leak check. After a successful leak check, the oil was injected by the syringe drive within 30 s for both oil and nitrogen. The oil injection (2 ml) always took 12 s, and afterwards 3 ml of N₂ were added within 18 s. After completion of injection, nitrogen was used to purge the system and the liquid and gas products were transferred into the receiver. At the end, the gas and liquid phases were taken from the receiver for GC analysis. The spent catalyst was separated from the glass beads and its coke content was determined using the CHN analyzer.

2.3.4.2 Product analysis and evaluation

The gas phase was analyzed in the GC as described in section 2.3.3.2. The gaseous products included CO₂, CO and gaseous hydrocarbons and is formally divided into dry gas (hydrogen, methane, ethane, and ethylene) and LPG (propane, propylene, butanes and butenes). The C₅+ gases were also quantified in this GC and this fraction was formally added to the gasoline fraction.

The liquid phase was analyzed by a GC-SIMDIS using an Agilent 7890 GC with electronic pressure control (EPC), configured with a FID (DB-1, 10 m × 530 μm × 2.65 μm). Temperature program: 40 °C to 350 °C at 20 K/min, held 5 min. The liquid products are classified into various fractions based on boiling ranges: gasoline (C₅ - 211 °C), LCO (221-360 °C), heavy cycle oil (HCO; > 360 °C).

The composition of gasoline fraction was analyzed using a GC-PIONA system (Agilent 7890A) equipped with Hydrocarbon Expert software from Separation System Inc. The GC configured with prefractionator inlet for gasoline separation and FID (SP-009, 100 m × 0.25 mm × 0.5 μm). This method helps to identify the hydrocarbons in the gasoline fraction group-wise roughly up to C₁₅ (n-paraffins, iso-paraffins, olefins, naphthenes and aromatics).

All calculation methods and software were provided by Grace Davison. The yield (Y) for products (gas, gasoline, LCO, HCO and coke) and the MAT conversion (X) based on weight (W) were calculated using the following equations. A balancing factor (f) was used as the mass balance was found not equal to 100%. Note that the recovery of coke is considered to be 100%. The mass balance was 96-101% of the injected feed in all runs.

$$f = \frac{W_{\text{feed}} - W_{\text{coke}}}{W_{\text{gas}} + W_{\text{liquid}}} \quad (\text{Eq. 2.13})$$

$$Y_{\text{Product } i} (\text{wt}\%) = \frac{W_{\text{product } i}}{W_{\text{feed}}} \times f \quad (\text{Eq. 2.14})$$

$$X = 100 - (Y_{\text{LCO}} + Y_{\text{HCO}}) \quad (\text{Eq. 2.15})$$

Chapter 3

Hydrodeoxygenation of Phenol as a Model

Compound for Bio-oil in a Batch Reactor

In this chapter, the performance of prepared catalysts in HDO of phenol as a probe model compound for bio-oil is addressed. The effect of second metal in bimetallic catalysts is illustrated based on various runs with phenol and intermediates and deep characterization of catalysts. Next, various reaction conditions and the influence of different supports are discussed.



PHENOL



3.1 Characterization of fresh and pre-reduced catalysts

3.1.1 Elemental analysis and N₂ physisorption

In this section, the HZSM-5 supported catalysts have been denominated as xNi, yCu, zCo and xNi_yCu or xNi_zCo, where x, y and z are the rounded contents (wt%) of nickel, copper and cobalt as measured by ICP-OES, respectively. Table 3.1 presents results from elemental analysis (metal content) and N₂ physisorption.

Table 3.1. N₂ physisorption results and metal content of the parent HZSM-5 and prepared catalysts

Catalysts	Metal loading (wt%)			N ₂ adsorbed volume at STP (cm ³ /g)	S _{BET} (m ² /g)
	Ni	Cu	Co		
Support (HZSM-5)				94.5	405
Monometallic catalysts					
4Ni	3.8	-	-	75.2	328
12Ni	12.3	-	-	73.4	315
21Ni	21.4	-	-	65.4	281
21Cu	-	20.9	-	64.7	278
19Co	-	-	18.7	63.2	271
Bimetallic catalysts					
17Ni ₂ Cu	16.7	2	-	63.0	269
16Ni ₄ Cu	15.8	4.3	-	65.3	280
11Ni ₁₀ Cu	10.9	9.5	-	63.3	271
4Ni ₁₄ Cu	4.1	14.3		63.1	270
16Ni ₂ Co	15.5	-	1.9	67.0	286
16Ni ₄ Co	16.2	-	3.6	63.7	274
10Ni ₁₀ Co	9.6	-	9.5	65.4	281
5Ni ₁₄ Co	4.5	-	13.7	63.5	272

Nitrogen physisorption studies revealed a steady decline in adsorption capacities with increasing metal loading, e.g. for the Ni-containing catalysts 4Ni, 12Ni and 21Ni. This is probably attributed to pore blocking by the increasing proportion of loaded metal species [113]. On the other hand, the adsorbed nitrogen quantity for mono- and bimetallic catalysts with ca. 20 wt% loading was more or less the same; that is, no differences in adsorption capacities were seen independent on the metal or metal combination used. The corresponding BET surface areas, which were also calculated based on the nitrogen adsorbed volume, reached 269-286 m²/g. Therefore, the differences in catalytic performances in all these latter samples must be related to other reasons than pore size effects because the micropore volume (more than 85% in these materials) is similar.

3.1.2 X-ray diffraction (XRD)

Figure 3.1 shows the XRD patterns of the pre-reduced monometallic catalysts. The existence of metallic Ni, Cu and Co was only observed in 21Ni, 21Cu and 19Co catalysts, respectively. The relative intensities of Cu and Ni reflections are similar. However, the intensities of Co reflections are much lower because Co atoms have a larger mass attenuation coefficient (used to describe how easily the sample can be penetrated by a beam of electromagnetic radiation) and thus the absorption of X-rays is higher.

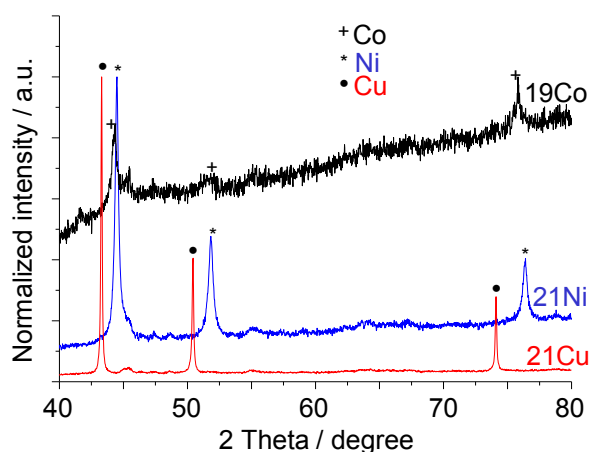


Figure 3.1. XRD patterns of monometallic reference catalysts.

Regarding the XRD patterns of the calcined and pre-reduced 11Ni10Cu and 4Ni14Cu bimetallic catalysts (Figure 3.2), the NiO and CuO phases were detected in the calcined catalysts, whereas the Ni-Cu alloy and metallic Cu were seen in both catalysts after reduction. Additionally the broad reflections in the range of 7-30° show the well-dispersed HZSM-5 structure.

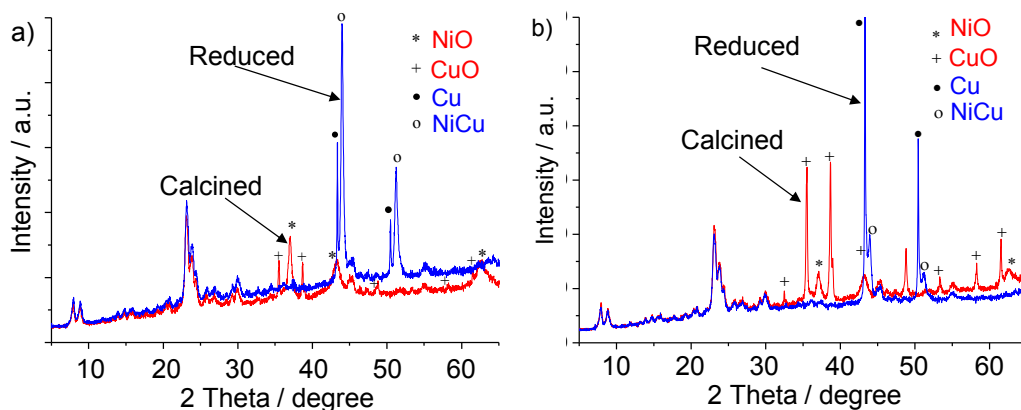


Figure 3.2. XRD patterns of the Ni-Cu/HZSM-5 bimetallic catalysts. a) 11Ni10Cu; b) 4Ni14Cu.

It should be noted that the formation of Ni-Cu alloy occurred during the reduction under H_2 flow at 600 °C. This result is in good agreement with data from Sinfelt [114] who suggested that Ni and Cu were completely miscible and form Ni-Cu alloy at high temperature (450 °C) during preparation process but Cu tends to segregate partly.

The XRD analysis of calcined 10Ni10Co and 5Ni14Co catalysts was also carried out (see Figure 3.3a). Obviously NiO, Co_3O_4 and/or $NiCo_2O_4$ spinel phases are found in the pattern of the calcined samples. In the case of the reduced Ni-Co/HZSM-5 catalysts, it was difficult to identify the state of metallic sites because the observed reflections were no exact matches with PDF data of metallic Ni or Co reflections. Nevertheless, the highly resolved XRD patterns in Figure 3.3b show that the largest reflections shifted from the right hand side (near metallic Ni reflection) to the left hand side (near metallic Co reflection) with increasing of the Co: Ni ratio. Thus, Ni and Co could coexist, alloys with a different composition of Ni and Co could be formed, and in the case of the Co-rich samples, Ni could be embedded in large Co domains as a result of the parent spinel phase in the calcined material. For instance, the discussed metal reflection for the reduced 10Ni10Co catalyst (green) was very broad, small and shifted toward the Co position. Moreover, the main reflections for samples 10Ni10Co and 5Ni14Co were smaller than the reflections for samples 21Ni, 16Ni2Co and 16Ni4Co, indicating a higher dispersion of metal particles in 10Ni10Co and 5Ni14Co samples than in other samples.

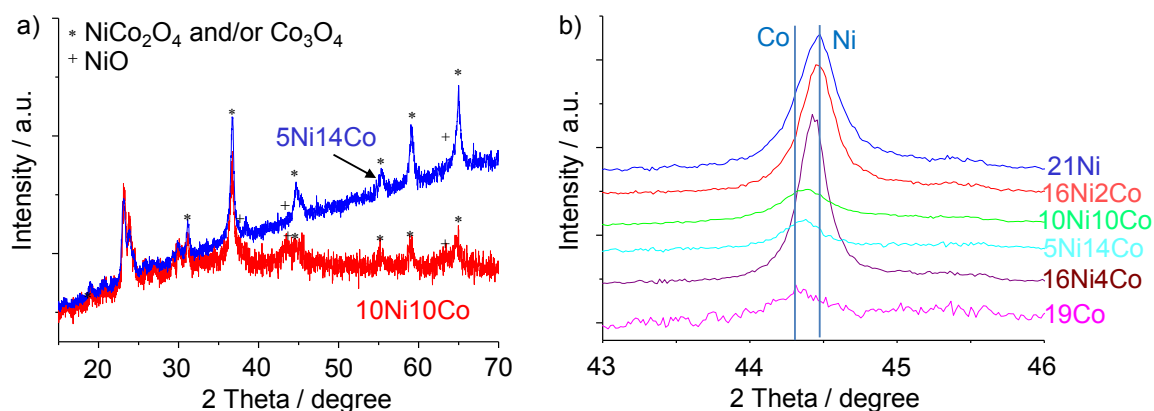


Figure 3.3. XRD patterns of the Ni-Co/HZSM-5 bimetallic catalysts. a) calcined catalysts; b) pre-reduced catalysts (high resolution).

3.1.3 Temperature programmed reduction (TPR)

In order to further understand the reducibility of the calcined precursors, TPR experiments were carried out. Figure 3.4a displays TPR profiles of monometallic (21Ni and 21Cu) and bimetallic precursors (16Ni4Cu, 11Ni10Cu, 4Ni14Cu). Obviously the broad reduction

profile of 21Ni sample consists of two peaks at low temperature (400 °C) and high temperature (550 °C), which can be explained via two possible effects as follows. First, nickel oxide could be reduced in two steps following equations 3.1 and 3.2, and this is supported e.g. by Hadjiivanov et al. [115, 116]. Second, different interaction strengths of Ni²⁺ species with HZSM-5 support because of their location outside or inside the zeolite framework may result in different reducibility [117]. Similar to the 21Ni sample, the TPR profile of the 21Cu sample also shows a low temperature (200-240 °C) and high temperature peak (280-330 °C), which can be explained similarly. However, both the peaks of the 21Cu sample were located at lower temperature compared to those of the 21Ni sample, which indicates that copper oxides are more easily reduced than nickel oxides on this support.

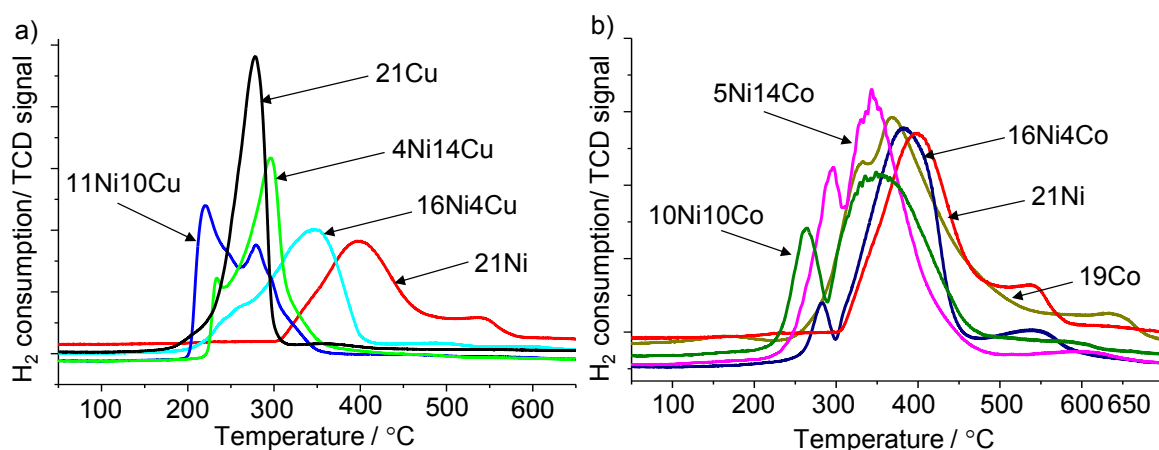


Figure 3.4. TPR profiles of precursors supported on HZSM-5. a) Ni, Cu and Ni-Cu; b) Ni, Co and Ni-Co.

In contrast, calcined supported Ni-Cu precursors could be reduced at a much lower temperature than the 21Ni sample (see Figure 3.4a). In absence of copper, nickel oxide was reduced step-wise at approximately 400 °C and 550 °C; however, it was mostly reduced at lower temperature (200-400 °C) with at least 3 peaks in the case of Ni-Cu precursors. This is likely to be due to synergistic interaction between the oxide phases and even physical mixing of NiO and CuO [118, 119]. In addition, the reduction profiles for Ni-Cu samples showed different intensities at high and low reduction temperature, which can be related to a different Ni: Cu ratio. Thus, it can be noted that the presence of Cu in the Ni-Cu bimetallic catalysts strongly promotes Ni reduction. The reduction temperature for the activation of Ni-Cu bimetallic catalysts was set to 600 °C.

Figure 3.4b represents TPR profiles of monometallic (21Ni and 19Co) samples and bimetallic Ni-Co/HZSM-5 precursor series. For 19Co catalyst, at least three peaks at low (300-450 °C) and high (650 °C) temperature were recorded. This result can be related to the intra-/extra framework species or the multiple oxidation states of Co and are in good agreement with reports from Wang et al. [120] and M. Zhao et al. [121]; the latter group detected CoO on Co/SBA-15 catalyst after reduction at 600 °C in H₂ flow. In comparison, the effect of Co addition to Ni on reducibility was not as strong as that of Cu in Ni-Cu bimetallic precursors. Although the reduction profile was still broad, complicated and consisted of at least three peaks, the maximum temperature was only slightly decreased compared to the 21Ni and the 19Co samples. Interestingly, a new peak at low temperature (250-300 °C) was observed in the Ni-Co bimetallic samples. This peak could be due to the reduction of the NiCo₂O₄ spinel, which was present in the calcined precursors, as confirmed by XRD analysis (Figure 3.3a). This peak is mainly visible in samples with a higher Co content (e.g., 10Ni10Co, 5Ni14Co), matching the stoichiometric requirements. This result is in good agreement with previous reports [122-124], which suggested that NiCo₂O₄ spinel was more easily reduced as compared with Co₃O₄, NiO and CoO. Based on these TPR results, the reduction temperature for catalyst activation of Ni-Co bimetallic catalysts was set to 650 °C.

In addition, the hydrogen consumption during TPR and the theoretical value were calculated and summarized in Table 3.2.

Table 3.2. Quantitative TPR results for selected precursors supported on HZSM-5.

Precursors	Metal contents (mmol/g)			H ₂ consumption (mmol/g)		H ₂ consumption (experimental/theory)
	Ni	Cu	Co	Theoretical ^[a]	experimental	(%)
21Ni	3.64	-	-	3.64	3.02	82
16Ni4Cu	2.68	0.68	-	3.36	3.11	93
11Ni10Cu	1.85	1.51	-	3.36	3.08	92
4Ni14Cu	0.70	2.25	-	2.96	3.00	101
21Cu	-	3.30	-	3.29	3.16	96
16Ni4Co	2.76	-	0.61	3.57	3.44	96
10Ni10Co	1.64	-	1.61	3.78	3.56	94
5Ni14Co	0.77	-	2.32	3.87	3.74	97
19Co	-	-	3.17	4.23	3.67	87

^[a] these theoretical values were calculated based on total reduction of NiO → Ni, CuO → Cu and Co₃O₄ → Co

Obviously the total amount of H₂ consumed during TPR of 21Ni and 19Co was clearly lower than the theoretical value (82% and 87%, respectively), whereas that of 21Cu was close to the theoretical value. This result indicates that nickel oxide and cobalt oxide are more difficult to reduce completely than copper oxide, which in turn explains the beneficial effect of Cu on Ni reducibility. On the other side, bimetallic precursors (Ni-Cu and Ni-Co) also showed H₂ uptake values similar to theoretical ones, suggesting that the addition of Cu and Co promotes the Ni oxide reduction, probably owing to the formation of a spinel phase in the latter case.

In these TPR studies, complicated and broad peaks were observed in the reduction profiles of monometallic and bimetallic catalysts owing to several reasons (e.g. the multiple oxidation states of the metals, different interaction between metals and support HZSM-5, metal positions in the lattice (extra- vs. intra-framework), as well as the formation of new structures like NiCo₂O₄ spinel. More importantly, the addition of Cu or Co promotes reduction of nickel oxide, leading to a shift of reduction peaks to lower temperature, and the effect of Cu is significantly stronger than that of Co. As a result, the reduction step and reaction can be performed at lower temperature.

3.1.4 X-ray photoelectron spectroscopy (XPS)

To get closer insight in surface properties, the elemental compositions in the near surface region of both calcined and reduced precursors (21Ni, 16Ni4Cu, 11Ni10Cu, 10Ni10Co, 5Ni14Co) as measured in XPS experiments are listed in Table 3.3.

Table 3.3. Change in elemental surface composition of the selected catalysts.

Samples		Ni: Si ratio	Cu(Co): Si ratio
21Ni	calcined	0.24	-
	reduced	0.11	-
16Ni4Cu	calcined	0.14	0.04
	reduced	0.04	0.03
11Ni10Cu	calcined	0.13	0.03
	reduced	0.02	0.06
10Ni10Co	calcined	0.06	0.04
	reduced	0.04	0.06
5Ni14Co	calcined	0.05	0.19
	reduced	0.07	0.19

It was observed that the surface Ni: Si ratio of reduced 21Ni precursor accounts for 46% of the initial Ni: Si ratio of the calcined 21Ni sample. This might be due to migration of

Ni into the pores (bulk) during reduction. The addition of either Cu or Co to Ni/HZSM-5 to form the bimetallic catalyst showed different effect on fraction of active Ni sites in the near surface region. In the case of Ni-Cu/HZSM-5 catalysts, the surface Ni: Si ratio substantially decreased to 29% and 15% for 16Ni4Cu and 11Ni10Cu samples, respectively, after reduction in comparison with that of 21Ni catalyst (46%), suggesting that adding of Cu does not stabilize Ni active sites at the surface. On the other side, the surface Cu: Si ratio was only slightly reduced for 16Ni4Cu after reduction, but significantly increased for 11Ni10Cu, leading to a Cu enrichment in the near surface region, which is in agreement with a report of Qiwu et al. [125].

In contrast, the Ni content in the near surface region is much more stable in presence of Co during the reduction. In general, a lower Ni: Si ratio was observed for the calcined Ni-Co samples than for the corresponding Ni-Cu samples, but after reduction this content remained stable. For 5Ni14Co sample, even with the lowest amount of Ni (Table 3.3), an increase of the surface amount of Ni was observed, whereas the surface Co: Si ratio was more or less the same for both Ni-Co samples. Thus, it is evident that the addition of Co to Ni/HZSM-5 strongly stabilizes the Ni sites at the surface, whereas the addition of Cu shows the reverse effect.

As a confirmation, a peak shift was observed in the XPS spectrum in the case of Ni2p for the Ni-Co series as compared to Ni catalysts (see Figure A2 in Appendix A), indicating the influence of Co admixture into Ni based catalyst.

3.1.5 Infrared spectroscopy of adsorbed pyridine (Py-IR)

To investigate the acid properties of selected reduced samples, the IR spectra of adsorbed pyridine were used and the results are shown in Figure 3.5 and Table 3.4. The bands at 1544 cm^{-1} and 1451 cm^{-1} are assigned to Brønsted and Lewis acid sites, respectively. Table 3.4 lists the total acidity of these HZSM-5 supported catalysts.

Table 3.4. Acidity data for the support and selected monometallic and bimetallic catalysts.

Samples	Acidity ($\mu\text{mol/g}$)		
	BAS	LAS	Total
HZSM-5	451	168	619
21Ni	243	345	588
10Ni10Co	162	509	672
5Ni14Co	166	527	693
19Co	165	460	624
BAS: Brønsted acid sites; LAS: Lewis acid sites			

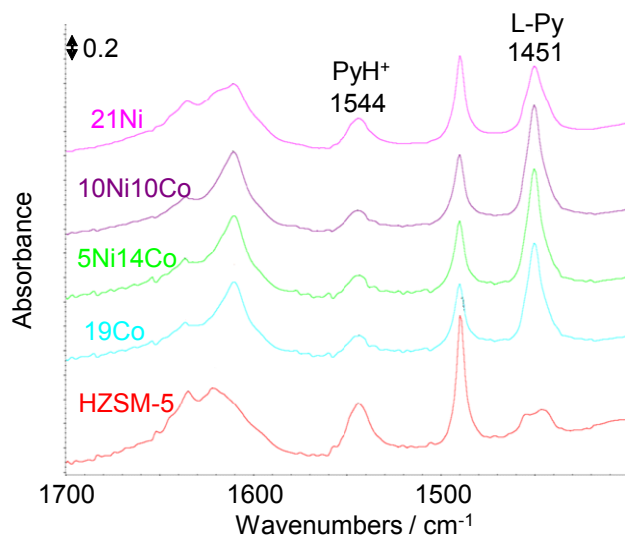


Figure 3.5. Py-IR spectra of adsorbed pyridine at 150 °C for HZSM-5 support and selected monometallic and bimetallic catalysts.

A significant decrease in overall Brønsted acidity of supported catalysts was observed compared to neat HZSM-5. This finding is consistent with previous suggestion [117] that metal species (e.g. Ni^{2+}) act as exchangeable cations and replace the H^+ from Brønsted sites. Conversely, overall Lewis acidity increases and significantly surpasses the remaining Brønsted acidity. As a result, the total acidity (pyridine amount) remains the same (588-693 $\mu\text{mol/g}$). Although the formation of the Lewis acid sites is not fully understood, this kind of acidity could be generated via dehydration of protonated oxide bridges after high temperature treatment in the calcination or reduction steps [126].

In general it has to be considered that all the catalysts derived from such precursors offer metal sites after reduction as well as a combination of Brønsted and predominant Lewis acid sites. Such combination is preferable for HDO reaction, as acid sites may cleave C-O bonds via protonation, and metal sites are able to activate hydrogen and to reduce aromatic rings.

3.1.6 Transmission electron microscopy (TEM)

In order to get more insight into morphology, particle size, elemental composition and dispersion of metallic species on support, the reduced 21Ni, 19Co and 10Ni10Co samples were selected for TEM analysis. In general, a broad distribution of particle size and very different shapes were observed on the three selected samples (Figure 3.6). In the 21Ni catalyst (Figure 3.6a), the particles from 20-30 nm represented the largest fraction while small particles with diameter less than 2 nm were detected by CS-corrected HAADF imaging. In addition, few bigger particles up to 80 nm were also seen.

In the case of the ^{19}Co catalyst, most of particles were found in the size range of 8-10 nm (Figure 3.6c). These particles were accompanied by a netlike structure consisting of particles less than 3 nm in diameter and some large particles. In the case of $^{10}\text{Ni}^{10}\text{Co}$ catalyst, mostly small (3-5 nm) and medium (10-20 nm) size particles were observed (Figure 3.6b). The 1:1 mixture of Ni and Co (Figure 3.6b) forms particle sizes in between the boundaries set by the pure Ni and Co systems.

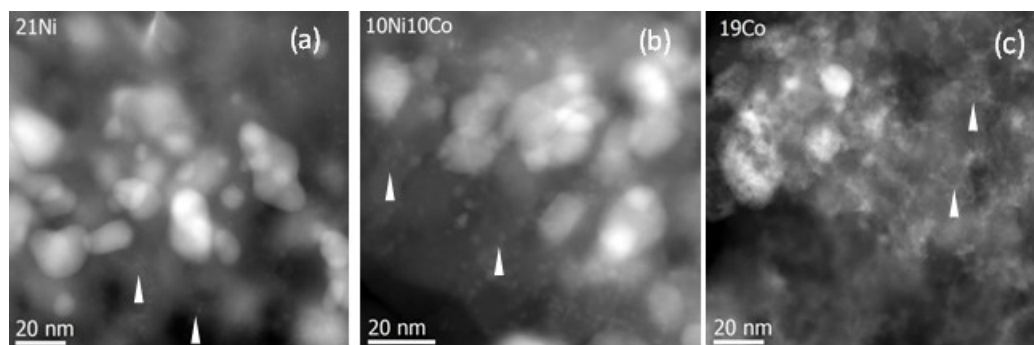


Figure 3.6. STEM-HAADF images of pre-reduced catalysts. a) ^{21}Ni ; b) $^{10}\text{Ni}^{10}\text{Co}$ and c) ^{19}Co ; The arrows indicate small particles with weak contrast.

Since Ni and Co are neighbors in the periodic table, neither difference in contrast in the HAADF images nor differences in the lattices at high resolution are expected. For that reason, EDXS mapping of all three samples was made in order to find out the elemental composition, especially in the case of $^{10}\text{Ni}^{10}\text{Co}$ (see Figure 3.7). During mapping, the samples were scanned by an electron beam of approximately 0.17 nm for 100-150 sweeps and additionally every minute an image was taken for drift control. Notably, the support material decomposed during EDXS measurement. Most zeolites tend to suffer damage by the strong and fast beam, in some cases at 200 kV within minutes.

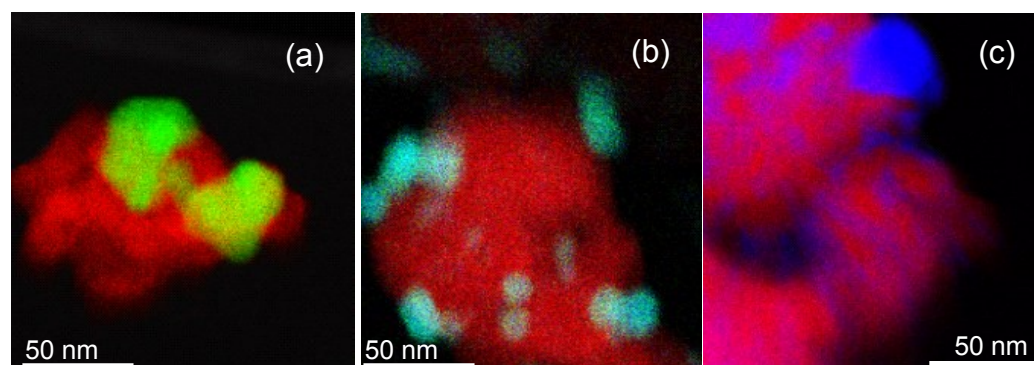


Figure 3.7. EDX mappings of pre-reduced catalysts. a) ^{21}Ni ; b) $^{10}\text{Ni}^{10}\text{Co}$ and c) ^{19}Co . Red: Si; Green: Ni; Blue: Co.

Figure 3.8 shows obtained images before and after EDXS mapping. Obviously the support HZSM-5 collapsed due to the loss of long range order (crystallinity) by the electron bombardment; however, the metallic particles remained in the same position. In fact, they seem to recrystallize under the measurement conditions because an increase of the size of the smallest particles and a change in contrast for the bigger ones were detectable. Possibly the loss of focus of the smallest particles was observed and the contours of the large particles were blurred due to the collapsed support.

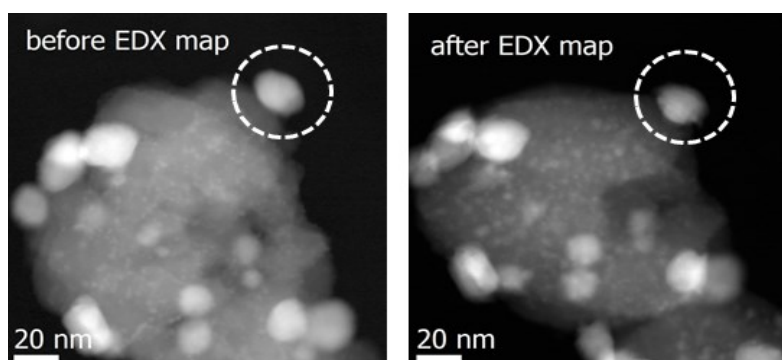


Figure 3.8. STEM-HAADF images of the same region before and after EDXS Mapping of pre-reduced 10Ni10Co catalyst. The same positions were marked by circles for significant positions in both images.

More importantly, the EDXS mapping gave information on the distribution of the different elements as shown in Figure 3.7. Different particle sizes and netlike structures are clearly visible in this figure. The color mix of metallic particles in Figure 3.7b showed that a homogeneous Ni-Co alloy with a characteristic ratio was found. These EDXS measurements showed that the Ni: Co ratio was independent from particle size as well as from position inside one metal particle, with the atomic ratio of Ni: Co being in the range of 41: 59 – 59: 41 (see Figure A3 in Appendix A).

In sum, a fairly homogeneous Ni-Co alloy was formed in 10Ni10Co catalyst at the given preparation conditions and its composition was independent on particle size. Moreover, the formation of Ni-Co alloy led to a reduced metal particle size on this material. As a result, the formation of Ni-Co alloy strongly enhances the dispersion in comparison with 21Ni catalyst.

3.2 Effect of second metal on catalytic performance of bimetallic catalysts

3.2.1 Feedstock and products analysis

In this study, phenol (99.9%, Merck) was used as a model compound for bio-oil. From the literature, it was found that phenol HDO leads to the hydrogenation products

(cyclohexanol, cyclohexanone) and various hydrocarbons (cyclohexane, cyclohexene, benzene, methylcyclopentane (MCP), bicyclohexane, ...) depending on catalyst and reaction conditions used [27, 36, 38, 127, 128]. On the other side, water was used as a solvent in this study due to several general reasons. First, the bio-oil from FP process already possessed large amount of water (15-30 wt%). Second, water is a by-product in HDO reaction. Last but not least, water seems to be “green”, environmentally suitable as well as easy and safe to handle.

It should be mentioned that some of the named products (e.g. hydrocarbons) are rarely soluble in water, indicating that the product mixture after reaction is not homogeneous causing some problems for analysis. This was validated with a synthetic model mixture of all relevant reactants. As a result, one extraction step was used after reaction to separate aqueous phase and organic phase (or mostly hydrocarbon phase). After trying several solvents (e.g. ethyl acetate, toluene, DCM, dodecane) with the product model mixture and using an existing GC in our lab, toluene was found to be a suitable solvent.

To identify the products from the real reaction with the prepared catalysts, several experiments were performed. Then, an extraction step was carried out to separate the organic and aqueous phases using toluene. The resulting phases were injected to GC and GC-MS for components identification. In addition, ethyl acetate was used to extract the organic phase to confirm that toluene was not formed at the selected reaction conditions. For quantification, mesitylene and 1,4 dioxane were used as the internal standards for organic phase (toluene phase) and aqueous phase, respectively. The typical chromatograms of the two phases are shown in Figure A4 in Appendix A.

Regarding the gas phase, a syringe was used to collect the sample and to inject it into a GC-MS. The identified compounds were mostly unreacted H₂ and very small concentrations of cyclohexane, benzene and cyclohexene. CO and CO₂ were not found in this reaction.

3.2.2 Catalyst performance in HDO of phenol and intermediates

In this section, the performance of two series of bimetallic catalysts (Ni-Cu/HZSM-5, Ni-Co/HZSM-5) and the corresponding monometallic catalysts is first illustrated. Figure 3.9 shows the results for bimetallic Ni-Cu/HZSM-5 with different Ni and Cu load and monometallic catalysts (Ni/HZSM-5 and Cu/HZSM-5) as well as for the pure support (HZSM-5). The test with the neat support showed that the conversion of phenol was less than 10% after 2 h reaction time at 250 °C. The supported monometallic catalysts 4Ni, 12Ni and 21Ni presented higher phenol conversions of 14%, 82% and 98%, respectively. With the last catalyst, selectivity reached 98% toward deoxygenated products, including

approximately 88% for cyclohexane and 8% for benzene. In contrast, the 21Cu catalyst exhibited extremely less activity, reaching 2% phenol conversion, and thus pure copper metal sites are likely to be inactive for this reaction.

The test with Ni-Cu/HZSM-5 with different Ni and Cu load showed that with the substitution of only 2 wt% of Ni (related to catalyst weight) for Cu (17Ni2Cu), the conversion strongly decreased from 98% to nearly 50%. In addition, the conversion steadily decreased with further substitution of Ni with Cu. It is explained by the exchange of Ni with Cu (an inactive site) resulting in a decrease in Ni amount (an active site) on the surface of the bimetallic Ni-Cu/HZSM-5 catalyst, and thereby leading to a reduction in activity. As shown above, the addition of Cu to Ni/HZSM-5 significantly reduced the number of Ni active sites at the surface as observed in XPS results (Table 3.3).

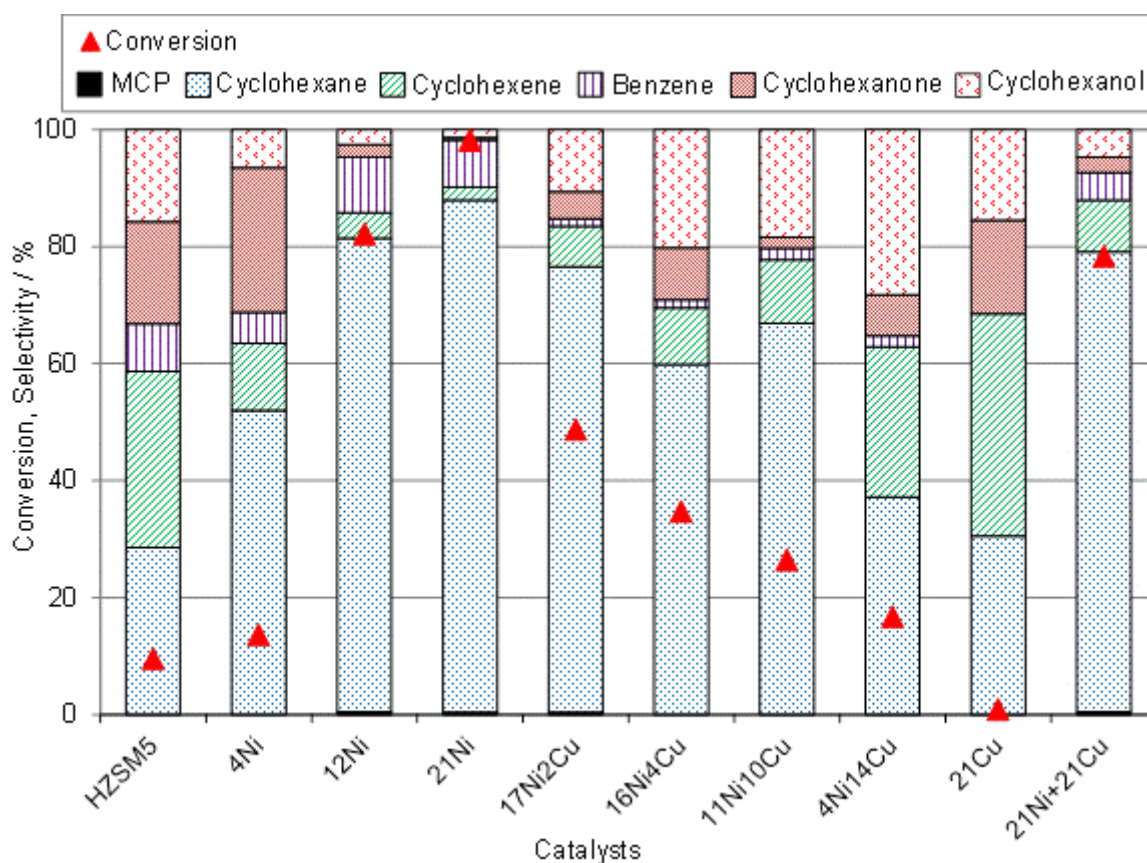


Figure 3.9. Phenol HDO on the parent HZSM-5 support, various monometallic and Ni-Cu/HZSM-5 samples. Reaction conditions: 5.3 mmol of phenol, 10 g of H₂O, 25 mg of catalyst, T = 250 °C, P = 50 bar at RT, t = 2 h.

These results suggest that 21Ni catalyst is highly active in the HDO of phenol, whereas 21Cu is greatly inactive. The combination of metal and acid sites is needed to efficiently eliminate oxygen from phenol. Tuning of the metal sites may provide additional control of

the hydrogenation severity (either attacking substituents or aromatic ring systems) and selectivity. Therefore, the substitution of Ni for Cu strongly affects both catalytic activity and selectivity. Such an effect is reported, e.g., by Sinfelt et al [129]. In their study, the activity of Ni-Cu alloys with different Ni: Cu ratio decreases substantially for ethane hydrogenolysis to methane, whereas the effect is very little for the cyclohexane dehydrogenation with the same catalysts. In the present study, the formation of Ni-Cu alloy was observed in both 11Ni10Cu and 4Ni14Cu catalysts together with metallic Cu (Figure 3.2), thus it might promote alternative reactions of phenol or intermediate products.

To clarify the effect of an admixture of Cu to Ni/HZSM-5 on catalytic performance, one catalyst was prepared by physical mixing of two reduced monometallic catalysts (21Ni and 21Cu) at a weight ratio of 1: 1 (denoted as 21Ni+21Cu), which was also tested at the same reaction conditions. The overall weight fractions of Ni, Cu metal and HZSM-5 of the 21Ni+21Cu were similar to those of 11Ni10Cu catalyst. However, as proven by the above characterization (section 3.1.2), the Ni-Cu alloy was present in 11Ni10Cu catalyst, but not in 21Ni+21Cu catalyst. Surprisingly, the conversion and selectivity toward deoxygenated products with the 21Ni+21Cu catalyst were much higher than those obtained with the 11Ni10Cu catalyst and were comparable to those obtained with 12Ni catalyst (Figure 3.9). It is explained that the presence of a significant amount of pure Ni metal particles on the surface of 21Ni+21Cu is sufficient to introduce high activity in such a catalyst. Cu species themselves proved to be inactive (see above) and cannot really interact with Ni particles. On the other side, as soon as Cu is alloyed to Ni and causes the above described changes in the surface region, activity is reduced.

Regarding the products distribution, the selectivity toward deoxygenated products of bimetallic Ni-Cu/HZSM-5 catalysts was lower than that with the monometallic Ni catalysts. In addition, the benzene selectivity was also lower with bimetallic Ni-Cu/HZSM-5 catalysts, which could be due to the fact that the separate Cu metal sites may be involved in consecutive reaction steps after phenol has been activated by Ni sites first. In addition, there could be also be an effect of formed Ni-Cu alloy, which is known to be active for aromatic hydrogenation [102]. Furthermore, the significant amount of Cu at the surface possibly influences the amount and performance of active Ni sites. For example, Ene et al. reported that the high strength of interaction of Cu with benzene and phenol was observed by using fourier transform infrared spectroscopy and electron paramagnetic resonance spectroscopy [130]. Anyhow, these results reveal that the admixture of Cu to bimetallic Ni-Cu/HZSM-5 catalysts significantly lowers the conversion and selectivity

toward hydrocarbons in phenol HDO, which can be considered as a negative synergistic effect.

The second series of Ni-Co/HZSM-5 bimetallic catalysts with different Ni and Co load as well as the monometallic catalyst Co/HZSM-5 were tested in phenol HDO at the same reaction conditions. Figure 3.10 shows results with respect to phenol conversion and product distribution.

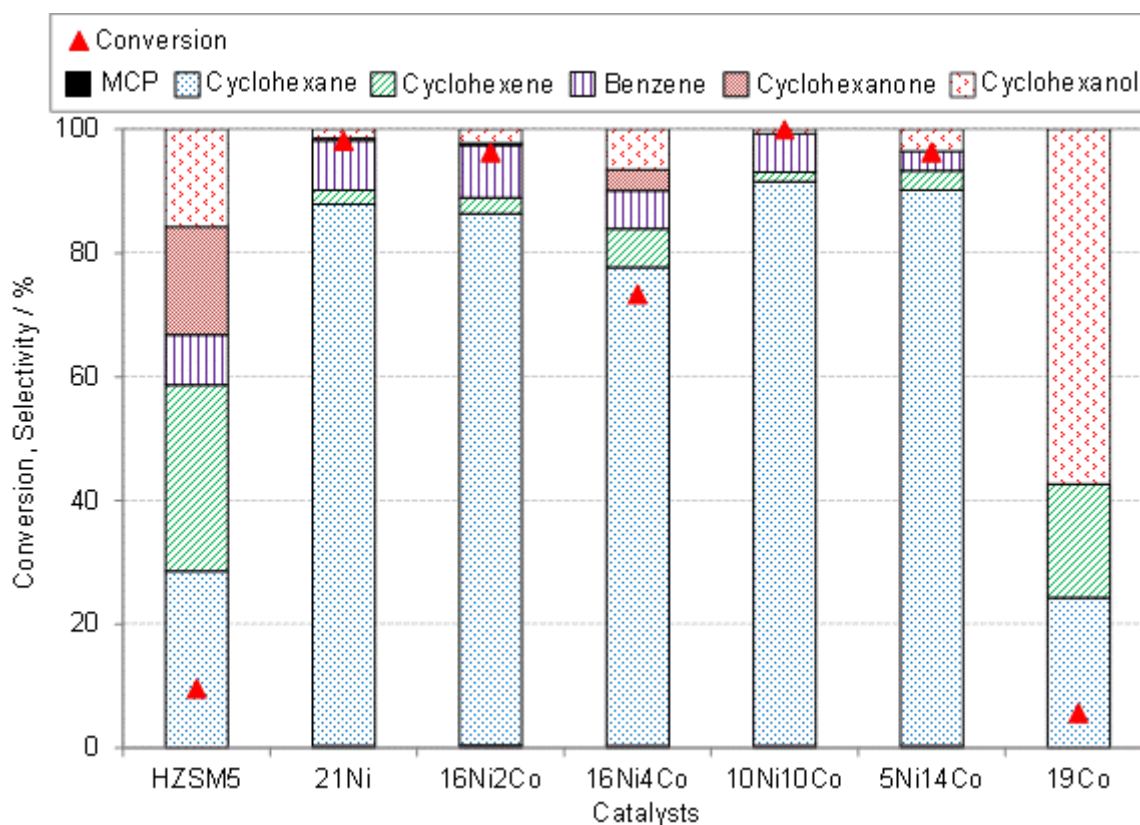


Figure 3.10. Phenol HDO on the parent HZSM-5 support, monometallic catalysts and Ni-Co bimetallic catalysts. Reaction conditions: 5.3 mmol of phenol, 10 g of H₂O, 25 mg of catalyst, T = 250 °C, P = 50 bar at RT, t = 2 h.

The 19Co catalyst showed poor activity for this reaction as conversion was less than 10%. Surprisingly, with the substitution of 5 wt% of Co (related to catalyst weight) for Ni (5Ni14Co), the conversion increased substantially to 96% and selectivity toward deoxygenated products reached approximately 96%. Conversion and HDO selectivity obtained with 5Ni14Co sample are much higher than those obtained with 4Ni and 12Ni samples (whereas adding of Cu to catalysts with a similar Ni content led to a strong activity decrease), which could be attributed to the higher number of active sites at the surface of 5Ni14Co, as observed in XPS result (see Table 3.3). Furthermore, for the catalyst with a Ni: Co ratio close to unity (10Ni10Co), the conversion was complete and

the selectivity toward deoxygenated products achieved the highest value observed (99.3%). These results are probably due to the formation of a NiCo_2O_4 spinel phase in the catalyst precursors, which leads to a higher dispersion of metal species in the case of 5Ni14Co and 10Ni10Co than in the samples containing less Co. As a proof, the addition of small amount of Co to Ni (16Ni2Co) reveals results similar to those obtained with the 21Ni sample. The addition of larger amounts of Co (16Ni4Co) but not in a ratio promoting a spinel formation further lowers the activity, because the formation of a spinel phase does not occur at all or not to a sufficient extent, as indicated in TPR result (see Figure 3.4b).

On the other side, little differences are observed in the product distribution, and 10Ni10Co showed the best selectivity toward hydrocarbons. In comparison with the 21Ni catalyst, the 10Ni10Co catalyst performed better with regard to cyclohexane selectivity. Notably, the Ni-Co catalysts clearly outperformed the Ni-Cu catalysts in terms of activity and deoxygenation selectivity.

Assuming that phenol hydrogenation is the rate-determining step in the HDO process [38], the above discussed effects of Co replacement for Ni in solid state properties as determined by TPR, XRD, XPS and TEM could explain the observed catalyst performances. The 21Ni sample is highly active due to highest Ni content among all catalysts. By adding Cu or Co, the Ni amount decreases; however, Co is more effective in forming highly dispersed alloys with Ni. Although the total amount of highly active Ni metal is lowered, this is compensated by a gain in dispersion. By generation of small metallic Ni particles in an alloy, the activation and insertion of H_2 into phenol could be significantly accelerated. Moreover, the formation of Ni-Co alloy with appropriate Ni: Co ratio also contributes to an improved catalyst performance.

On the other side, selectivity could be controlled by the adsorption mode of phenol on the surface. If adsorption would occur via the hydroxyl group on Brønsted sites, the weakening of the O-C bond would make it more susceptible for hydrogen attack, e.g. from hydrogen that was dissociated on surface metal sites before, leading to benzene formation. If the adsorption would occur via the aromatic ring, possibly on Lewis sites, the reduction towards cyclohexanol would be the first step, leading to another pathway via cyclohexene.

To further understand the effect of metallic Ni or Ni-Co alloy sites on catalytic performance, pure Ni and two Ni-Co alloys with different Ni: Co ratios (50:50 and 25:75) were prepared without support and tested in phenol HDO. Accordingly, these bulk materials should be considered as non-acidic. The catalytic activities of pure Ni and Ni-Co alloy (50:50) were comparable and slightly higher than that of Ni-Co alloy (25:75) (Figure 3.11). The results therefore indicate that the Ni-Co alloy itself has capability for catalyzing

the phenol hydrogenation to cyclohexanone/cyclohexanol comparable to the pure Ni. Furthermore, only cyclohexanone and cyclohexanol were obtained in the product mixture, which confirmed that the phenol HDO requires both metal and acid sites to take place. The latter were not provided by these three catalysts and therefore the reaction stopped at the ketone-alcohol stage. The impact of both the sites on the product distribution can be seen in the work of Hong et al. [28], who used Pt doped on different acidic supports under typical conditions (250 °C, 40 bar H₂ at RT). In contrast, Ohta et al. [86] reported on HDO of 4-propylphenol over a highly active acid-free Pt/active carbon catalyst at higher temperature (280 °C). As expected, hydrogenation is catalyzed by Pt; however, the subsequent dehydration of the formed cyclohexanol also occurs. The authors claim an in-situ generation of protons in hot compressed water ($pK_w = 11.2$ at 280 °C), which catalyze the dehydration step.

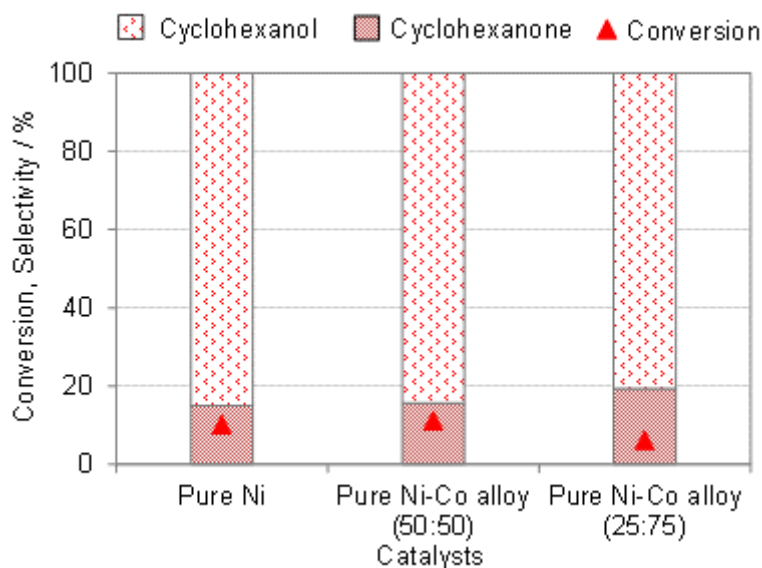


Figure 3.11. Phenol HDO on bulk Ni and Ni-Co alloy. Reaction conditions: 5.3 mmol of phenol, 10 g of H₂O, 25 mg of catalyst, T = 250 °C, P = 50 bar at RT, t = 2 h.

To gain more insight into the effect of the catalysts on the individual reaction steps, intermediate products cyclohexanol, cyclohexanone, cyclohexene and benzene were tested under the same reaction conditions as used in phenol HDO. Figure 3.12a shows the results of cyclohexanol HDO on 21Ni, 10Ni10Co and 19Co catalysts. Conversion on the two Ni containing catalysts was almost complete, whereas 19Co was less active than 21Ni and 10Ni10Co. This result correlates well with the overall acidities of these materials (Table 3.4), being the properties that mostly govern the catalytic activity. In this context, all three catalysts led to very high deoxygenation selectivities via dehydration owing to the

high acidities provided by the support. The product distribution also reveals that the elimination of oxygen attached to saturated rings is easier than that from phenol (compare Figure 3.10). Nevertheless, the severity of hydrogenation toward cyclohexane on these catalysts was significantly different and revealed the hydrogenation activity of the metal sites. In the case of 19Co, cyclohexene accounted for 35% in the product mixture, whereas it was converted almost completely to cyclohexane on both 21Ni and 10Ni10Co catalysts.

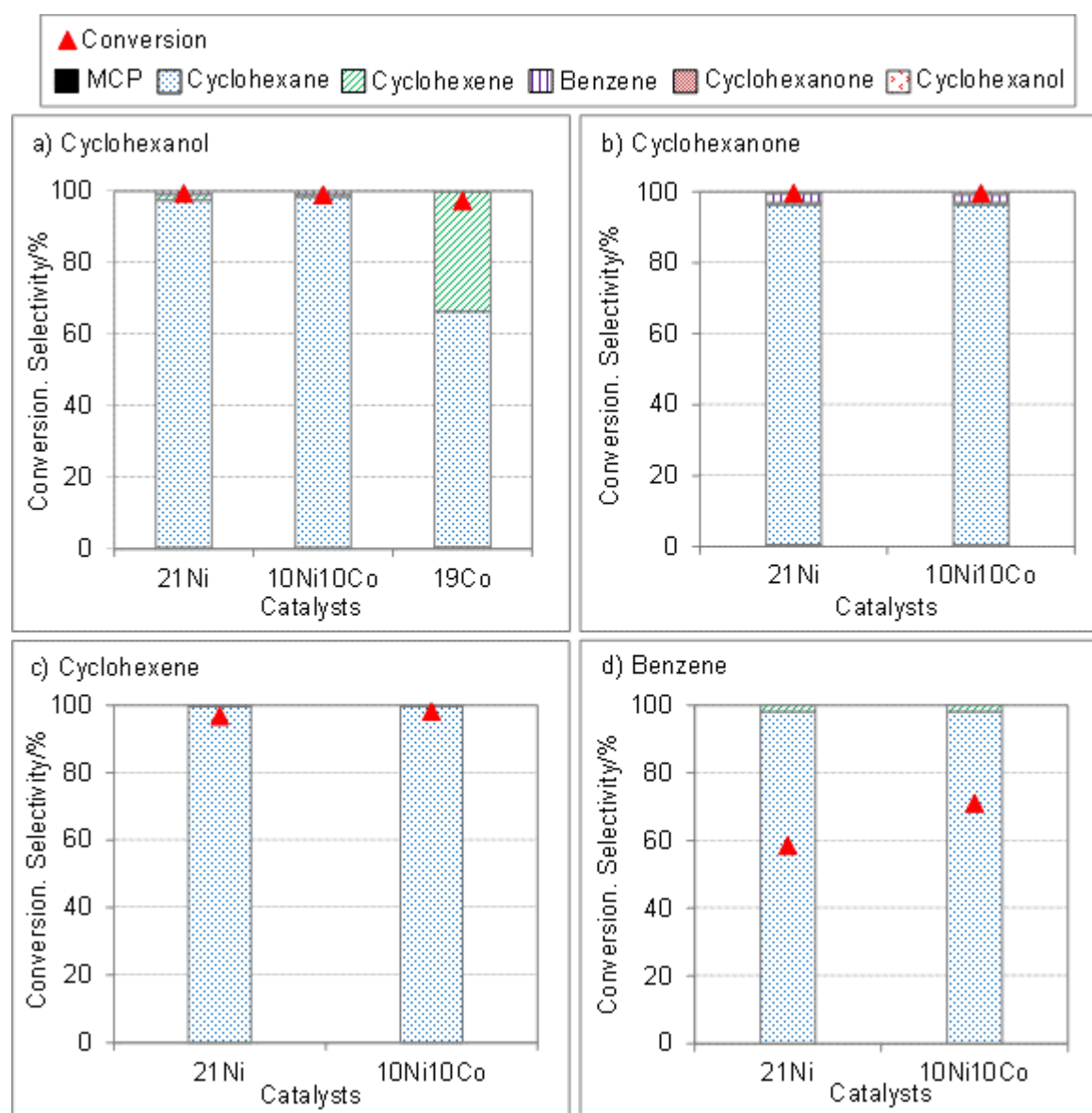


Figure 3.12. HDO of selected intermediate products. Reaction conditions: 5.3 mmol of phenol, 10 g of H₂O, 25 mg of catalyst, T = 250 °C, P = 50 bar at RT, t = 2 h.

In the following experiments, conversion of other intermediates was studied only on 21Ni and 10Ni10Co catalysts. In the case of cyclohexanone feed (Figure 3.12b), both

catalysts showed very similar performance with regard to conversion and selectivities. Among hydrogenation products, cyclohexane was predominant with more than 90% selectivity, together with cyclohexanol and MCP. The latter product points at the effect of the available Brønsted sites, which guides to the isomerization of the carbon skeleton, which most likely occurs only at high cyclohexane concentration (consecutive reaction). The conversion of cyclohexanone (requiring hydrogenation to cyclohexanol and hydrogenolysis) is most likely ruled by the metal sites which activate hydrogen as a first step.

Cyclohexene was almost completely converted with the Ni containing catalysts (conversion > 95%) to cyclohexane with more than 99% selectivity and very small amount of benzene was detected due to dehydrogenation of cyclohexene (Figure 3.12c). This is not surprising because it is known that Ni can act as hydrogenation and dehydrogenation catalyst and the extent is controlled by equilibrium.

Regarding the benzene conversion under HDO conditions, 10Ni10Co catalyst showed higher activity than the 21Ni catalyst (Figure 3.12d). These results help to understand why the selectivity for cyclohexane in phenol HDO with 10Ni10Co catalyst was higher than with 21Ni catalyst (Figure 3.10). The bimetallic catalyst is more powerful and able to attack the benzene ring and thus promotes the final steps toward cyclohexane at higher reaction rate. This catalyst seems to provide an excellent balance of acid and metal sites.

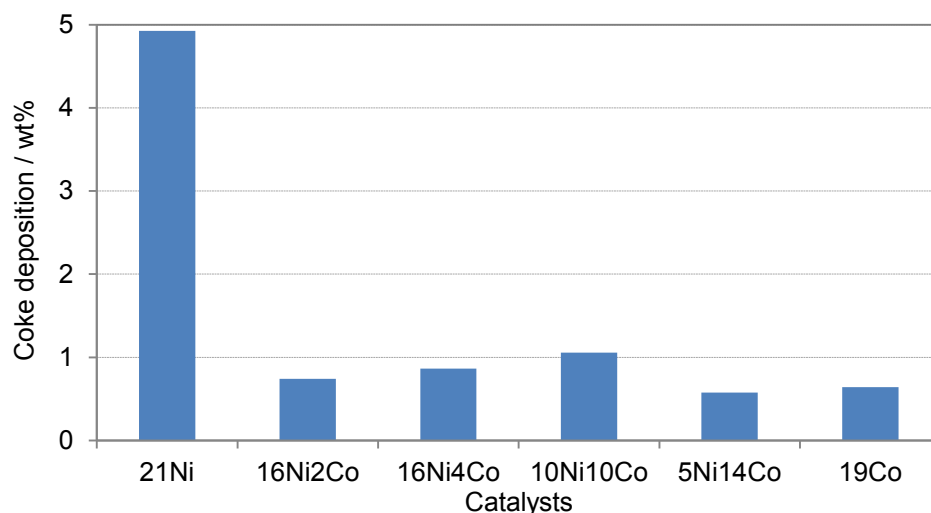


Figure 3.13. Coke deposition after phenol HDO reaction.

In order to evaluate coke formation on the catalysts, the carbon content of the used catalysts after 2 h reaction time was measured with CHN analyzer. As shown in Figure 3.13, monometallic 21Ni catalyst showed much more coke formation in comparison to any

other catalyst in this series. The formation of alloy reduces the particle size, which possibly also helps to lower the rate of coke deposition [131, 132]. In addition, stabilization of Ni active sites by the presence of Co could affect the coke formation. Last but not least, the considerably lower Brønsted acidity of Co-containing catalysts (see Table 3.4) may also suppress the coke formation [133].

Based on the above results, it can be concluded that the substitution of Co into Ni based catalyst not only improves the catalytic performance but also reduces coke formation. However, the addition of Cu shows the reverse trend. As a result, the Ni-Co bimetallic and monometallic Ni catalysts are further investigated in next sections.

3.3 More insight into effect of reaction conditions

It is known that reaction time is one of the most important parameters in batch reactor operation, in particular when studying consecutive reactions. Hence, the impact of reaction time was investigated for mono- and bimetallic catalysts (Figure 3.14). The real-time sampling during aqueous phase HDO in the autoclave is very difficult due to biphasic reaction mixture and small reaction volume, thus those data were collected after separate runs with different reaction time, pressure and temperature.

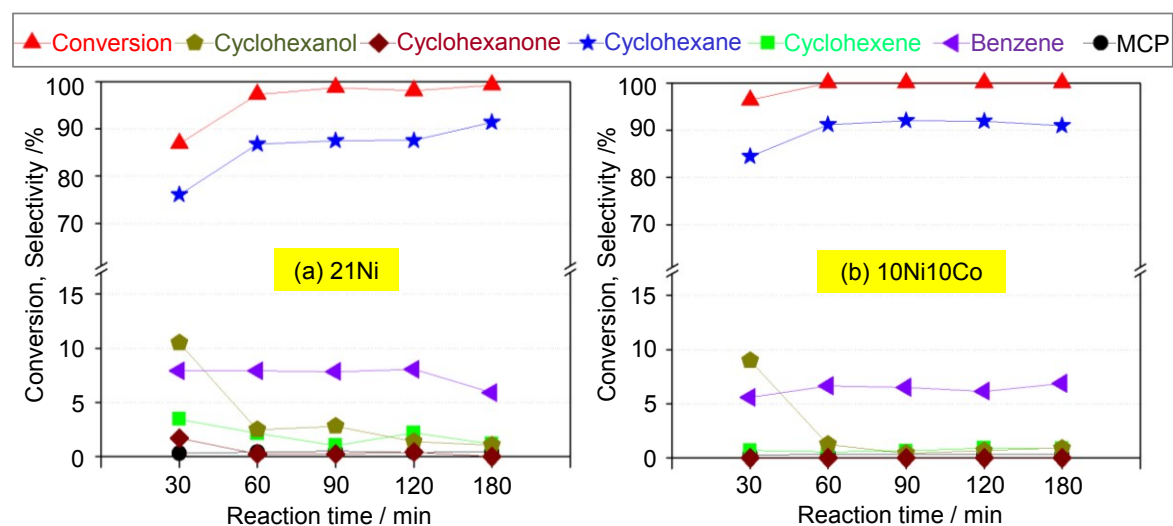


Figure 3.14. Phenol HDO of 21Ni (a) and 10Ni10Co (b) as a function of reaction time. Reaction conditions: 5.3 mmol of phenol, 10 g of H₂O, 25 mg of catalyst, T = 250 °C, P = 50 bar at RT.

It was found that after 30 min of reaction time, the conversion achieved 90% and 95% for 21Ni and 10Ni10Co samples, respectively. The selectivity toward deoxygenated products on 10Ni10Co was 90% and slightly higher compared to monometallic catalyst. Nevertheless, both catalysts showed nearly 100% of conversion after 60 min reaction

time. It should be noted that the high selectivity toward deoxygenated products and particularly cyclohexane are clearly seen in Figure 3.14.

The impact of pressure and temperature on the catalytic performance of 10Ni10Co was evaluated next (see Figure 3.15). Obviously, increasing the pressure led to an increase of the saturated hydrocarbon selectivity. This can be explained by the increased solubility of hydrogen in the reaction mixture and a higher hydrogen concentration near the metal sites, which boosts the hydrogen consuming reactions (e.g. hydrogenation reaction of benzene/cyclohexene to cyclohexane and hydrogenation of phenol). Meanwhile, starting with a pressure of 20 bar H₂ at RT, the selectivity of oxygenated products (cyclohexanol, cyclohexanone) achieved approximately 20% at a conversion of 82%, which indicates that a lower hydrogen pressure can not affect the cyclohexane formation and stabilizes the ketones intermediates, being consistent with Zhao et al. [94].

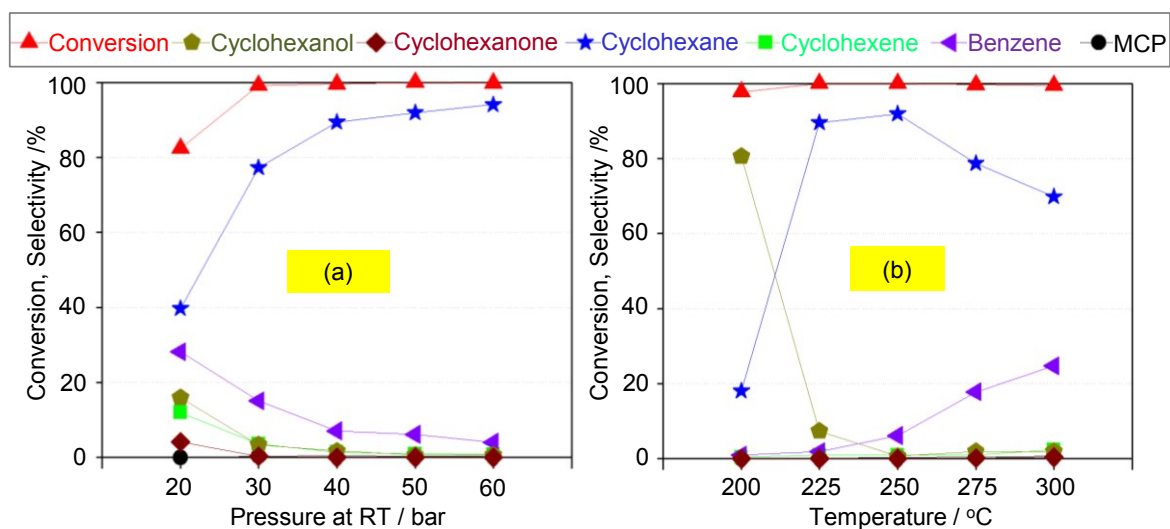


Figure 3.15. Effect of reaction conditions on catalytic performance of 10Ni10Co: a) Pressure and b) Temperature. Reaction conditions: 5.3 mmol of phenol, 10 g of H₂O, 25 mg of catalyst, t = 1 h.

Rising the temperature led to an increase of benzene selectivity. That is not surprising because the higher temperature favours the formation of benzene as dehydration and dehydrogenation are endothermic reactions [127]. A low temperature led to a higher fraction of oxygenated products (cyclohexanone, cyclohexanol) even when the conversion was almost complete. This result can be attributed to the dependence of temperature on dehydration step of cyclohexanol, which is an important step in HYD reaction route.

To elucidate this, the dehydration of intermediate cyclohexanol was investigated more in detail (Figure 3.16). As expected, conversion and the hydrocarbon selectivity increased with temperature. This result is also in line with the work of Zhao et al. [37] who showed that conversion of cyclohexanol over aqueous H₃PO₄ was significantly raised from 8.6% to

95% with increasing temperature from 180 to 200 °C. In addition, the authors also showed that raising temperature leads to more oxygen-free components at the expense of oxygenated products in HDO of 4-n-propylphenol over Pd/C combined with different solid acid (e.g. HZSM-5, Amberlyst 15, sulfated zirconia, Nafion/SiO₂) [94].

Moreover, higher temperature enhances the formation of benzene, indicating that the higher temperature promotes the dehydrogenation of cyclohexene to benzene. Figure 3.16 also presents the result from cyclohexanol dehydration over bare support at 250 °C. Cyclohexene was found to be the dominant product with more than 95% in the product distribution, confirming the importance of Ni active sites for hydrogenation step to completely transfer cyclohexene to saturated hydrocarbon because with HZSM-5 dehydration runs, but not hydrogenation. Thus, the presence of Ni active sites in supported catalyst accelerates the hydrogenation reaction of cyclohexene which in turn shifts the dehydration reaction toward cyclohexane product. As a result, the combination of both metal and acid sites is therefore needed to efficiently promote the HDO reaction.

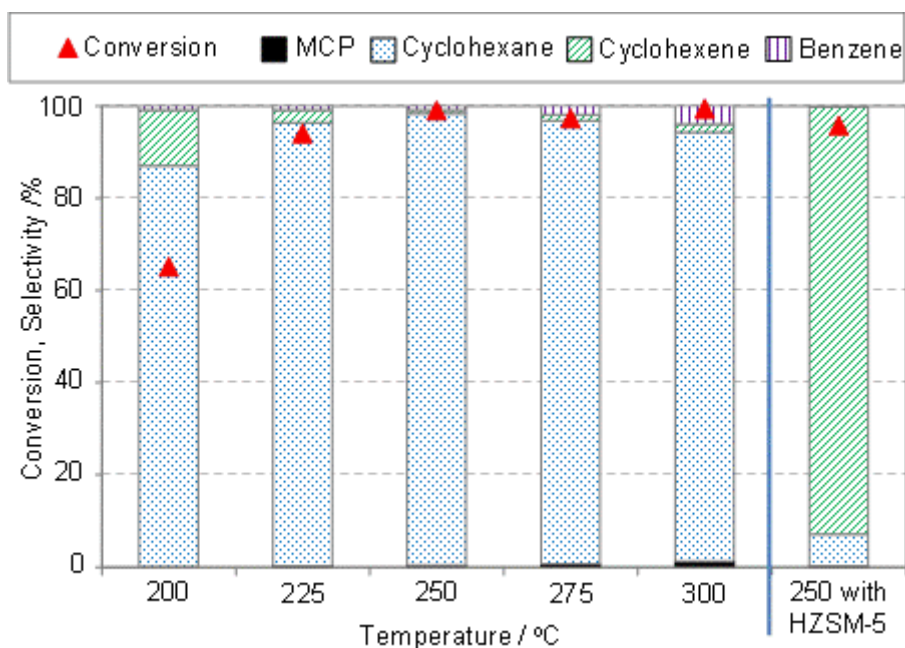


Figure 3.16. Dehydration of cyclohexanol as a function of temperature over 10Ni10Co and parent HZSM-5. Reaction conditions: 5.3 mmol of cyclohexanol, 10 g of H₂O, 25 mg of catalyst, t = 1 h.

3.4 Effect of support nature on bimetallic Ni-Co catalysts

Here the focus is put on the influence of supports on performance of bimetallic Ni-Co catalysts. The three most common zeolites HZSM-5, HBeta and HY were selected as supports and zirconia, which is weakly Lewis acidic and lacks any Brønsted acidity, was

included in this series. Table 3.5 lists typical properties of the resulting bimetallic Ni-Co catalysts, and the above discussed data of HZSM-5 supported Ni and Ni-Co catalysts are also included for comparison. To distinguish the samples, the catalysts are now denoted as xNi_yCo/Z, where x and y are the rounded content (wt%) of nickel and cobalt, respectively, and Z is the name of the supports. Obviously, 10Ni10Co/ZrO₂ possessed a mesoporous structure and significantly lower surface area compared to the others catalysts. The average crystallite size of metallic sites was calculated with Scherrer's equation from XRD results and revealed that 10Ni10Co/HZSM-5 exhibits the smallest one with only 15 nm, whereas in the other catalysts it varies from 19-30 nm. This is remarkable as the crystallites in ZrO₂ are smaller though surface area is smaller. The XRD patterns of the pre-reduced catalysts are displayed in Figure 4.2 in chapter 4.

Table 3.5. Textural and acidity properties of the Ni-Co catalysts prepared on different supports

Catalysts	N ₂ adsorbed volume at STP (cm ³ /g)	S _{BET} (m ² /g)	S _{micro} (m ² /g)	V _t (cm ³ /g)	V _{micro} (cm ³ /g)	Crystallite size (nm)	Acidity (μmol/g)		
							BAS	LAS	BAS/LAS
10Ni10Co/ZrO ₂	12.1	40	-	0.16	-	29.8	0	44	-
10Ni10Co/HBeta	101.5	434	368	0.24	0.16	23.3	137	984	0.14
10Ni10Co/HY	131.8	568	499	0.32	0.20	19.0	259	505	0.51
10Ni10Co/HZSM-5	65.4	281	195	0.23	0.09	15.1	162	509	0.32
21Ni/HZSM-5	65.4	281	184	0.25	0.08	29.7	243	345	0.70

S_{micro} = micropore area; V_t = total pore volume; V_{micro} = micropore volume

Quantitative estimation of their acidities (calculated from integral intensities of the peaks at 1545 and 1450 cm⁻¹ in the spectra of adsorbed pyridine py-IR (see Figure A5 in Appendix A) is also shown in Table 3.5. As expected, 10Ni10Co/ZrO₂ is only possessed few Lewis acid sites and no Brønsted sites. It is well known that zeolite possesses bridging hydroxyl groups (Si-OH-Al) in the framework (tetrahedral Al) which are indicated as strong Brønsted sites, whereas the Lewis acid sites are generated by partial extraction of Al from framework (octahedral Al) [134, 135]. The Brønsted acid site concentrations follow the support order: HY > HZSM-5 > HBeta > ZrO₂. If normalized to the specific surface area, the respective Brønsted site concentration of these samples showed another trend: HZSM-5 > HY > HBeta > ZrO₂, confirming the high density of strong Brønsted sites of HZSM-5 support. As the density of Lewis sites in HBeta supported catalyst is significantly higher than for others samples, 10Ni10Co/HBeta has the highest total acidity among these series.

The performance results of bimetallic and corresponding monometallic catalysts are depicted in Figure 3.17. Notably, all bimetallic catalysts (10Ni10Co) outperformed the corresponding monometallic catalysts (20Ni) in terms of activity and selectivity toward deoxygenated products for all named supports, which again confirms the benefit of the addition of Co into Ni based catalysts [136]. The bimetallic catalyst 10Ni10Co/HZSM-5 showed the best catalytic performance compared to all other materials. The poor activity of catalysts with HY support seems to be related to the poor hydrothermal stability of support (for detailed discussion see Figure 4.2 in Chapter 4).

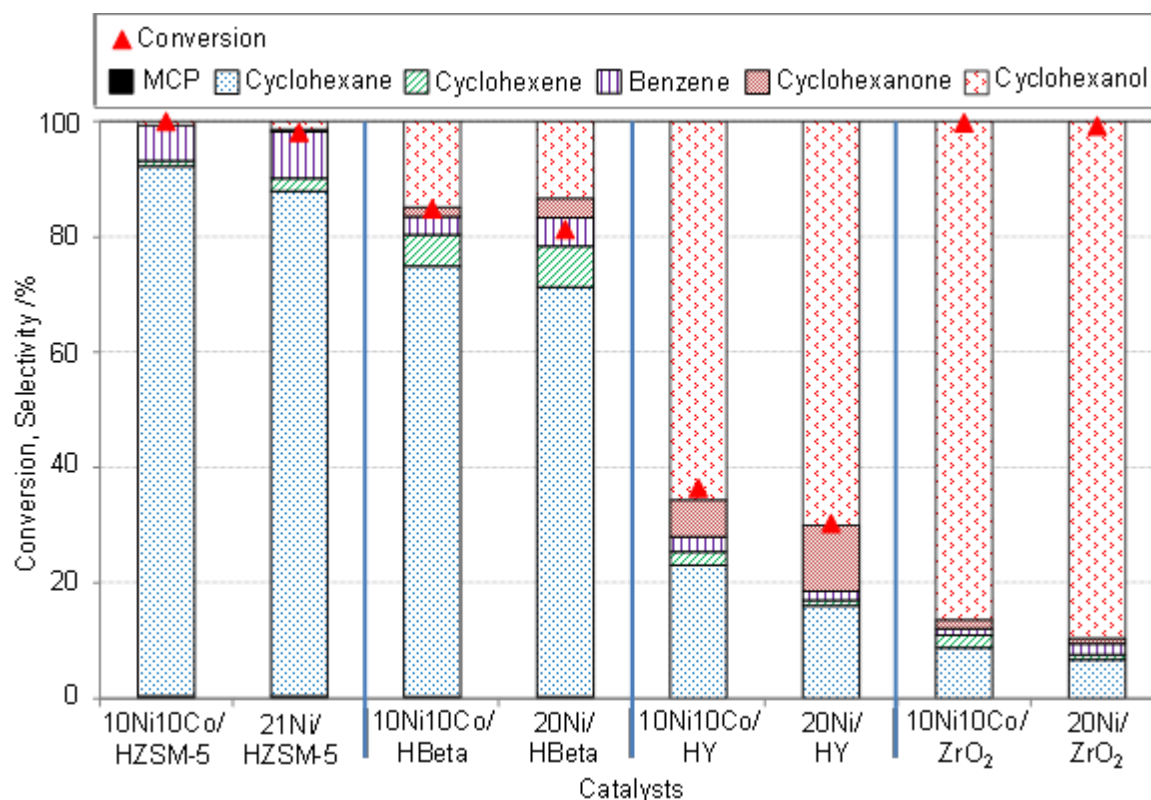


Figure 3.17. Phenol HDO on supported monometallic and bimetallic catalysts. Reaction conditions: 5.3 mmol of phenol, 10 g of H₂O, 25 mg of catalyst, T = 250 °C, P = 50 bar at RT, t = 2 h.

To further understand the influence of different supports, an investigation on reaction time impact was performed over the bimetallic Ni-Co catalysts (Figure 3.18). The bimetallic catalyst with the least acidic support (10Ni10Co/ZrO₂) reached complete conversion after only 60 min but hydrocarbon selectivity was less than 12% even when the reaction time was extended to 180 min. The low hydrocarbon selectivity can be attributed to the very low acidity of ZrO₂ compared to the zeolite supports (Table 3.5). Thus, 10Ni10Co/ZrO₂ is only active in hydrogenation, whereas the dehydration step needs acidic sites to proceed, and thus ZrO₂ is not able to promote dehydration steps under

given conditions. Over 10Ni10Co/HY, the conversion increased with the first 60 min and then it seems to be almost stable, whereas the conversion and selectivities toward deoxygenated products gradually increased with reaction time over the 10Ni10Co/HBeta.

The catalytic performance on HZSM-5 supported catalysts as function of reaction time at same conditions is already shown in Figure 3.14, and comparison reveals that the 10Ni10Co/HZSM-5 shows the best performance in phenol HDO compared to other supported 10Ni10Co catalysts at any given reaction time. This can be attributed to the metal particle dispersion, acidity properties of supports and hydrothermal stability.

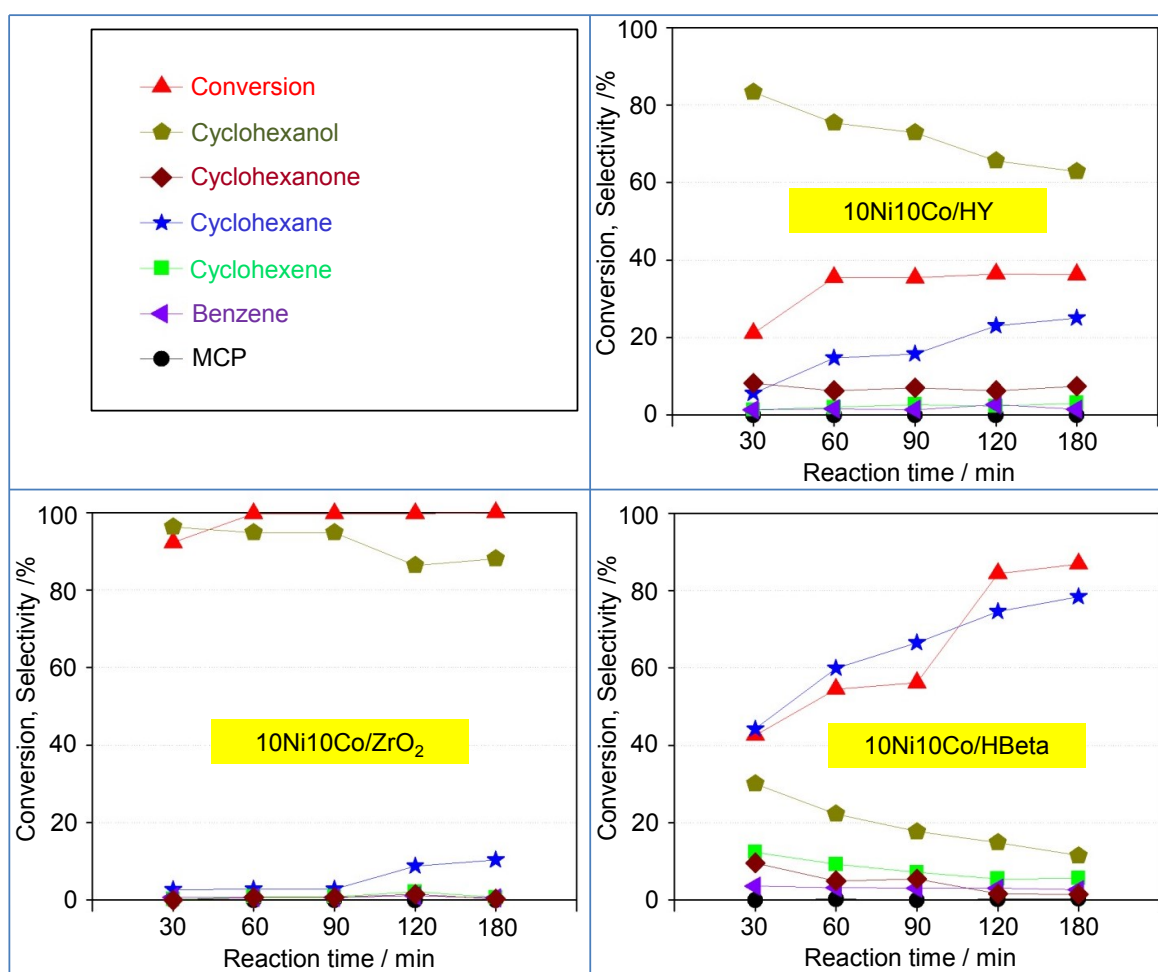


Figure 3.18. Catalyst performance with reaction time for the bimetallic Ni-Co catalysts. Reaction conditions: 5.3 mmol of phenol, 10 g of H₂O, 25 mg of catalyst, T = 250 °C, P = 50 bar at RT.

3.5 Summary and conclusions

In this chapter, various monometallic Ni, Cu or Co containing HZSM-5 supported catalysts and two series of bimetallic catalysts (Ni-Co/HZSM-5 and Ni-Cu/HZSM-5) were prepared,

characterized and studied in HDO of phenol as model compound in batch experiments. The results show that Ni/HZSM-5 is more active than Cu/HZSM-5 and Co/HZSM-5 for phenol HDO, most likely due to its outstanding capability of H₂ activation and dissociation. For bimetallic catalysts, adding Cu to Ni/HZSM-5 strongly promotes Ni reducibility, leads to the formation of Ni-Cu alloy, and generates separate Cu species with larger size. The latter could cause a loss of Ni active sites, Ni dispersion and increase of the number of inactive Cu sites at the surface, and finally lower the conversion and selectivity to deoxygenated products. In contrast, substitution of Co into Ni/HZSM-5 not only improves catalytic activity but also changes product distribution toward deoxygenated products, as some key hydrogenation steps in the reaction sequence were accelerated. Co addition also suppresses carbon deposition remarkably compared to monometallic catalysts.

Several tests at various reaction conditions with phenol and individual intermediate products gave more insight in catalyst performance and in particular the effect of Co addition to Ni based catalysts. High pressure is needed to increase the solubility of hydrogen into the reaction mixture to promote hydrogenation toward saturated hydrocarbons. The impact of temperature dependency of benzene-cyclohexene-cyclohexane equilibrium on the product distribution was observed. As phenol HDO toward cyclohexane is a consecutive reaction, thus any effect in reaction rates of individual steps finally change the overall reaction efficiency.

Moreover, the bimetallic Ni-Co catalysts supported on different acidic materials (HZSM-5, HY, HBeta and ZrO₂) show different activity and products distribution, which leads to the following conclusions:

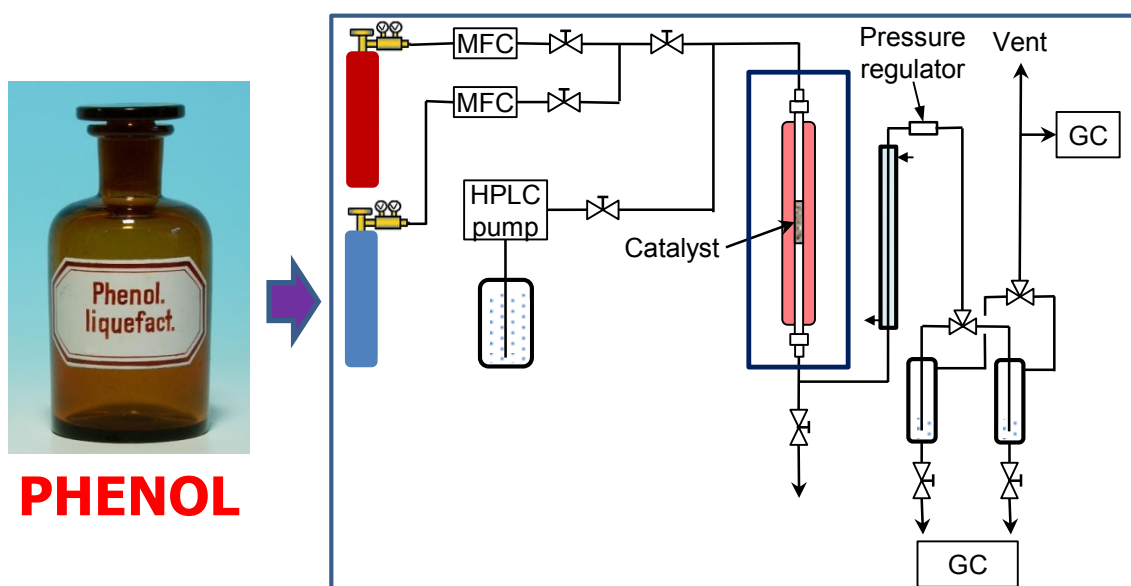
- The supports determine the surface area of the catalyst;
- They also introduce acidity into the catalyst, which is necessary to perform the dehydration step in reaction network.
- The combination of metal and acid sites must be tuned to effectively catalyze all the individually necessary reaction steps.
- last but not least, the support must be hydrothermally stable in aqueous phase environment.

Among these materials, 10Ni10Co/HZSM-5 shows the best performance in terms of conversion and selectivity toward saturated hydrocarbons. In the next chapters, the Ni-Co bimetallic catalyst and Ni monometallic catalyst are selected for further investigation.

Chapter 4

Hydrodeoxygenation of Phenol in a Continuous Fixed Bed Reactor

This chapter presents the performance of several catalysts in a continuous fixed bed reactor to check the catalyst stability and the influence of several reaction conditions. First, the effect of supports in bimetallic catalysts is illustrated. Then, various reaction conditions are applied for further comparison with the batch reactor results and to study stability of catalysts over prolonged run time. The relationship between the catalyst structure and performance are elaborated and finally the proposed reaction pathway is discussed.



4.1 Effect of supports on bimetallic catalysts

4.1.1 Performance of supported bimetallic Ni-Co catalysts

The effect of different supports on bimetallic catalysts was evaluated in a continuous flow reactor at the selected conditions (250 °C, 60 bar, WHSV = 1.8 h⁻¹, H₂: phenol molar ratio = 28). The conversion and product distribution over the different bimetallic catalysts with time on-stream is presented in Figure 4.1. The testing without catalyst showed that already 8% of conversion was obtained due to the impact of hot compressed water.

After reaching steady-state (3 h), the conversion was complete over 8 h on-stream for named catalysts, except the 10Ni10Co/HY, which reached a maximum conversion of approximately 90% but showing a slight decrease at longer run time. On the other side, a significant difference in selectivity toward products was observed for the named catalysts. For 10Ni10Co/ZrO₂ (least acidic support), mainly cyclohexanol was found with more than 95% selectivity, whereas 10Ni10Co/HZSM-5 and 10Ni10Co/HBeta (high acidity supports) led to nearly 100% selectivity toward deoxygenated products (cyclohexane, benzene, cyclohexene and MCP) for initial 6 h on-stream. After 8 h on-stream, 10Ni10Co/HZSM-5 showed a slight rise of cyclohexene and benzene fraction at the expense of cyclohexane selectivity. Compared to 10Ni10Co/HZSM-5, 10Ni10Co/HBeta showed a gradual drop in selectivity toward deoxygenated product with time on-stream. Interestingly, 10Ni10Co/HY possessed high acidity; however, it generated roughly 40% selectivity toward the deoxygenated products after 1 h on-stream and a subsequent gradual decay. It might be attributed to the poor stability of HY at hydrothermal conditions (see XRD pattern in Figure 4.2 in chapter 4.1.2) and loss of acidity (see Table 4.1 in chapter 4.1.2). Regarding the HZSM-5 supported catalysts, 21Ni/HZSM-5 gave 100% in conversion; however, the selectivity toward unsaturated hydrocarbon (benzene, cyclohexene) was always higher than those obtained with 10Ni10Co/HZSM-5. This is in line with the result from the batch tests in previous chapter owing to the outstanding capability of Ni-Co alloy in some individual hydrogenation steps.

As a result, it can be concluded that the acidities of the supports play an important role for catalytic performance, especially for the selectivity toward deoxygenated products at the given conditions. Moreover, the hydrothermal stability of supports should be taken into account. Among the named catalysts, 10Ni10Co/HZSM-5 shows the best performance in terms of catalytic performance and stability with time on-stream. Based on these results, 10Ni10Co/HZSM-5 was further studied with different reaction conditions (temperature, pressure and WHSV) and in a prolonged test to understand the catalyst stability and to elucidate the relationship between catalyst structure and performance.

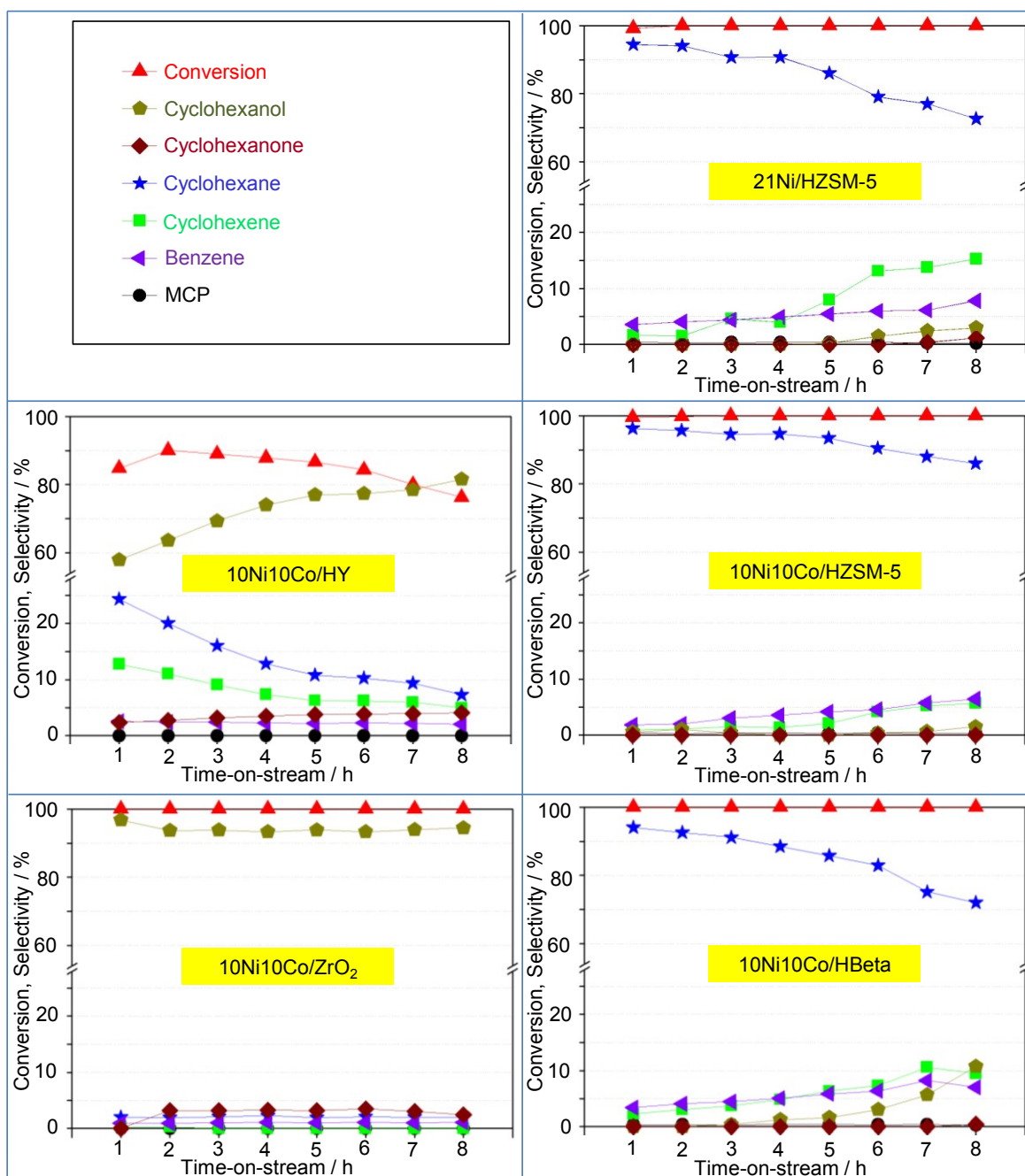


Figure 4.1. Performance of various supported bimetallic catalysts and 21Ni/HZSM-5 in phenol HDO. Reaction conditions: $T = 250\text{ }^{\circ}\text{C}$, 60 bar, $\text{WHSV} = 1.8\text{ h}^{-1}$, H_2 : phenol molar ratio = 28.

4.1.2 Spent catalyst characterization results

Various techniques were used for characterization of fresh and pre-reduced catalysts as described in the section 3.1; however, the analysis of spent catalysts has been not performed due to the small amount of catalyst and short run times. Therefore, in this section, some selected spent catalysts after prolonged time on-stream in a continuous flow reactor were recovered and compared with the pre-reduced ones.

The XRD patterns of the fresh pre-reduced catalysts are shown in Figure 4.2a. The reflections of metallic sites in the bimetallic catalyst occur between known reflections of Ni and Co metallic sites because of formation of Ni-Co alloy as proved via TEM and XRD measurements in chapter 3.1 and our previous study [137, 138]. The patterns of spent catalysts after 8 h on-stream were also measured and are shown in Figure 4.2b. Obviously, the sharp reflections of zeolite Y in the range of 6-32° almost disappeared after 8 h on-stream, indicating the considerable deterioration of its crystal structure. This observation is in line with the literature and can be attributed to the conversion of the crystal structure of zeolite Y into an amorphous phase [139]. Similarly, XRD pattern showed a significant decrease in intensity of the reflection of zeolite Beta (2 theta = 4.5°, 23°). In contrast, HZSM-5 and ZrO₂ supported catalysts showed no appreciable change in both metallic site and support reflections. Although the crystallinity of supports changed, particularly of 10Ni10Co/HY and 10Ni10Co/HBeta, the crystal structure of metallic domains of all named catalysts seems to be fairly stable.

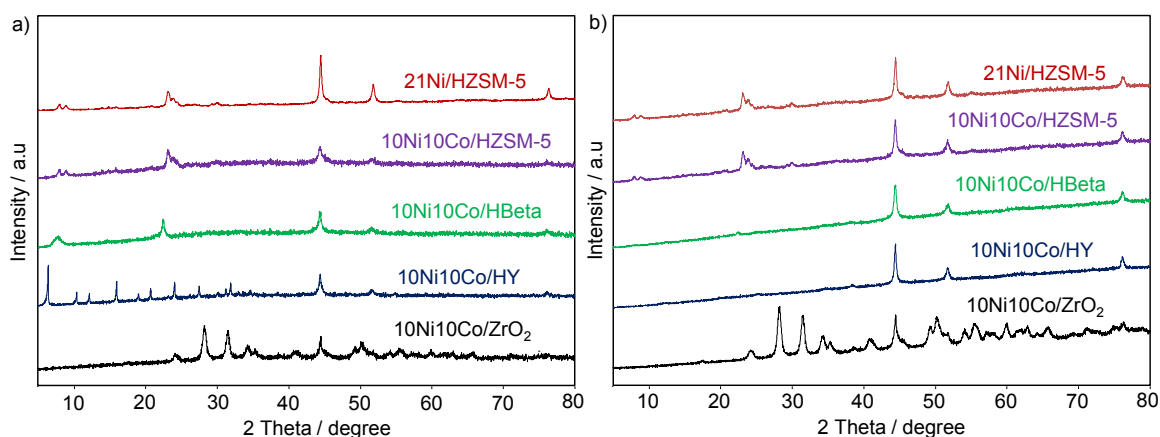


Figure 4.2. XRD patterns of pre-reduced catalysts (a) and spent catalysts (b) from a continuous reactor ($T = 250\text{ }^{\circ}\text{C}$, 60 bar, WHSV = 1.8 h^{-1} , H₂: phenol molar ratio = 28, 8 h on-stream).

Table 4.1 lists the textural and acid properties of the spent catalysts. The specific surface areas of 10Ni10Co/HY and 10Ni10Co/Beta were significantly reduced compared to those of fresh catalysts. Interestingly, the decay in surface areas of spent HZSM-5 and ZrO₂ supported catalysts was negligible as compared to the fresh catalysts. Nonetheless, after 24 h on-stream test (entry 6 and 7 in Table 4.1), the surface area of 10Ni10Co/HZSM-5 slightly dropped, whereas that of 21Ni/HZSM-5 was fairly reduced. The decline in surface area of 21Ni/HZSM-5 was possibly related to the high coke formation as shown in Table 4.1.

Table 4.1. Textural and acid properties of the spent catalysts.

Catalysts ^[a]	N ₂ adsorbed volume at STP (cm ³ /g)	S _{BET} (m ² /g)	S _{micro} (m ² /g)	V _t (cm ³ /g)	V _{micro} (cm ³ /g)	Coke deposits (wt%)	Acidity (μmol/g)		
							BAS	LAS	BAS/LAS
10Ni10Co/ZrO ₂	12.4	44	-	0.17	-	0.6	15	41	0.37
10Ni10Co/HBeta	27.4	117	98	0.2	0.04	1.7	50	189	0.27
10Ni10Co/HY	16.4	71	45	0.19	0.02	0.7	29	125	0.23
10Ni10Co/HZSM-5	62.3	265	190	0.30	0.08	1.0	112	440	0.25
21Ni/HZSM-5	63.8	271	198	0.29	0.08	1.9	117	251	0.47
10Ni10Co/HZSM-5 ^[b]	41.2	176	143	0.22	0.06	1.3	91	434	0.21
21Ni/HZSM-5 ^[b]	33.4	142	136	0.14	0.06	3.9	129	188	0.68

^[a]: 8 h on-stream, T = 250 °C, P = 60 bar, WHSV = 1.8 h⁻¹, H₂: phenol molar ratio = 28
^[b]: 24 h on-stream, T = 250 °C, P = 60 bar, WHSV = 1.8 h⁻¹, H₂: phenol molar ratio = 28

Regarding the acidity, overall acidities of 10Ni10Co/HY and 10Ni10Co/HBeta significantly decreased, whereas the 10Ni10Co/ZrO₂ showed a small increase of Brønsted acid sites (compare entries 1-3 in Table 4.1 to Table 3.4 in chapter 3.1.5). With HZSM-5 supported catalysts, the acidities decreased slightly on 10Ni10Co/HZSM-5 after 8 h on-stream (entry 4 in Table 4.1). However, weaker Lewis sites were created (1444/1597 cm⁻¹) at the expense of the stronger sites (1450/1622 cm⁻¹) on 21Ni/HZSM-5 (entry 5 in Table 4.1). This might be attributed to the dehydration of protonated oxide bridges during reaction under aqueous environment [126]. The decrease in acidities also happened with the samples tested at 24 h on-stream. The detailed py-IR spectrum is shown in Figure A6 in Appendix A.

Table 4.2 presents the change in elemental composition in the near surface region of the HZSM-5 supported catalysts with different time on-stream. For 21Ni/HZSM-5 sample, the Ni content in the near surface region in the spent catalyst after 8 h on-stream is slightly lower compared to that of the pre-reduced catalyst. However, this value slightly increased after 24 h on-stream and is relatively similar to reduced catalyst. As for the oxidation state in spent 21Ni/HZSM-5, oxidic and metallic Ni species were found in the sample before and after testing over 8 h and 24 h on-stream (see XPS spectra in Figure A7 in the Appendix A). That means that a strong re-oxidation occurred during recovery steps (washing and drying) of the sample. As discussed in section 3.1, a peak shift was seen in the case of Ni2p for Ni-Co/HZSM-5 due to the influence of Co addition into Ni/HZSM-5. In the spent 10Ni10Co/HZSM-5, the peak of metallic Ni seems to shift slightly toward the oxidic Ni compared to that in the pre-reduced one. Interestingly, a significant increase of both Ni and Co fraction in the near surface region during these tests was

observed. This further confirms the stabilization of Ni in the near surface region by substitution of Co into Ni/HZSM-5.

Table 4.2. Changes in elemental in spent catalysts compared to pre-reduced catalysts.

Samples	21Ni/HZSM-5	10Ni10Co/HZSM-5	
	Ni: Si ratio	Ni: Si ratio	Co: Si ratio
Pre-reduced	0.11	0.04	0.06
8 h on-stream - spent	0.10	0.09	0.13
24 h on-stream - spent	0.12	0.09	0.14

Two selected spent catalysts (10Ni10Co/HZSM-5 and 21Ni/HZSM-5), recovered after different time on-stream (8 h and 24 h), were studied by TEM method. Similar to pre-reduced catalyst, Figure 4.3a presents a broad distribution of particle sizes with different shapes in the spent 10Ni10Co/HZSM-5 after 8 h on-stream. Besides large and small particles with different shapes, a new domain/crystalline species of a metal was formed. It appears to consist of Ni-Co alloy located on the edge or the top of support HZSM-5 (so called edge domain). Detail in different particles size or domain is shown in Figure A8 (Appendix A). These observations are not fully understood, probably due to the agglomeration and re-structuring of metallic sites during reaction. Regarding the elemental composition, a minor change in Ni: Co atomic ratio (in Figure 4.3b,c) was noticed compared to the pre-reduced catalyst.

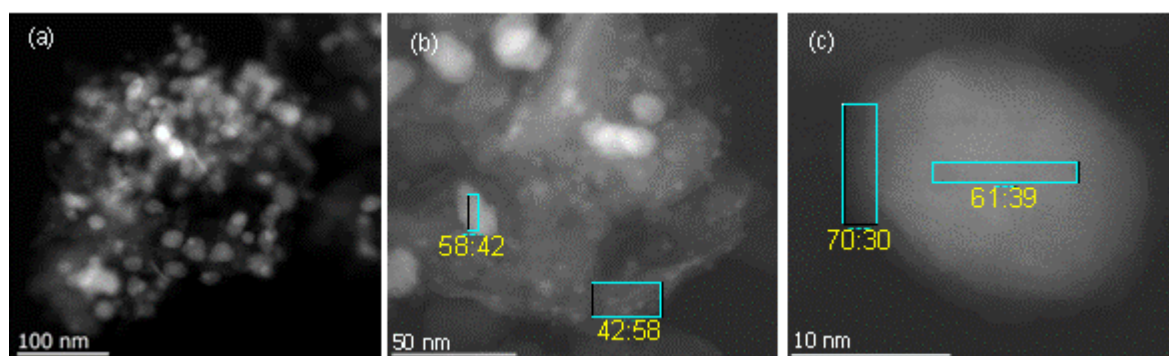


Figure 4.3. TEM images of spent 10Ni10Co/HZSM-5 catalyst after 8 h on-stream. The numbers represent Ni: Co atomic ratio.

On the other side, a core-shell domain in most large particles was observed, in which an oxide layer with the presence of Ni, Co and O (shell) covers the Ni-Co alloy in the core (Figure 4.3c). This result can be related to the formation of oxides in the near surface region due to contact with air during the catalyst recovery and handling, being consistent with the XPS results.

After 24 h on-stream with 10Ni10Co/HZSM-5, a broad distribution with large, small particles and the edge domain were observed (Figure 4.4a,b). In this sample, the new species seem to be more pronounced compared to the sample with 8 h on-stream, further confirming the edge domain develops during the long-term reaction. A slight change in Ni: Co atomic ratio was also noticed (see Figure 4.4c).

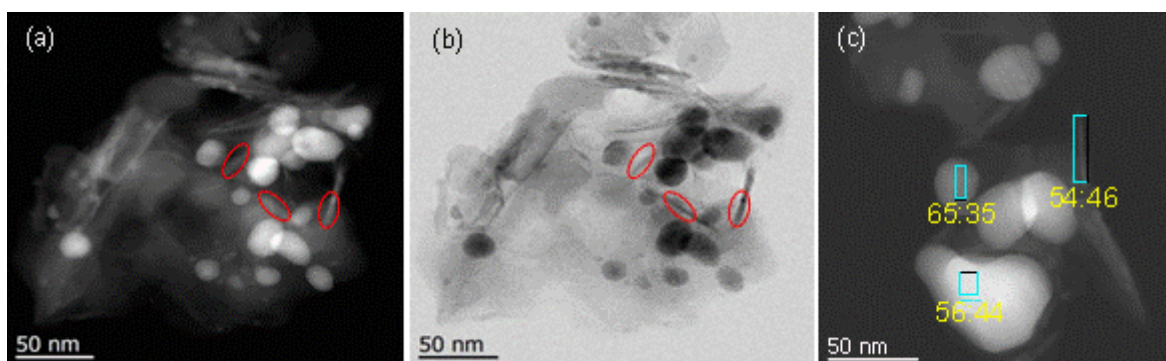


Figure 4.4. TEM images of spent 10Ni10Co/HZSM-5 catalyst after 24 h on-stream. The ellipses indicate the edge domain species of metal and the yellow numbers represent Ni: Co atomic ratio.

Different types of particles/species comparable to 10Ni10Co/HZSM-5 are also present in the case of 21Ni/HZSM-5 after 8 h on-stream; however, the edge domain is much more pronounced (see Figure 4.5a). In addition, very large Ni particles, possibly owing to the fast agglomeration, surrounded by a thin oxide shell were noticed in this sample. Different domains of Ni particles that sit on the surface of HZSM-5 are shown in Figure 4.5b.

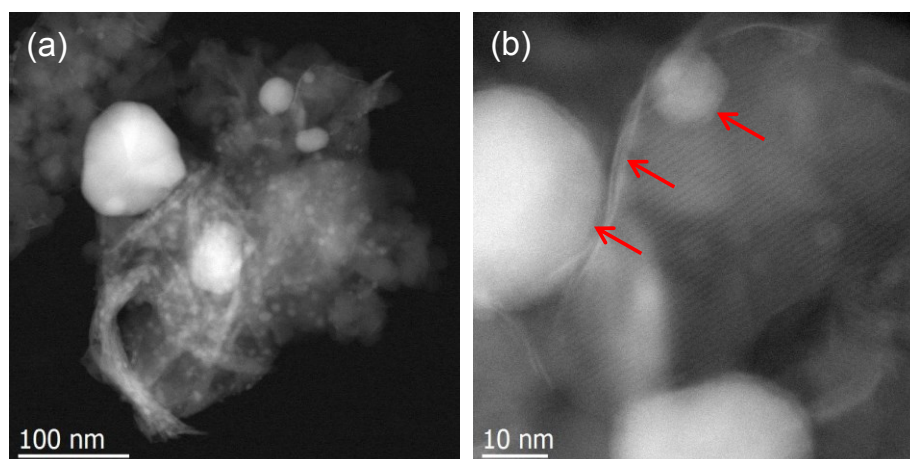


Figure 4.5. TEM images of spent 21Ni/HZSM-5 catalyst after 8 h on-stream. The arrows show different particles; the edge domain sit on the top of support.

After 24 h on-stream, the 21Ni/HZSM-5 catalyst clearly shows a fast agglomeration resulting in formation of large metallic particles (Figure 4.6). In addition, the edge domain

was also evident in here (more in detail see Figure A9 Appendix A). An enrichment of aluminium (correlates to Si: Al atomic ratio) in the edge domain was noticed compared to the original support (see Figure 4.6), indicating that the support was modified during time on-stream.

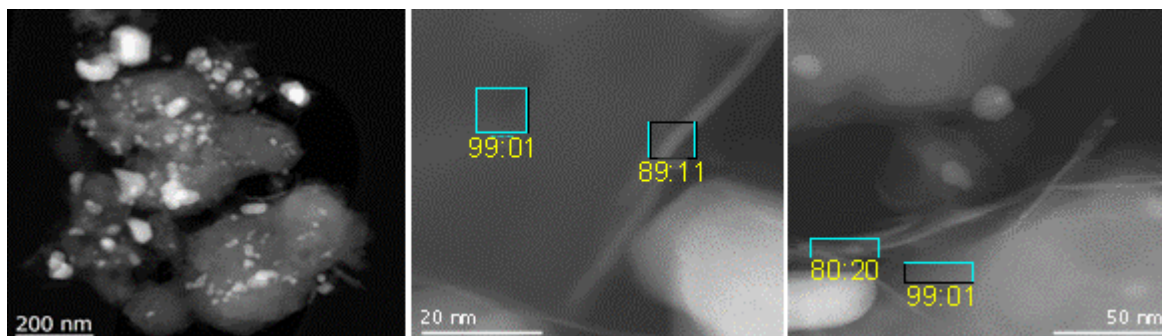


Figure 4.6. TEM images of spent 21Ni/HZSM-5 catalyst after 24 h on-stream.

In summary, although both catalysts showed a change in particle sizes and also the formation of new domain/crystallite species of metal, however, the observation was much more pronounced in the case of 21Ni/HZSM-5 compared to 10Ni10Co/HZSM-5. Based on this observation, it can be concluded that the addition of Co could help to reduce the fast agglomeration and to stabilize the Ni active sites during the long-time reaction owing to the formation of Ni-Co alloy.

4.2. Effect of various reaction conditions

4.2.1 Temperature

As discussed in previous chapter, increasing the temperature strongly support the formation of benzene. Almost complete phenol conversion over 10Ni10Co/HZSM-5 was observed in the temperature range of 200-300 °C, whereas a slight drop in conversion was observed at 350 °C (Figure 4.7). Besides, a change in product distribution was clearly seen. An increase of selectivity toward benzene, cyclohexene and methylcyclopentane at the expense of cyclohexane was observed especially at 350 °C. This observation points to the increase of back reaction rate (dehydrogenation of cyclohexane to cyclohexene/benzene). On the other side, MCP might form by isomerization of cyclohexane due to the presence of Brønsted acid sites in catalyst at high temperature. It is well known that the isomerization and dehydrogenation are favored at high temperature and/or the presence of strong acid catalysts [140]. This finding is consistent with the observation of Echeandia et al. who reported that the selectivity for MCP was increased from 0 to 17% when the temperature increased from 250 to 300 °C

on Pd/HY catalyst [141]. Moreover, a significant change in product distribution with increasing temperature can be explained by the benzene-cyclohexene-cyclohexane equilibrium which depends on temperature [141].

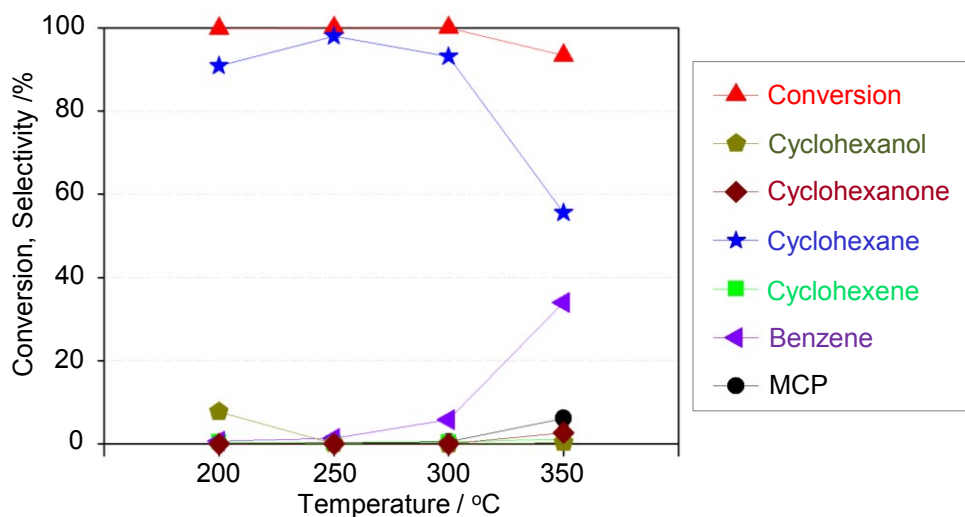


Figure 4.7. Phenol HDO as a function of temperature over 10Ni10Co/HZSM-5. Reaction conditions: T = 250 °C, P = 60 bar, WHSV = 1.8 h⁻¹, H₂: phenol molar ratio = 28.

On the other side, cyclohexanone was also detected in the product mixture at 350 °C (see Figure 4.7), indicating a lower hydrogenation performance of metal sites at the surface, probably linked with coke formation, because usually this product was rapidly hydrogenated to cyclohexanol on the metal sites. In addition, at higher temperature (>300 °C), a high yield of benzene and cyclohexene was observed, leading to less hydrogen consumption compared to runs with high cyclohexane yield. Thus, it seems to be a positive economic aspect because high hydrogen consumption leads to an increased operation cost. Nevertheless, a high concentration of unsaturated hydrocarbons in the product mixture could act as precursor for coke formation, which in turn finally limits catalysts lifetime. This is one of the most important parameters for the catalyst development. As a result, the HDO of phenol at 250 °C was selected for further investigation.

4.2.2 Pressure

The effect of pressure on 10Ni10Co/HZSM-5 performance was also carried out at the given conditions (250 °C, WHSV = 1.8 h⁻¹, H₂: phenol molar ratio = 28) (see Table 4.3). The test with a lower pressure (at 40 bar) showed high yields of oxygenates and unsaturated hydrocarbon, in accordance with the test in batch autoclave. This is most

likely attributed to the low hydrogen solubility in the reaction mixture, which keeps the reaction rates low and makes the HDO insufficient toward cyclohexane. Increasing the pressure thus results in a slight increase of saturated hydrocarbon (cyclohexane) in the product mixture, which is linked to enhanced solubility of hydrogen and more available high hydrogen in the reaction. This can be seen as the major pressure impact on HDO. A minor drop in cyclohexane selectivity was observed with time on-stream, coming along with a slight increase of cyclohexene, benzene and cyclohexanol yields. An increase of oxygenates in the product mixture was found after 8 h on-stream. It seems first to be linked to the acidity or stability of the support at the high pressure. In addition, the competitive adsorption of phenol and intermediates onto the two types of active sites (metal and acid sites) should be considered. Phenol and polar intermediate products (cyclohexanol, cyclohexanone) might prefer Brønsted acid sites, whereas non-polar products (benzene, cyclohexene, cyclohexane, MCP) might also prefer metal sites. The degree of surface coverage is controlled in each case by adsorption/desorption equilibria which depend also on total pressure. In addition, hydrogen is mostly adsorbed on metal sites, and high pressure might promote that effect. As a result, the pressure of 60 bar was selected for further investigation.

Table 4.3. Effect of pressure on performance of 10Ni10Co/HZSM-5.

Time on stream	Pres. (bar)	Conv. (%)	Selectivity (%)					
			Cyclo-hexane	Benzene	Cyclo-hexene	MCP	Cyclo-hexanol	Cyclo-hexanone
1 h	40	100	77.7	9.6	8.3	0.3	4.1	-
	60	99	96.3	1.8	0.9	0.5	0.5	-
	80	100	97.3	1.1	1.3	0.3	-	-
	100	100	99.1	0.6	-	0.3	-	-
4 h	40	100	71.6	8.6	11.2	0.3	7.6	0.8
	60	100	94.6	3.6	1.4	0.4	-	-
	80	100	95.2	1.4	3.1	0.3	-	-
	100	100	97.9	1.3	0.4	0.4	-	-
8 h	40	100	60.4	8.6	16.2	0.3	12.7	1.8
	60	100	86.0	6.5	5.7	0.3	1.5	-
	80	100	85.2	3.9	8.1	0.4	2.5	-
	100	100	85.7	1.7	5.0	0.3	7.2	-

Reaction conditions: T = 250 °C, WHSV = 1.8 h⁻¹, H₂: Phenol molar ratio = 28

4.2.3 WHSV

Table 4.5 shows the effect of WHSV on catalyst performance after 8 h on-stream. Though conversion is almost complete as varying the WHSV from 1.8 h^{-1} to 3.0 h^{-1} , a selectivity change is clearly observed. In the beginning of the reaction (1 h on-stream) the conversion and selectivity toward deoxygenated products both reach nearly 99 %, with the selectivity to cyclohexane ranging from 93-96%. However, after 8 h on-stream, the cyclohexanol selectivity rises from 2% to 36% and the decrease of cyclohexane selectivity from 86% to 42% when the WHSV is increased from 1.8 h^{-1} to 3 h^{-1} , respectively. Considering the reaction pathway of phenol HDO as reported in literature, parallel and consecutive reactions take place in two general reaction pathways, such as the primary hydrogenation of phenol to cyclohexanone/cyclohexanol and the dehydration of cyclohexanol to cyclohexene which is finally hydrogenated to cyclohexane. Thus, the low WHSV leads to a high contact time of catalyst with phenol and intermediate products, promoting the subsequent reactions of intermediates (e.g. cyclohexanol, cyclohexene) toward cyclohexane or MCP in the reaction network. This observation also seen in Figure 3.14 with the increasing of reaction time in a batch reactor.

Table 4.5. Effect of WHSV on Phenol HDO over 10Ni10Co/HZSM-5.

Time on stream	WHSV (h^{-1})	Con. (%)	Selectivity (%)					
			Cyclo-hexane	Benzene	Cyclo-hexene	MCP	Cyclo-hexanol	Cyclo-hexanone
1 h	1.8	99.5	96.3	1.8	0.9	0.5	0.5	-
	2.2	100	95.5	1.9	2.5	-	-	-
	3.0	100	92.9	2.4	4.0	0.3	0.5	-
4 h	1.8	100	94.6	3.6	1.4	0.4	-	-
	2.2	100	91.9	2.6	4.8	0.3	0.5	-
	3.0	100	77.9	3.9	11.2	-	6.6	0.4
8 h	1.8	100	86.0	6.5	5.7	0.3	1.5	-
	2.2	100	77.9	5.2	11.2	0.3	5.5	-
	3.0	100	42.2	4.4	14.5	-	35.8	3.0

Reaction conditions: T = 250 °C, P = 60 bar, H₂: phenol molar ratio = 28.

4.2.4 Long term evaluation of 10Ni10Co/HZSM-5 and 21Ni/HZSM-5

To better understand the catalyst stability, a prolonged evaluation with 24 h on-stream was performed with 10Ni10/HZSM-5 at the optimum conditions (T = 250 °C, P = 60 bar,

WHSV = 1.8 h^{-1} , H_2 : phenol molar ratio = 28). The corresponding monometallic catalyst 21Ni/HZSM-5 was also checked for comparison (see Figure 4.8).

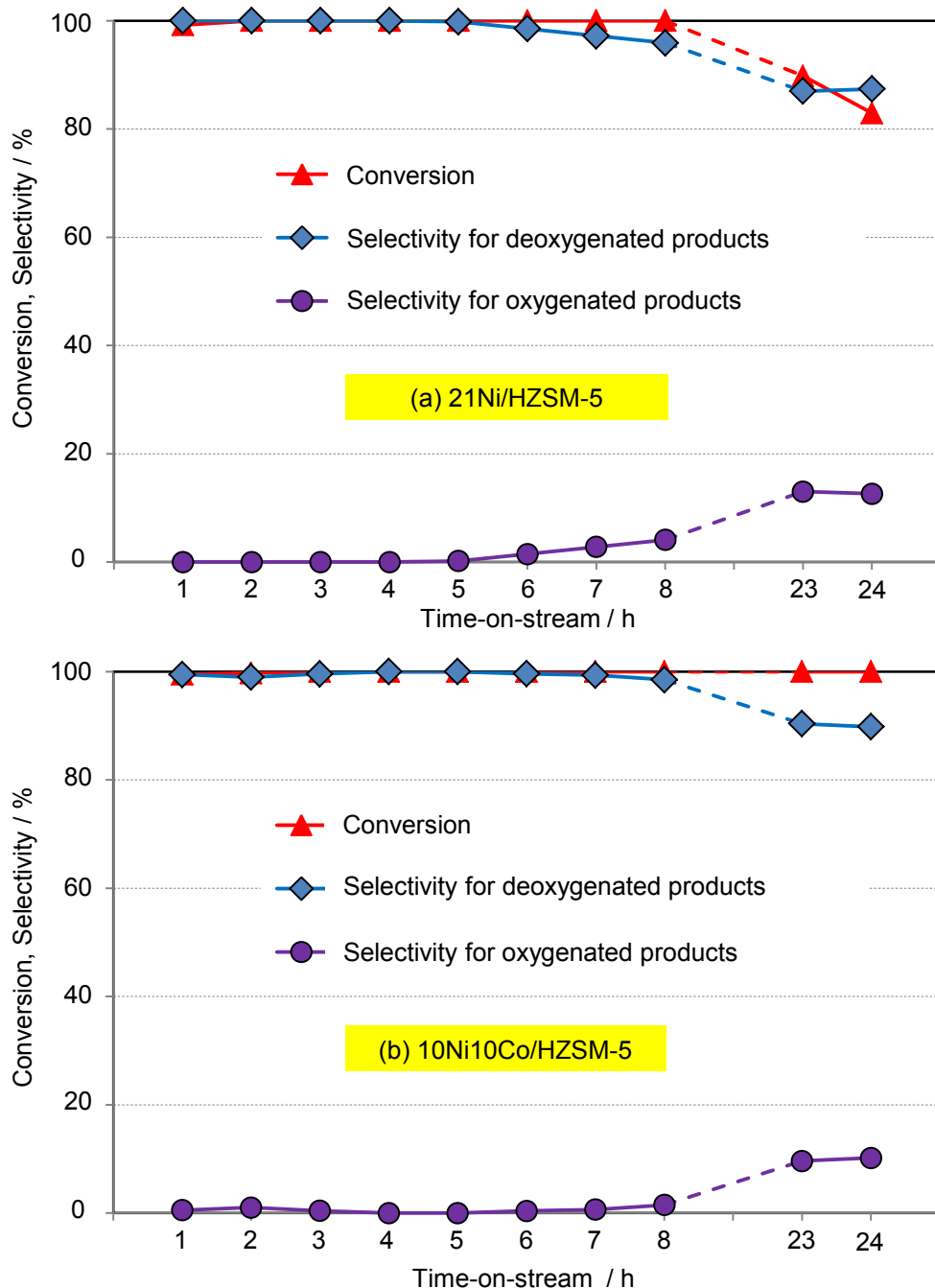


Figure 4.8. Phenol HDO over (a) 21Ni/HZSM-5 and (b) 10Ni10Co/HZSM-5. Reaction conditions: $T = 250 \text{ }^\circ\text{C}$, $P = 60 \text{ bar}$, $\text{WHSV} = 1.8 \text{ h}^{-1}$, H_2 : Phenol molar ratio = 28.

With 10Ni10Co/HZSM-5, conversion remained complete after 24 h on-stream, whereas a decrease of conversion was observed for 21Ni/HZSM-5 (from 100 to 83%). A possible reason for this loss in activity is the loss of active metal by leaching. According to ICP-

OES and AAS results (Table A1 in Appendix A), the Ni content in 21Ni/HZSM-5 was reduced by 6.5wt%, whereas the Ni, Co contents in 10Ni10Co/HZSM-5 were reduced by 1.9% and 1.8%, respectively. The Si and Al content of the support in 21Ni/HZSM-5 were also slightly reduced by roughly 5 wt% and 0.7 wt%, respectively, whereas those obtained in the 10Ni10Co/HZSM-5 amounted to 4.7 wt% and 0.9 wt%. These results are attributed to the dissolution of Si and Al (desilication, dealumination) in aqueous phase during reaction [142-144]. The decrease of the above elements is connected with the increase of coke formation on 21Ni/HZSM-5 compared to the 10Ni10Co/HZSM-5 (see Table 4.1).

Table 4.6 shows detailed information on product distribution as a function of time on-stream. With respect to the oxygen-free hydrocarbons, a slight decrease in selectivity was noticed resulting in 10% of selectivity toward oxygenated products. The increase of selectivity for oxygenated products (e.g. cyclohexanone, cyclohexanol) after 23-24 h on-stream can be attributed to the slight loss of acidity properties of catalysts (Table 4.1) and the agglomeration of metal particles to form other types of particles.

Table 4.6. Product distribution over HZSM-5 supported catalysts.

Time on stream	Catalysts	Con. (%)	Selectivity (%)					
			Cyclo-hexane	Benzene	Cyclo-hexene	MCP	Cyclo-hexanol	Cyclo-hexanone
1 h	21Ni	99.2	94.4	3.6	1.6	0.4	-	-
	10Ni10Co	99.5	96.3	1.8	0.9	0.5	0.5	-
4 h	21Ni	100	90.8	4.9	4.0	0.4	-	-
	10Ni10Co	100	94.6	3.6	1.4	0.4	-	-
8 h	21Ni	100	72.6	7.8	15.3	0.2	2.9	1.2
	10Ni10Co	100	86.0	6.5	5.7	0.3	1.5	-
24 h	21Ni	83.1	59.1	10.1	17.8	0.5	8.5	4.1
	10Ni10Co	100	68.1	10.4	11.0	0.3	7.5	2.6

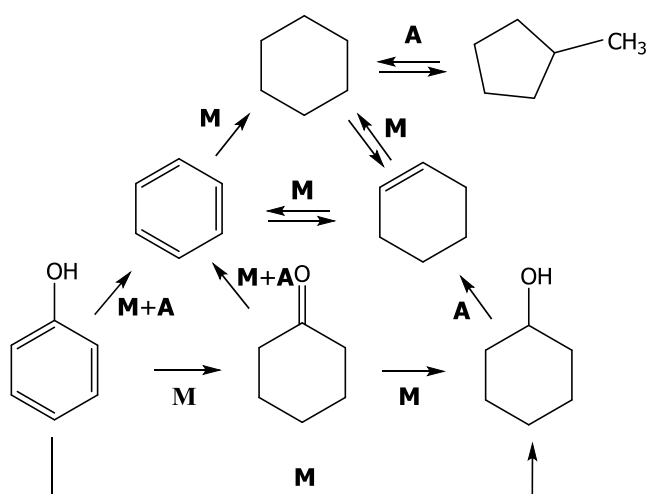
Reaction conditions: T = 250 °C, P = 60 bar, WHSV = 1.8 h⁻¹, H₂: Phenol molar ratio = 28.

Interestingly a slight increase of benzene and cyclohexene selectivities at the expense of cyclohexane selectivity was noticed with time on-stream from 1 to 24 h which has been not properly seen in batch-wise experiments. To find out the answer for this observation, one has just to look at the result of characterization of spent catalyst after 8 h and 24 h on-stream. Significant coke deposition was observed, which can have an impact on the rates of the individual reaction steps. The observed change of particle size and shape of metal sites in the spent catalysts, as proved by TEM method, might influence the adsorption modes of reactant or intermediates on various sites (e.g. steps and corners), resulting in

different yield of products with time on-stream. Similar to coke impact, the change of particle size can affect the conversion of intermediate products and ultimately product distributions. In line with this, Newman et al. [35] also suggested that the particle sizes of active sites could be related to different pathways, whereby different product distribution can be achieved. Mortensen et al. [145] found that various Ni active sites in Ni/SiO₂ catalyst shows different in hydrogenation and dehydration reaction. The authors reported that the later reaction was hindered at small particles due to competitive adsorption of alcohols on the nickel sites. The change in the product selectivities is therefore attributed to the slight drop of acid sites, a reduction of metal site and also the changing in shapes and particle sizes.

4.3. Proposed reaction pathways

Based on above experiments on phenol HDO in batch and continuous flow reactors with phenol and intermediates feeds, the reaction pathway was proposed as shown in Figure 4.9.



M: metal sites (metal or alloy) **A:** acid sites (zeolites, oxides)

Figure 4.9. Proposed reaction pathways of phenol HDO over supported Ni based catalysts.

In general, phenol can undergo two pathways for deoxygenation toward oxygen-free hydrocarbons (benzene, cyclohexane, cyclohexene and MCP): direct deoxygenation or hydrogenolysis (DDO route) and hydrogenation (HYD route). The latter pathway involves several steps such as phenol hydrogenation to cyclohexenol, an unstable intermediate that rapidly tautomerizes to cyclohexanone, which is further hydrogenated to cyclohexanol. Subsequently, cyclohexanol may dehydrate to form cyclohexene and finally be hydrogenated to cyclohexane. The isomerization of cyclohexane to MCP also

occurred, especially in the presence of acidic support. The results from HDO of intermediate products (Figure 3.12) indicate that benzene was formed via dehydrogenation of cyclohexene. This might be assigned to the ability of Ni to act also as a dehydrogenation catalyst.

As expected for this consecutive reaction, different supports, and various reaction conditions have a clear impact on the reaction network, the individual reaction steps and finally on the selectivity [95, 146]. Particularly in this study a long contact time between catalyst and the reaction mixture (including reactant and intermediates) leads to high conversion and selectivity toward saturated hydrocarbons (cyclohexane, MCP). High acidity promote the dehydration step in HYD route. A high temperature enhances the DDO route which linked to high yield of benzene, cyclohexene due to equilibrium dependence on temperature. In addition, solvent properties also influence on the reaction network, particularly in the case of aqueous phase reaction, e.g. Ohta et al [86] interpreted an in situ generation of protons in hot compressed water catalyzes the dehydration step over Pt/C catalyst at 280 °C.

It should be emphasized that the phenol adsorption modes can be related to nature of support, particularly in the case of supports possessing both Brønsted and Lewis acid sites. If the adsorption would occur via the hydroxyl group on Brønsted sites, leading to the formation of benzene as a first step (DDO route). If the adsorption would occur on the aromatic ring on Lewis sites, guiding the saturation of aromatic rings as a first step and leading to another pathway via cyclohexene (HYD route).

The proposed pathways are supported by findings of Zhang et al. [27], Hong et al. [28] and Massoth et al. [29] with two main routes. The later group conducted the gas phase HDO of phenol on sulfided CoMo/Al₂O₃ at 300 °C and 48.4 bar. In contrast, Zhao et al. [93] proposed that hydrogenolysis of phenol to benzene is inhibited, and hydrogenolysis of cyclohexanol to cyclohexane is also suppressed when using carbon-supported noble metal catalyst (Pt/C, Ru/C, Pd/C) and a mineral acid at the given reaction conditions (200 °C, 50 bar H₂ at RT). Moreover, the same group reported that benzene did not form in phenol HDO using Ni/HZSM-5 and Ni/Al₂O₃-HZSM-5 at lower temperature (200 °C, 50 bar H₂ at RT) [38]. This can be explained by the fact that hydrogenation is thermodynamically favorable at low temperature and promotes the HYD route.

As shown in above Figure 4.9, the deoxygenation process needs a combination of metal function and acid sites to take place. Metal functions (Ni or Ni-Co alloy) promote hydrogenation reactions (e.g. phenol to cyclohexanone/cyclohexanol, cyclohexene to cyclohexane) and dehydrogenation of cyclohexene to benzene, whereas acid sites (HZSM-5, oxides) appear as crucial for dehydration of phenol and cyclohexanol. Besides

that, the combination of metal function and acid site also affects the hydrogenolysis of phenol or converting cyclohexanone to benzene.

4.4. Summary and conclusions

Phenol HDO over Ni-Co based catalysts using several acidic supports in a continuous flow reactor confirms that the outstanding performance of HZSM-5 compared to other carriers (HBeta, HY and ZrO₂) depends on its high acidity and hydrothermal stability. It is evident that the acidity of the support plays an important role in HDO of phenol, as it affects the oxygen removing steps.

The investigation of the effect of reaction conditions (pressure, temperature, WHSV) on catalyst performance reveals that high H₂ pressure obviously leads to an increase of H₂ solubility in the reaction mixture and subsequently promotes hydrogen consuming reactions steps toward saturated hydrocarbon. The strong temperature-selectivity dependence also results in significant changes in product distribution, especially the formation of benzene and MCP at high temperature. The dependency of selectivity from (intermediate) conversion is evident from the test varying the WHSV.

The long-term tests at the given condition (T = 250 °C, P = 60 bar, WHSV = 1.8 h⁻¹, H₂: phenol ratio = 28) show that 10Ni10Co/HZSM-5 is highly stable with almost 100% conversion and a slight loss (from 100 to 90%) in selectivity toward deoxygenated products after 24 h on-stream. In contrast, 21Ni/HZSM-5 shows a decline in both the phenol conversion (from 100 to 83%) and deoxygenated products selectivity (from 100 to 86%), possibly due to high coke formation and fast agglomeration of metal sites compared to 10Ni10Co/HZSM-5.

Finally, the proposed reaction network is illustrated, which further confirms that two reaction pathways are available over the prepared catalysts and that the combination of metal and acidic sites is needed in an effective catalyst for HDO of phenol toward oxygen free hydrocarbon (cyclohexane, benzene, cyclohexene and MCP). These continuous tests offer a better insight into consecutive reactions as residence time can be better controlled.

Chapter 5

Hydrodeoxygenation of Bio-oil in a Batch Reactor

In this chapter, the results of batch-wise HDO of bio-oil over selected catalysts are presented and discussed. The effect of different acidic materials is discussed. The effect of different experimental HDO conditions on the product yields and product properties is given to get more insight into the upgrading of bio-oil.



BIO-OIL



5.1 Feedstock

For this study, PYTEC GmbH supplied bio-oil, which was produced by FP of wood chips, where the wood is pressed continuously against a hot rotating disk and pyrolyzed [147]. Table 5.1 shows some typical properties of such bio-oil. In addition, a bottom residue from crude oil atmospheric distillation in a commercial refinery in Vietnam was used as a representative of a FCC conventional feed (denoted as BH-Residue) and its properties are shown in Table 5.1 as well. The difference in the nature of the bio-oil and the conventional feed are evident in this table, e.g., oxygen content, water content and HHV. The properties of UBO with 10Ni10Co/HZSM-5 are also given here that will be discussed in following sub-chapter.

Table 5.1. Typical properties of bio-oil and Bach Ho residue.

Properties		Bio-oil	Bach Ho Residue	UBO (run 11)
Wet basis	H ₂ O (wt%)	32.58	-	-
	pH	3.2	-	-
Dry basis (wt%)	C	55.32	86.17	66.4
	H	6.90	13.51	10.6
	N	0.25	0.32	0.3
	O	37.41	-	22.8
HHV (MJ/kg)		21.9	48.6	33.6

5.2 Effect of the catalyst supports on bio-oil HDO

The optimum HDO conditions (5 g of bio-oil, 25 g of H₂O, 1 g of catalyst, P = 60 bar H₂ at RT, T = 300 °C, t = 4 h) were taken for tests with the Ni-Co bimetallic catalysts. The sample 21Ni/HZSM-5 was included in this series to provide a benchmark.

With phenol as a model compound (chapter 3 and 4), the catalytic activity is calculated based on consumption of a single feed compound. For evaluation of bio-oil HDO, however, this definition can not be used because the feed is very complex and the exact molecular composition is unknown. Therefore, the product yields, the DOD and a van Krevelen plot are common tools for catalytic evaluation. The experimental results (product yields and DOD) are shown in Figure 5.1. It should be noted that the evaporation of DCM solvent and work-up procedure (filtration) typically caused a loss in the mass balance (8-15 wt%) in this study.

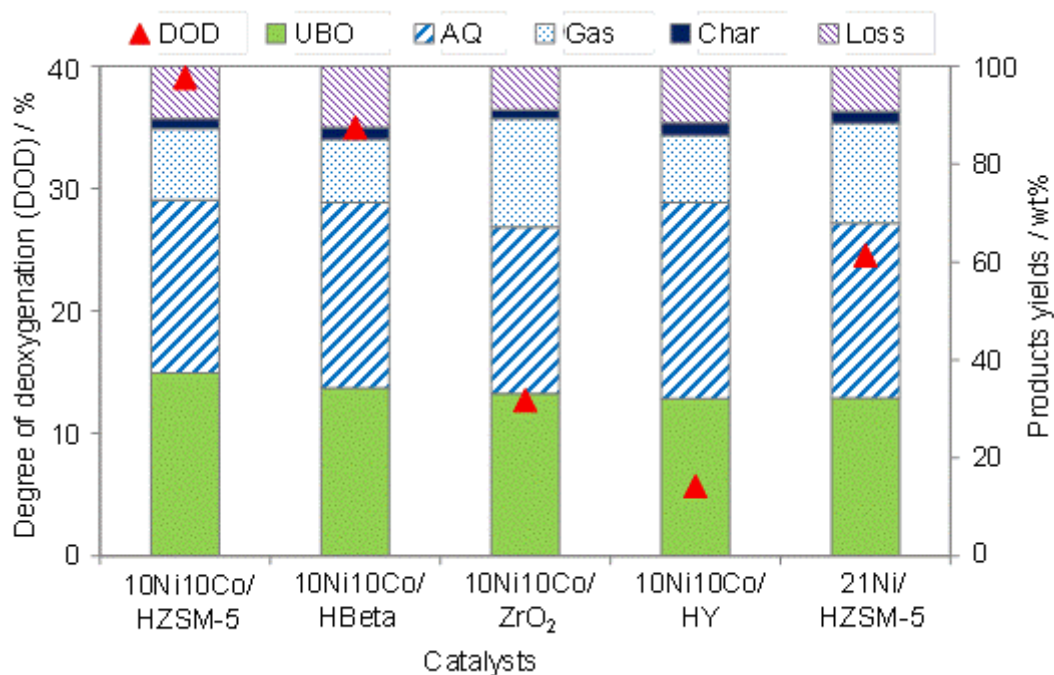


Figure 5.1. Performance of 21Ni/HZSM-5 and 10Ni10Co-catalysts in bio-oil HDO. Reaction conditions: 5 g of bio-oil, 25 g of H₂O, 1 g of catalyst, P = 60 bar H₂ at RT, T = 300 °C, t = 4 h.

Regarding the product yields, the oil fractions (UBO) obtained with all catalysts reached more or less the same values (32-37 wt%), whereas the amount of products found in the aqueous phase (AQ) was slightly higher in the case of 10Ni10Co/HY and 10Ni10Co/HBeta than with other catalysts. This indicates that more polar products (e.g. alcohols, carbonyl compounds) which are highly soluble in water must have formed. Considerable amounts of gas phase were produced in all runs, corresponding to 13-22 wt% related to feed. It is well known that high acidity promotes the cracking reactions. However, in the case of zeolite Y with a relatively high number of Brønsted acid sites, a smaller gas fraction was observed (Figure 5.1). It might be due to the change of acidity of 10Ni10Co/HY during reaction because of its lower hydrothermal stability. In contrast, the formation of a large amount of gas fraction was observed with 10Ni10Co/ZrO₂ even though it does not offer Brønsted acid sites. It might be due either to the effect of Lewis acid site of ZrO₂ or its mesoporous structure, which offers improved accessibility to acid sites for the feed molecules or intermediate products, leading to an increase of the fraction of gaseous products. It should be considered that ZrO₂ is also reported to be active in deoxygenation of biomass in hot compressed water at temperatures above 350 °C [36]. The main components in the gas phase were non-converted H₂, methane, CO₂, CO and various hydrocarbons (C₂ to C₅₊) (see Figure 5.2). Compared to the model reaction, CO₂

and CO were now observed in these tests due to the presence of several functional groups (e.g. carboxylic acids, aldehydes, guaiacols, syringols) in the starting feed.

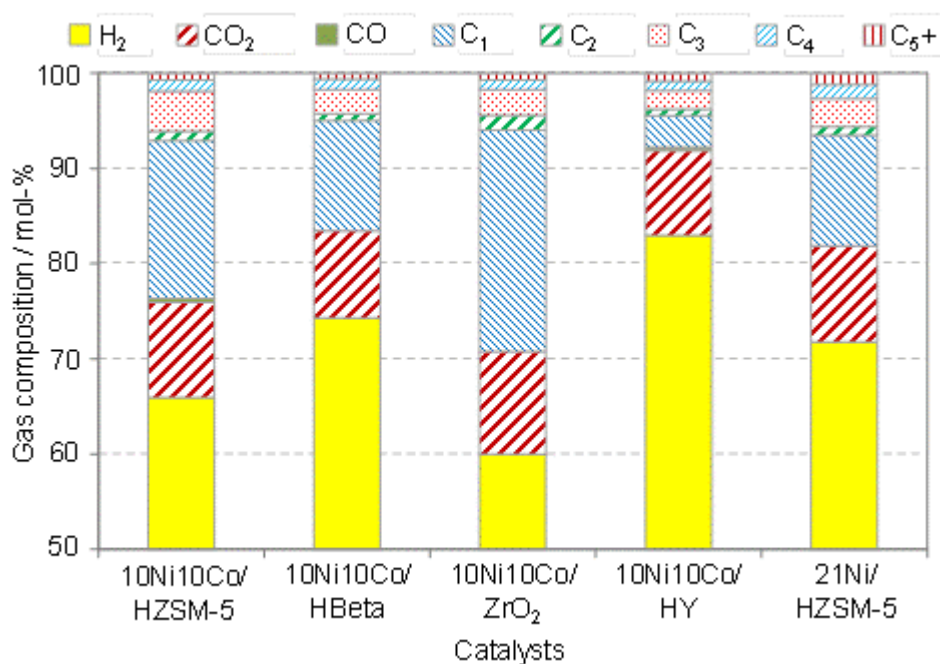


Figure 5.2. Gas distribution of bio-oil HDO over 21Ni/HZSM-5 and 10Ni10Co/HZSM-5 catalysts. Reaction conditions: 5 g of bio-oil, 25 g of H₂O, 1 g of catalyst, 60 bar H₂ at RT, T = 300 °C, t = 4 h.

The bimetallic catalyst 10Ni10Co/HZSM-5 showed a higher activity for oxygen elimination than the 21Ni/HZSM-5. This can be related to the higher dispersion with smaller metal particle size (see Table 3.5) and to TEM results [137]. The second reason could be the lower coke formation with 10Ni10Co/HZSM-5 as determined by elemental analyzer (see Table 5.2) and the hard coke formation as indicated by TPO result (see Figure 5.5, chapter 5.3).

More important, the DOD with the bimetallic catalysts follows the support order HZSM-5 > HBeta > ZrO₂ > HY. This demonstrates the advantage of HZSM-5 compared to the other materials, which could be related to its hydrothermal stability and acid properties. The low DOD with the 10Ni10Co/ZrO₂ can be attributed to its much lower surface area and acidity compared to other catalysts (Table 3.5). The HDO performance is also displayed in a van Krevelen plot (Figure 5.3). The molar O: C ratio of the liquid UBO samples was considerably lower and the molar H: C was higher compared to those obtained from original bio-oil (O: C ~ 0.51, H: C ~ 1.5). The far distance of the original bio-oil to the fossil feed (BH-Residue) is clearly seen in this Figure. The upgrading with all catalysts improved the bio-oil quality toward to that of the fossil feed. In fact, the molar H: C ratio of UBOs upgraded with 10Ni10Co/HBeta and 10Ni10Co/HZSM-5 is higher

although the molar O: C ratio is still higher than compared to those of fossil feed. It should be noted that the high molar H: C ratio and low molar O: C ratios in the UBOs compared to fossil fuels are linked with an effective HDO reaction.

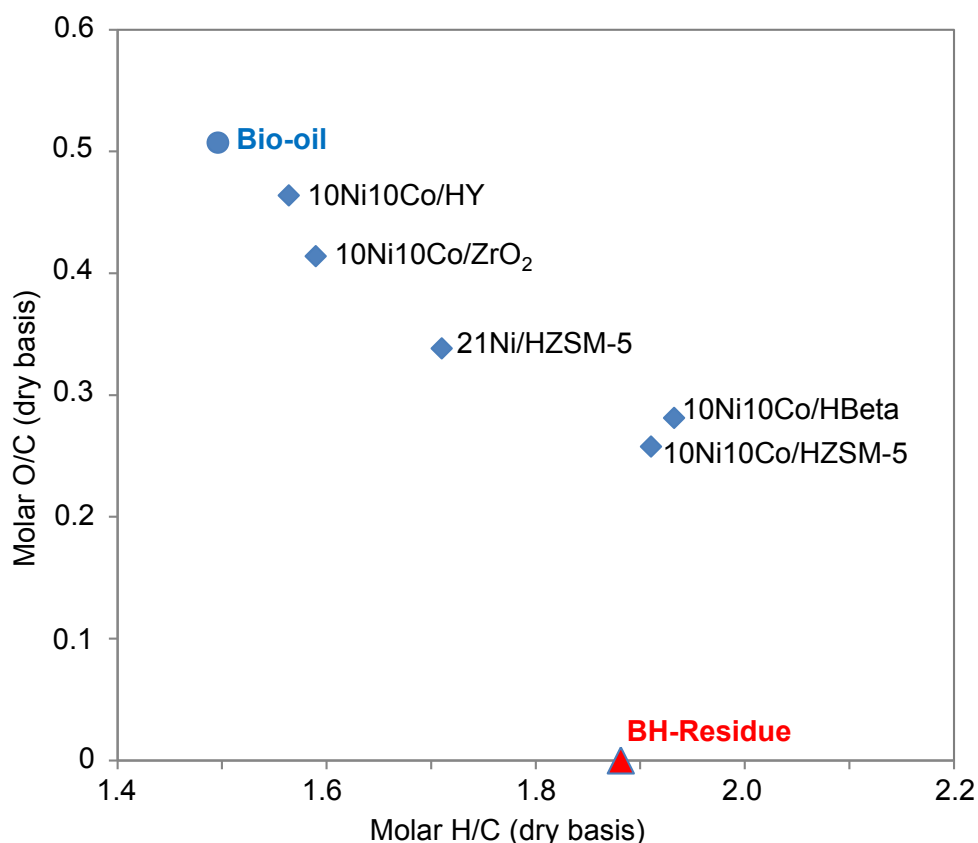


Figure 5.3. van Krevelen plot for bio-oil, BH-Residue and UBO upgraded with named catalysts. Reaction conditions: 5 g of bio-oil, 25 g of H₂O, 1 g of catalyst, 60 bar H₂ at RT, T = 300 °C, t = 4 h.

As discussed in previous chapters, a combination of metal and acid sites is essential for elimination of oxygen from phenol. The above results also follow the same manner with bio-oil. Additionally it is believed that the higher acidity of catalysts, the greater the coke formation, which can be clearly seen via CHN analyser (Table 5.2 in chapter 5.3).

5.3 Characterization of spent catalysts

The properties of the fresh catalysts (textural properties, acidity) were already presented in previous chapter (Table 3.5). This paragraph shows the results for the spent catalysts recovered from the above-discussed tests described in Chapter 5.2.

The XRD patterns of the pre-reduced catalysts (Figure 4.2a) are shown again in Figure 5.4a for comparison together with the patterns of spent catalysts (Figure 5.4b). Similar to

the spent catalysts from the phenol tests, the sharp reflections of zeolite Y in the range of 6-32° almost disappeared after the reaction, whereas 10Ni10Co/HZSM-5 and 10Ni10Co/ZrO₂ retained their structure. The sample 10Ni10Co/HBeta presents a moderate decrease in intensity of the reflection of zeolite Beta (2 theta = 4.5°, 23°). Together with this, a dramatic loss of surface area was evidenced (Table 5.2). The catalyst 21Ni/HZSM-5 experienced a higher surface loss than 10Ni10Co/HZSM-5.

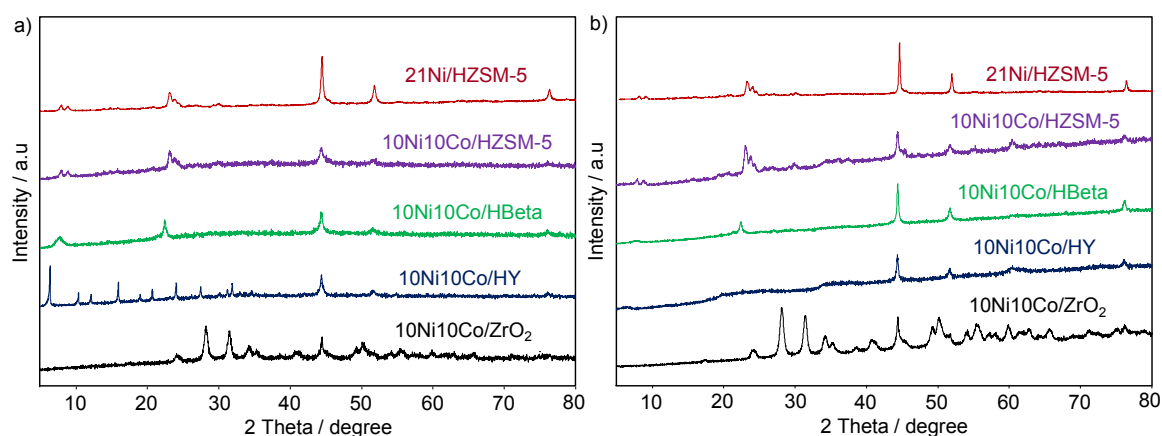


Figure 5.4. XRD patterns of reduced catalyst before (a) and after reaction (b).

Table 5.2. Textual properties of the selected spent catalysts

Catalysts ^[a]	N ₂ adsorbed volume at STP (cm ³ /g)	S _{BET} (m ² /g)	S _{micro} (m ² /g)	V _t (cm ³ /g)	V _{micro} (cm ³ /g)	Coke deposition (wt%)
10Ni10Co/ZrO ₂	14.0	50	-	0.17	-	2.5
10Ni10Co/HBeta	20.1	70	39	0.10	-	5.4
10Ni10Co/HY	29.0	110	7.8	0.28	-	6.3
10Ni10Co/HZSM-5	53.7	229	123	0.35	0.06	4.8
21Ni/HZSM-5	39.1	167	151	0.11	0.06	6.3

^[a] Reaction conditions: 5 g of bio-oil, 25 g of H₂O, 1 g of catalyst, P = 60 bar H₂ at RT, T = 300 °C, t = 4 h.

A relatively high coke formation was found in such samples compared with the model reaction tests (see results of CHN analyzer Table 5.2). The observation can be attributed to the presence of the highly reactive unsaturated functionalities (aldehydes, ketones, ...) in the feed, which can act as coke precursors better than phenol.

In order to gain more insight in the nature of coke species formed on the spent catalysts, three samples were studied by the TPO method. Figure 5.5 displays the TPO profiles for CO₂ and H₂O desorption. These profiles show a sharp peak at medium

temperature (280-340 °C), whereas only for HZSM-5 supported catalysts a broad shoulder is visible at higher temperature (400-500 °C). The latter peak is much clearer for the 21Ni/HZSM-5 than for 10Ni10Co/HZSM-5. This indicates that two types of carbonaceous material (at medium and high temperature) are formed over the HZSM-5 supported catalysts compared to the ZrO₂-based catalyst.

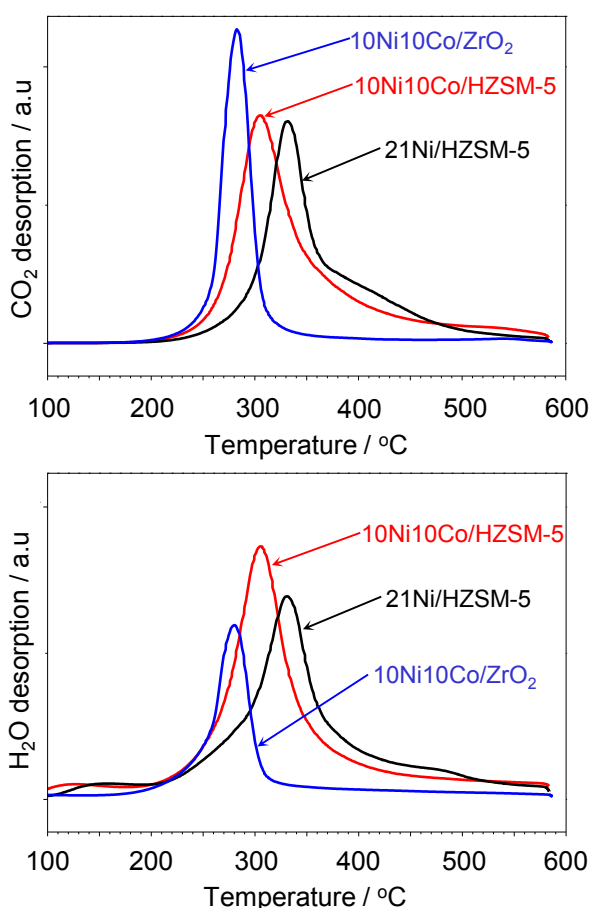


Figure 5.5. TPO results of selected spent catalysts.

In addition, the CO₂ desorption curves (correlated with peak area) of HZSM-5 supported catalysts look quite similar (peak areas of 293×10^6 and 268×10^6 for 10Ni10Co/HZSM-5 and 21Ni/HZSM-5, respectively) and much higher than that of 10Ni10Co/ZrO₂ (peak area of 190×10^6). On the other side, the peak areas of H₂O desorption curves for the HZSM-5 supported catalysts (286 - 314×10^6) were much higher than for 10Ni10Co/ZrO₂ (139×10^6), suggesting that highly H containing species were formed with the zeolite supported catalysts. In the case of 10Ni10Co/ZrO₂ catalyst, the CO₂ desorption is generally much more pronounced than the corresponding H₂O desorption, indicating that this sample was covered with less hydrogenated coke species. Notably, the maximum temperatures of the two peaks in 21Ni/HZSM-5 were higher than

for 10Ni10Co/HZSM-5, which in turn illustrates the beneficial effect of the addition of Co to Ni/HZSM-5 in terms of a strong decrease of hard coke formation.

5.4 Effect of reaction conditions on bio-oil HDO over 10Ni10Co/HZSM-5

As mentioned in Chapter 1, various parallel and/or consecutive reactions (e.g. hydrogenolysis, hydrogenation, dehydration, decarbonylation, decarboxylation, cracking, hydrocracking, polymerization) run in the upgrading of bio-oil [51, 54, 55]. Those reactions are favoured at different reaction conditions (e.g. temperature, pressure) or on different catalysts. In this respect, hydrogenation is normally favoured at a lower temperature (170-250 °C), whereas high temperature (> 250 °C) and/or acidic catalysts support the HDO and (hydro)cracking.

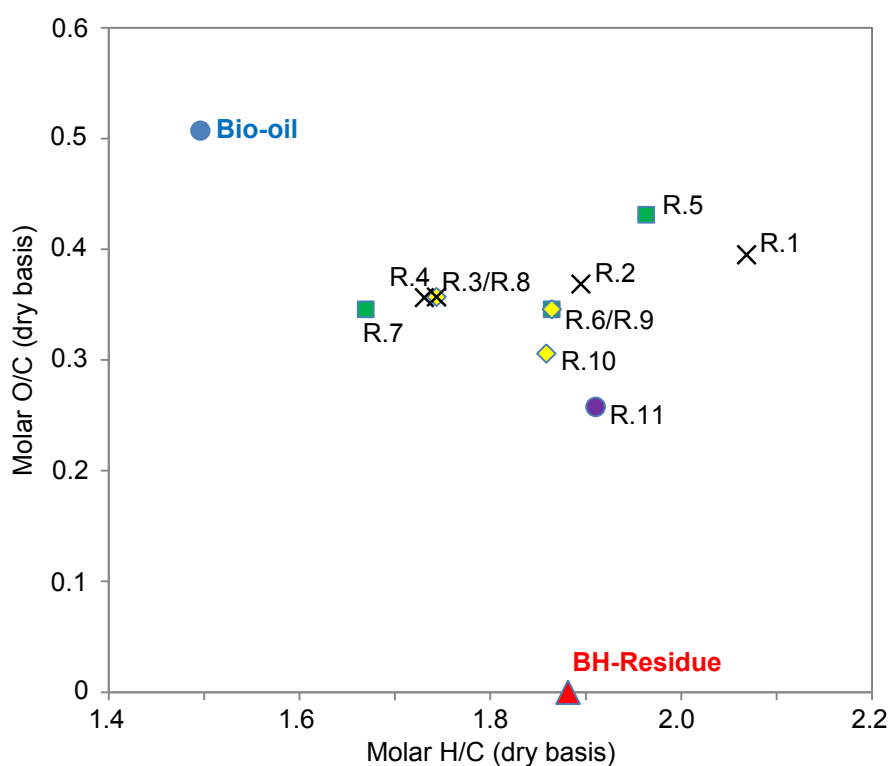
Thus, in order to get more insight into the effect of reaction conditions on catalytic performance of the best performing catalyst 10Ni10Co/HZSM-5, several test series were performed. First, the reaction was performed at different temperature (250, 280, 300, 320 °C) while keeping other parameters (5 g of bio-oil, 25 g of H₂O, 0.5 g of catalyst and P = 40 bar H₂ at RT) (runs 1-4 in Table 5.3). Second, the effect of reaction time on HDO performance with 10Ni10Co/HZSM-5 was investigated with three tests over 2 h, 4 h and 6 h (runs 5-7). Next, testing with different H₂ initial pressure (40, 50 and 60 bar at RT) was carried out (runs 8-10). Furthermore, a run with higher catalyst to bio-oil ratio of 20 wt% was conducted (run 11). The range of the catalyst to bio-oil ratio was selected based on the results of Duan and Savage [63]. Higher catalyst loadings lead to more light gas components and coke formation, hence more carbon was lost and DOD was decreased.

Table 5.3 provides the experimental results of these runs together with the elemental compositions of the starting material bio-oil (run 0). In addition, a van Krevelen plot for the product properties from those runs is depicted in Figure 5.6. The diagram shows that the molar H: C ratios of oil phases from all runs are always higher than that of bio-oil (H: C ~ 1.5), whereas the molar O: C ratios are always less. The impact of the reaction conditions is also visualized in Figure 5.7, which summarizes the composition of the gas phase from each run with 10Ni10Co/HZSM-5.

Table 5.3. Effect of the different reaction conditions of bio-oil HDO on 10Ni10Co/HZSM-5.

runs [a]	T (°C)	P (bar)	t (h)	Product yields [c]					Elemental composition of bio-oil and oil phase (dry)				DOD (%)	HHV (MJ/kg)
				UBO	AQ	Gas	Char	Loss	C	H	N	O		
0				Bio-oil					55.3	6.9	0.3	37.4		21.9
1	250	40	4	36.0	39.8	8.2	1.67	14.4	58.6	10.1	0.4	30.9	17	28.8
2	280	40	4	34.4	40.3	9.2	1.76	14.4	60.4	9.5	0.3	29.7	21	28.9
3	300	40	4	35.5	40.5	9.8	1.93	12.2	61.5	8.9	0.4	29.3	22	28.4
4	320	40	4	33.9	36.1	13.8	2.02	14.1	61.6	8.9	0.3	29.2	22	28.4
5	300	50	2	35.9	38.5	8.3	2.10	15.2	57.3	9.4	0.3	33.0	12	27.0
6	300	50	4	36.9	39.3	9.6	1.79	12.4	61.7	9.6	0.3	28.4	24	29.6
7	300	50	6	35.0	39.6	10.2	1.92	13.3	62.3	8.7	0.4	28.7	23	28.4
8	300	40	4	35.5	40.5	9.8	1.81	12.3	61.5	8.9	0.4	29.3	22	28.4
9	300	50	4	36.9	39.3	10.2	1.79	11.8	61.7	9.6	0.3	28.4	24	29.6
10	300	60	4	37.0	38.4	10.2	1.62	12.8	63.8	9.9	0.3	26.0	30	29.7
11 ^[b]	300	60	4	36.7	35.3	14.6	2.03	11.3	66.4	10.6	0.3	22.8	39	33.6

[a] Reaction conditions: 5 g bio-oil, 25 g H₂O, 0.5 g catalyst; [b] 1 g catalyst.
[c] UBO = upgraded bio-oil or oil phase, AQ = aqueous phase, Gas = gas phase.

**Figure 5.6.** van Krevelen plot of bio-oil and UBO products at different reaction conditions over 10Ni10Co/HZSM-5.

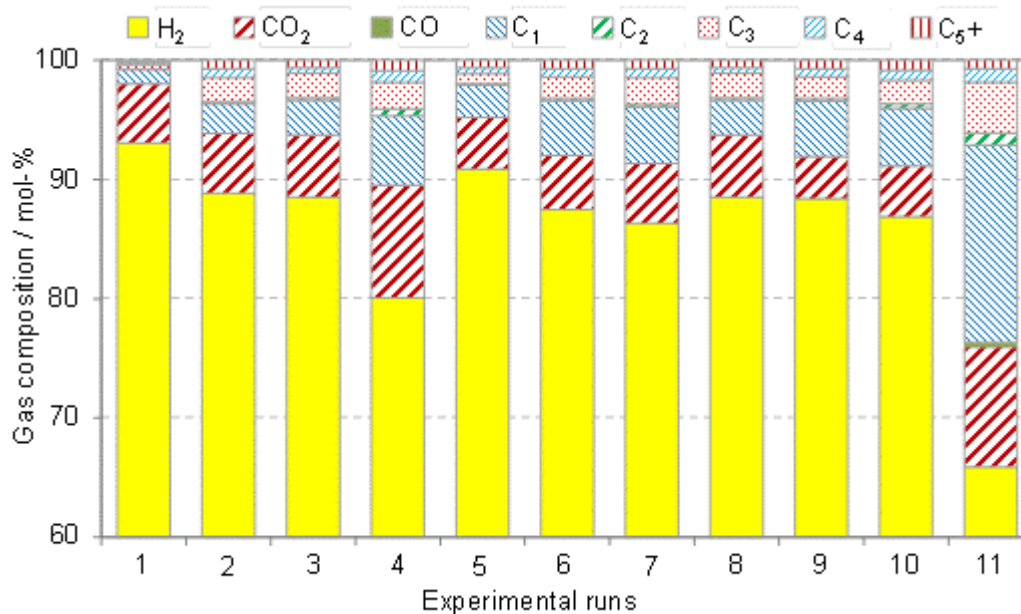


Figure 5.7. Gas distribution obtained with 10Ni10Co/HZSM-5 catalyst at different conditions.

5.4.1 Effect of reaction temperature

Rising the temperature from 250 °C to 320 °C (runs 1-4) led to an increase in DOD from 17 to 22%, and simultaneously the yield for oil phase dropped slightly from 36 to 33.9%. The higher DOD comes along with a decrease in molar O: C ratio of the liquid product. Figure 5.6 shows that already at 250 °C the molar O: C ratio was lowered significantly (~ 0.39) compared to original bio-oil (O: C ~ 0.51), and dropped further at 300 °C (O: C ~ 0.35). The formation of high amount of CO₂ and in particular methane (see Figure 5.7) via hydrocracking could be responsible for the lower oil yield. Moreover, the molar H: C ratio at 250 °C (H: C ~ 2.1) was significantly higher than that of bio-oil. This can be attributed to initial hydrogenation of oxygenated compounds (aldehydes, ketones) which is favourable at lower temperature [77, 82]. However, the molar H: C ratio was reduced with the increase of temperature. This might be due to dehydrogenation on the metal sites and dehydration on the available Brønsted acid sites of the support at higher temperature, forming olefins and aromatics, the latter of which might also act as coke precursors. The result from HDO of phenol as a model compound with the same catalyst in previous chapter confirmed that the selectivity toward benzene and cyclohexene increases with temperature. As the objective of this study is to decrease the oxygen content and to retain the oil yield, the temperature of 300 °C was therefore selected for further investigation.

5.4.2 Effect of reaction time

Obviously, the oil yield slightly increased with prolongation of the reaction time from 2 h to 4 h at 300 °C, but decreased slightly after 6 h (runs 5-7), implying that the oil phase is further hydrocracked to gaseous products [51]. This observation is confirmed by an increase of the concentration (respective total amount) of gaseous components such as CO₂ (via deoxygenation) and gaseous alkanes via cracking (Figure 5.7). Similar to the increase of temperature, the prolongation of run time makes the reaction conditions more severe, and hydrocracking comes to the foreground. Simultaneously, the DOD was increased significantly from 2 h to 4 h, but only little from 4 h to 6 h. This may point to a higher reaction rate of HDO compared to conventional hydrocracking (which is usually run at higher pressure and temperature). Furthermore, the amount of solids (char) decreases slightly from 2 h to 4 h but increases slightly at the longest reaction time. Further prolongation of reaction time leads to a slight rise of molar O: C ratio in the oil phase, most likely due to a shift towards oxygen-free hydrocarbons in the gas phase; at the same time, the molar H: C ratio is lowered. Therefore, 4 h reaction time is considered as optimum in terms of oil yield.

5.4.3 Effect of pressure

The DOD was increased gradually by raising the initial hydrogen pressure at RT from 40 to 60 bar (at 300 °C, runs 8-10, Table 5.3). Due to the pressure limit of the autoclave, the reaction was not run at higher pressure. The product gas composition also changed with the pressure increase, particularly the concentrations of methane and other hydrocarbons increased at the cost of CO₂, whereas the decreasing hydrogen fraction indicates higher hydrogen conversion (Figure 5.7). A higher initial hydrogen pressure enhances the solubility of hydrogen in the reaction mixture, and thereby increases the hydrogen concentration near the active sites and consequently the rates of hydrogen consuming reactions [18]. This is in connection with a slight growth of oil phase yield, but more importantly, the oxygen content of the oil phase was decreased gradually. Interestingly, the CO₂ fraction in the gas phase drops slightly at higher pressure, which might indicate that other reactions than decarboxylation or decarbonylation (C-C bond cleavage) come to the foreground, e.g., hydrogenolysis of C-O bonds or methanation of CO/CO₂ is promoted. As a consequence, more water would be formed and the molar O: C ratio would drop. The nature of the functional groups will be discussed in one of the following chapters according to NMR results (chapter 5.4.5). The effect of pressure can be seen in Figure 5.6, in which the molar H: C ratio is higher and molar O: C is lower with increasing pressure.

5.4.4 Effect of catalyst amount

One more experiment was conducted at 300 °C with an initial hydrogen pressure of 60 bar, but with doubling the catalyst to bio-oil ratio to 20 wt% (run 11 in Table 5.3). The DOD increased significantly and reached 39%, while the amount of oil phase was reduced slightly. The gas distribution (Figure 5.7) showed that the hydrogen conversion was significantly increased, whereas the concentrations of CO₂, methane and other hydrocarbons were increased significantly compared to those obtained with lower amount of catalyst (run 10). For instance, the total yields of CO₂ and methane (with respect to the feed) are 6.3 and 11.2 wt% for run 10 and run 11, respectively. The increase of molar H: C ratio and even more the decrease of molar O: C ratio (Figure 5.6) at higher catalyst to bio-oil ratio points to a higher overall contact time between oxygenates and catalyst, allowing deeper hydrogenation of the feed and leading to an improved performance [63].

Thus, the highest oil yield on wet basis (37 wt%) and DOD (39%) were achieved with the bimetallic catalyst 10Ni10Co/HZSM-5 under the investigated conditions. The typical properties of this UBO fraction are shown in Table 5.1. Obviously, the hydrogen content in UBO was increased significantly and the oxygen content was decreased, leading to higher molar H: C and lower molar O: C ratios and finally higher HHV compared to original bio-oil. The change in functional groups during reaction will be discussed in following sub-chapter. Finally, an UBO obtained with a higher catalyst amount (produced in separate experiments, not described here) was used for co-processing tests that will be described in Chapter 6.

5.4.5 Chemical analysis

In order to get more insight into transformations of functional groups during reaction, ¹³C-NMR spectra of original bio-oil and the UBO obtained with the best performing catalyst 10Ni10Co/HZSM-5 were recorded. The spectra of the two samples are presented in Figure 5.8. Obviously, there are numerous peaks in the range of 10-50 ppm for both samples; however, signals of aliphatic carbon atoms in the range of 10-20 ppm were much more pronounced for the UBO compared to the parent bio-oil. In addition, various peaks in the 50-65 ppm range, which corresponds to R-CH₂-OH (alcohol), disappeared in the UBO spectrum. This points to the remarkable capability of this catalyst to activate hydrogen and to cleave C-O bonds. Furthermore, the feed showed resonances at 160-180 ppm and 180-210 ppm, which are attributed to carboxylic acids, aldehydes and ketones. These peaks vanished almost completely in the UBO spectrum. Both spectra show peaks at 110-160 ppm, which relate to the alkenyl and aromatic carbon atoms;

however, these peaks are much more prominent in the UBO, especially for the 120-130 ppm region.

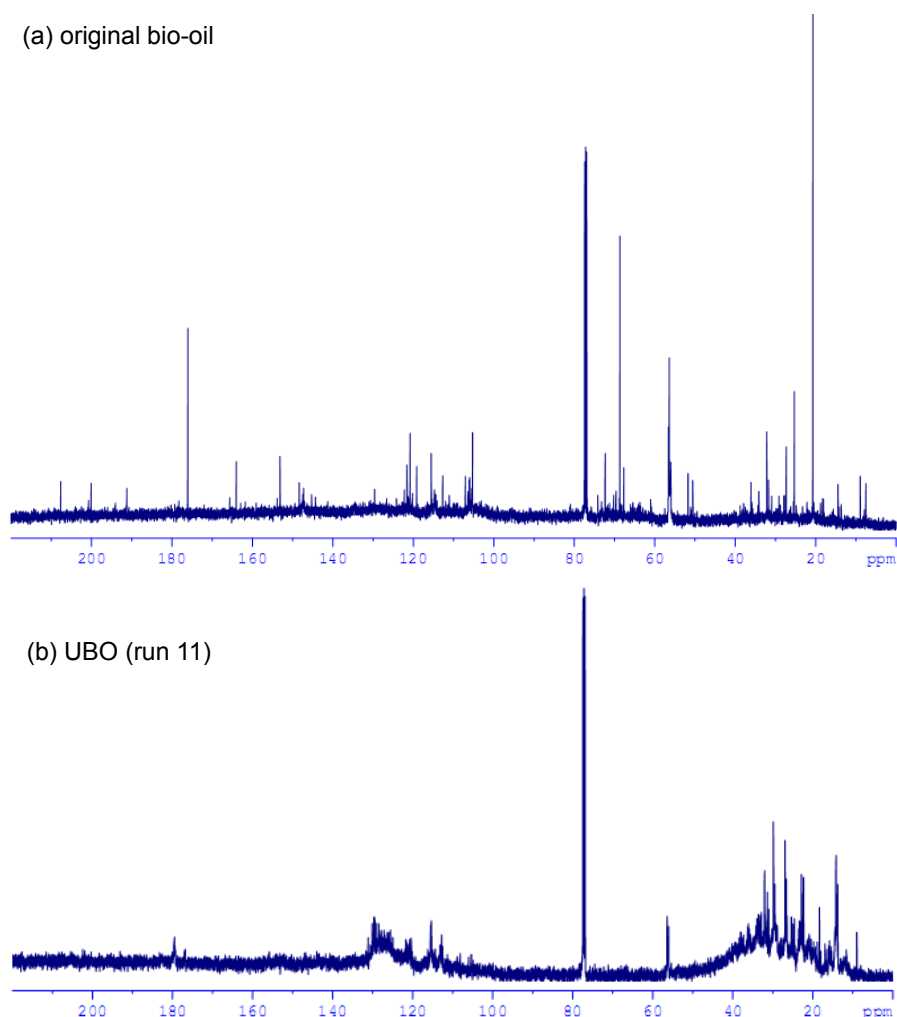


Figure 5.8. ^{13}C -NMR spectrum of original bio-oil (a) and UBO (b).

The NMR results evidence that there are significant changes in the chemical nature of the bio-oil during HDO. The fractions of carboxylic acids, ketones, aldehydes and alcohols are reduced significantly, whereas the fractions of aliphatic and aromatic carbon atoms increased strongly. This result is also in line with the GC-MS analysis of both samples (see Figure A10 in Appendix A).

5.5 Summary and conclusions

The transfer of reaction conditions and processing concepts from model reaction (phenol HDO) to the conversion of bio-oil is challenging due to its complex composition. In the course of investigation of reaction conditions over 10Ni10Co/HZSM-5, pressure, reaction time and catalyst amount showed significant effect on the DOD, the oil yield and the molar

H: C and molar O: C ratios. Temperature showed weaker impact on catalyst performance, as increasing temperature leads to slight increase of DOD and volume of gas phase, leading to an reduced oil phase.

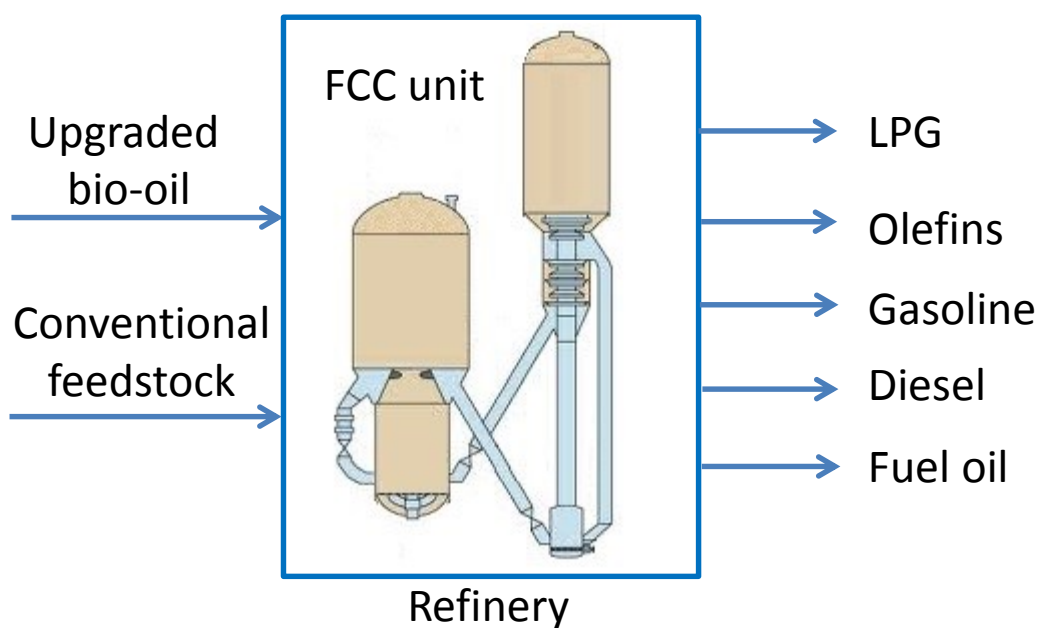
In addition, the influence of the supports in 10Ni10Co based catalyst shows that HZSM-5 is the best compared to other supports. This can be related to acid properties, surface area, particle size and hydrothermal stability. Therefore, the results from this chapter, i.e. using bio-oil, further confirm the established reaction network from model reaction described in previous chapters.

As a result, bio-oil upgraded with 10Ni10Co/HZSM-5 (UBO) was selected for further tests in co-processing with conventional feed in a FCC unit.

Chapter 6

Co-processing of Upgraded Bio-oil with Conventional Feed in a FCC unit

The target of this chapter is to demonstrate the effect of co-processing of upgraded bio-oil with conventional feed in a FCC unit using an equilibrated catalyst. Therefore, the product obtained from HDO of bio-oil over 10Ni10Co/HZSM-5 was selected as a feed for co-processing with different percentages with conventional feed.



6.1 Feedstocks and catalyst

A schematic configuration of a commercial refinery in Vietnam is shown in Figure 6.1 [148]. FCC is one of the most important conversion processes used in petroleum refineries and might offer sufficient capacity to co-process large streams of UBO. FCC unit is responsible in the refinery for conversion of heavy oil (bottom residue from crude oil atmospheric distillation, denoted as BH-residue) to light valuable components, e.g LPG and gasoline. Thus, to stay as close as possible to the regular FCC conditions, a typical equilibrated FCC catalyst and conventional feed from the named refinery were used.

Table 6.1 shows the physico-chemical properties of an equilibrated Re-USY FCC catalyst. The bio-oil was upgraded with 10Ni10Co/HZSM-5 at the given conditions ($T = 300\text{ }^{\circ}\text{C}$, 60 bar at RT, $t = 4\text{ h}$, catalyst to oil mass ratio = 0.2 g/g) as described in previous chapter. The conventional FCC feed and equilibrated catalyst for the tests were obtained from Vietnam Petroleum Institute (VPI). The properties of BH-residue and UBO are already shown in Table 5.1 in previous chapter. Various fractions (0, 5, 10 and 20 wt%) in the feed were used. The obtained FCC feed samples were denoted according to weight percentage of the UBO in the feeds (0UBO, 5UBO, 10UBO, 20UBO).

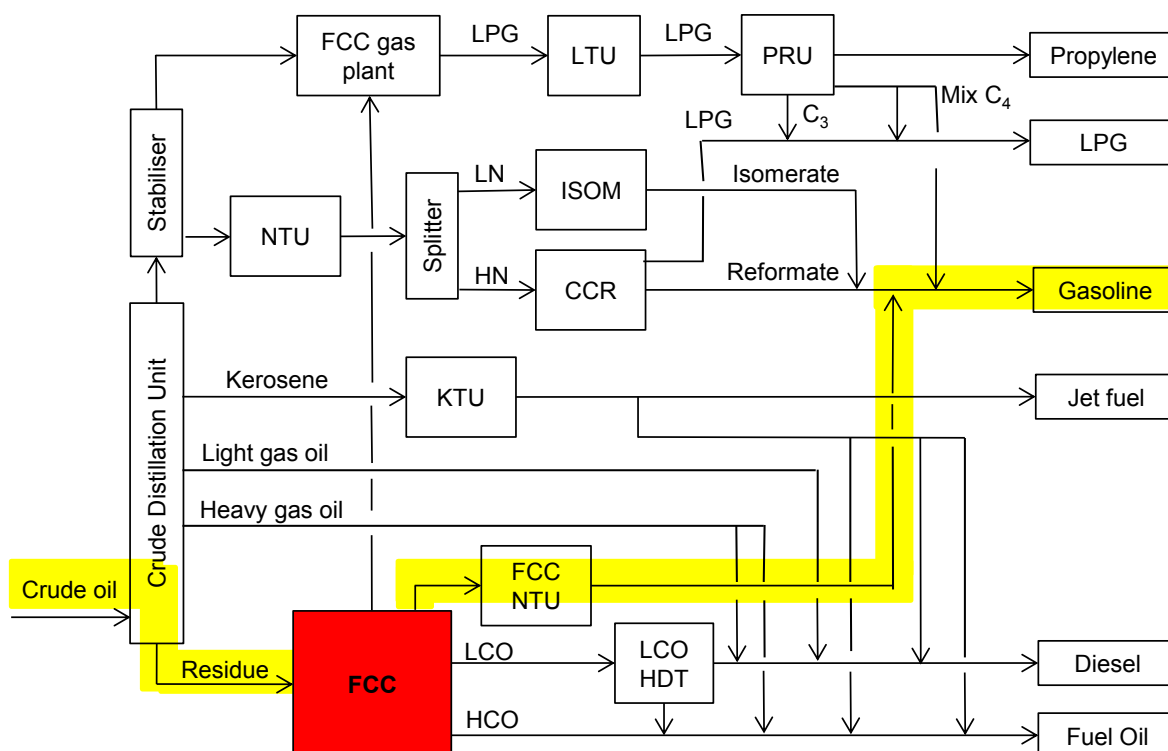


Figure 6.1. Schematic configuration of a commercial refinery in Vietnam.

Table 6.1. Physico-chemical properties of the equilibrated FCC catalyst (Re-USY).

Properties	
BET area (m ² /g)	125
Zeolite area (m ² /g)	63
Matrix area (m ² /g)	62
Pore size (nm)	8.8
Unit cell (nm)	2.43
Chemical composition (wt%)	
Al ₂ O ₃	55.30
Re ₂ O ₃	1.14
CaO	0.17

6.2 Catalytic cracking

In a commercial FCC unit, the catalytic cracking reactions normally runs in a riser-reactor, where the feed contacts with a catalyst and reacts within very short time (1.5-3 seconds) [149]. The catalyst and products are quickly separated at the reactor outlet (using cyclones) in order to avoid thermal and non-selective cracking reactions of the desirable products. The spent catalyst falls into a stripper and finally regenerates in a regenerator. To predict and evaluate FCC catalyst activity and selectivity, the MAT technique has become a widely applied method in laboratory, instead of performing time-consuming and costly test runs in pilot plants or commercial units. In this study, the use of fixed bed SR-SCT-MAT unit simulates accurately the commercial cracking unit. The system operates with a single shot at very short contact time, the reactor was designed with no dead volume and a feed injection with both oil and nitrogen was modified to simulate a transition state from the feed injection to the stripping phase as in standard unit, and finally a single receiver serves to collect liquid and gaseous products [150].

Several MAT runs with the same equilibrated catalyst and various fractions of UBO in the feed and different CTO ratios were performed at FCC conditions (520 °C, 1 bar, CTO = 2.5 or 3) in order to demonstrate the effect of co-feeding of UBO on the cracking of BH-residue. The product distribution from the MAT runs with these co-feed mixtures (5UBO, 10UBO, 20UBO) will be discussed and compared with that of the 100% conventional feed (0UBO). Table 6.2 presents the main results observed with respect to the conversion and product yields as a function of the various fractions of the UBO in the feed and the CTO ratios.

Table 6.2. The effect of the CTO ratios and the UBO fractions in co-processing tests.

Samples	0UBO	5UBO	10UBO	20UBO	0UBO	5UBO	10UBO	20UBO
	2.5				3			
CTO ratio (g/g)								
Mass balance (wt%)	99.2	99.3	100.6	97.0	100.0	97.6	99.9	95.8
Conversion (wt%)	80.3	76.8	70.9	64.0	79.2	81.2	80.3	78.1
Product yields (wt%)								
Gas	21.4	19.8	17.4	16.8	21.3	21.7	22.2	21.0
Gasoline	55.6	54.0	49.9	43.9	53.5	55.5	54.2	52.6
LCO	10.8	10.8	15.1	12.2	10.3	11.1	13.0	13.6
HCO	8.8	12.4	14.0	23.8	10.5	7.7	6.6	8.3
Coke	3.3	3.0	3.6	3.3	4.4	3.9	3.9	4.6

Obviously, at a CTO ratio of 2.5 (g/g), which correlates to somewhat milder reaction conditions in terms of residence time and respective catalyst load, the conversion decreased gradually with the increase of the UBO fraction from 80% to 65% (with the 20UBO sample). In contrast, the conversions of all samples were slightly higher at the CTO ratio of 3 (g/g). This demonstrates that the oxygenated compounds in the UBO are more recalcitrant to cracking due to the many O-containing functional groups and the lower H-content (e.g. phenols, guaiacols, syringols and dimers) as discussed in previous chapters. This observation is in line with the results of Mercader et al. [77], who stated that a slightly higher CTO ratio is required for co-processing of UBO with conventional feed (Long residue) in order to obtain an equivalent conversion.

Regarding the product distribution at the CTO ratio of 2.5 (g/g), the gas and gasoline yields decreased slightly when raising the amount of UBO, whereas the LCO and HCO fractions increased gradually. The slight increase of the LCO content could be related to either the existence of components in the LCO range in the UBO or to cracked products of the co-feed in the LCO range. It should be noted that the LCO fraction from the FCC unit is normally used for diesel fuel blending. The gas and gasoline yields at the CTO ratio of 3 (g/g) were similar for both the BH-residue and the co-feeds, whereas a considerable change in the yield of the LCO and HCO fractions was observed. The LCO yield was increased gradually and the HCO yield showed the reverse trend (especially with 20UBO), indicating the subsequent cracking of heavy components in the HCO fraction to form lighter components in the LCO range (particularly for the 5UBO and 10UBO samples) or the gas range.

This result was in line with the observation of increasing fractions of gas components (dry gas (C₁, C₂), LPG (C₃, C₄) and CO/CO₂) with increasing UBO fraction in the feed (see Table 6.2 and Figure 6.2). However, at the CTO ratio of 2.5 (g/g), the contents of LPG and

olefins ($C_2=$, $C_3=$) were reduced gradually with the increase of the UBO fraction in the feed, whereas dry gas fraction was increased slightly (see Figure 6.2). The detailed gas composition can be seen in Table A2 in Appendix A.

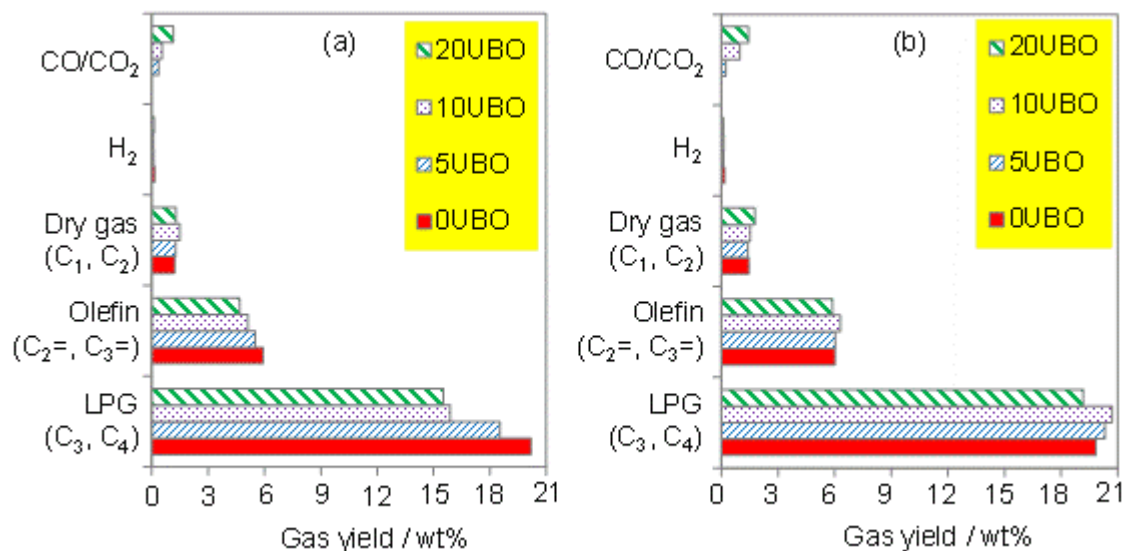


Figure 6.2. Gas yield in the co-feed tests at (a) CTO = 2.5 (g/g) (b) CTO = 3 (g/g).

It should be noted that CO and CO₂ were solely formed with the co-feed samples as a result of cracking of oxygenated compounds and these amounts were increased with raising the UBO fraction. It is well known that the gas fraction from the FCC unit is normally fed to gas processing unit in which the gases will be separated to get more valuable gaseous fractions for further uses (e.g. olefins, LPG). Some of them will be converted to other product (e.g. H₂S will be converted to sulfur via the Claus process). The remaining gases are used internally as refinery fuel. The release of CO/CO₂ should be taken into account to fulfil the specification from gas emission in refinery.

Furthermore, the hydrogen fraction was reduced for the co-processed feeds compared to 100% conventional feed, possibly due to hydrogen consumed in other reactions (e.g. hydrogenation, hydrogenolysis) of oxygenated components in UBO [73, 78].

As catalytic cracking of oxygenates runs via complex reaction pathways involving different classes of reactions, namely, cracking of large molecules to smaller molecules, dehydration, hydrogen-producing reactions (e.g. steam reforming, dehydrogenation), hydrogen-consuming reactions (hydrogenation, hydrogenolysis, dehydration), Aldol condensation or Diels Alder reaction [73]. As a consequence, the catalytic cracking of such biomass derived feedstock in presence of a fossil feed showed a synergetic effect due to coupling of such reactions [151]. This can be seen from the result above, as BH-Residue can act as hydrogen donor, which provides the hydrogen to reduce the

oxygenated compounds in UBO, resulting in high hydrogen consumption in co-feeds test as well as to increase the cracking of oxygenates in UBO. The effect is also known from cracking of model compound (m-cresol) with hexanes over HY zeolite as recently reported by To and Resasco [152], who reported that co-feeding of small amounts of m-cresol at low reactant concentrations caused fast deactivation of catalyst. Nevertheless, increasing the paraffin concentration interestingly hindered the deactivating effect of m-cresol. The authors proposed the observation due to the hydride transfer between a phenolic compound and the paraffin.

Graça et al. [75] also reported on catalytic cracking of a mixture of conventional gas oil with several model compounds (acetic acid, phenol or hydroxyacetone). An increase in yields towards fuel gas, LPG and gasoline and a slight coke decrease were observed. The authors interpreted this by a preferential adsorption of the feed and intermediates on the catalytic surface instead of the oxygen containing compounds.

Coke deposition appears as a major problem in heterogeneous catalysis, particularly in the case of cracking of oxygenated model compounds and untreated bio-oils [77, 153, 154]. In this study, a slight increase in coke yield was observed with the increase of the CTO ratios and cracking severity. However, there was no significant difference in observed coke yield between co-feeds and 100% conventional feed, independent of the CTO ratios. It is difficult to explain the observed trends compared with literature data because different FCC catalysts, feeds and set-ups with different contact times were used [68]. Coke deposition is well-known to be a function of several factors such as catalyst activity, space time, temperature and molar H: C ratio of the feed [155, 156]. However, these results indicate that the FCC process seems to be rather insensitive to UBO admixture with regard to coking.

The gasoline fraction is the primary objective of a FCC unit as highlighted in Figure 6.1. Therefore, the composition of the gasoline fraction obtained with the 4 samples tested at a CTO ratio of 3 (g/g) was analyzed to see the impact of co-feed on this product range (Figure 6.3). Clearly, co-processed feeds give larger amounts of aromatic compounds in the gasoline as compared to 100% conventional feed. This is not surprising as the UBO initially contains aromatic compounds (see Figure 5.8 b) and additionally they are more refractory to cracking than a paraffinic feedstock because of the lower H-content. Additionally, the iso-paraffins and olefins fractions were reduced compared to 100% conventional feed while the n-paraffins and naphthenes fraction was more or less the same. The increase of aromatics in co-processed feeds can be countered by optimizing the blend ratio of gasoline fractions from the different units in a standard refinery (e.g. FCC, reforming, isomerization) to adapt the limit values of aromatics in gasoline.

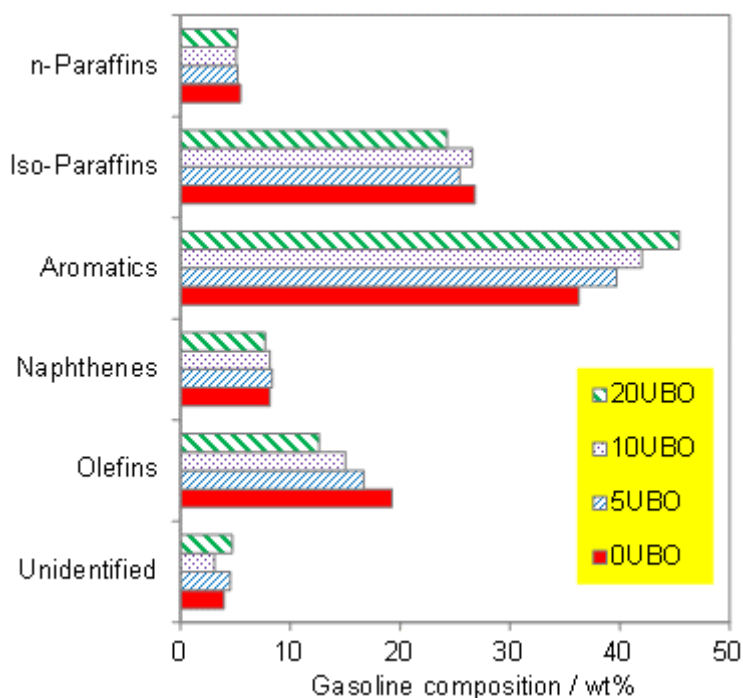


Figure 6.3. Gasoline composition in the products from co-feed tests at 520 °C and CTO = 3 (g/g).

6.3 Summary and conclusions

In sum, it is revealed that the co-processing of the UBO containing roughly 23 wt% oxygen with a conventional feedstock using a commercial catalyst in a lab-scale FCC unit is successful and thus provides valuable data on the effect of the most important process parameters related to co-processing. Conversion and selectivities toward desired products (gas, gasoline, LCO) are reduced at the mild conditions (lower CTO ratio). However, at the higher CTO, the HCO yield is reduced gradually, leading to a slight increase in the desired fractions at a similar conversion. It is suggested that higher CTO ratio should be used for the application of UBO in the standard FCC unit in the conventional refinery. The successful co-processing points out that the preliminary mild HDO step is indeed necessary to reduce the fraction of highly active components (coke precursors) and stabilize the bio-oil without the full deoxygenation.

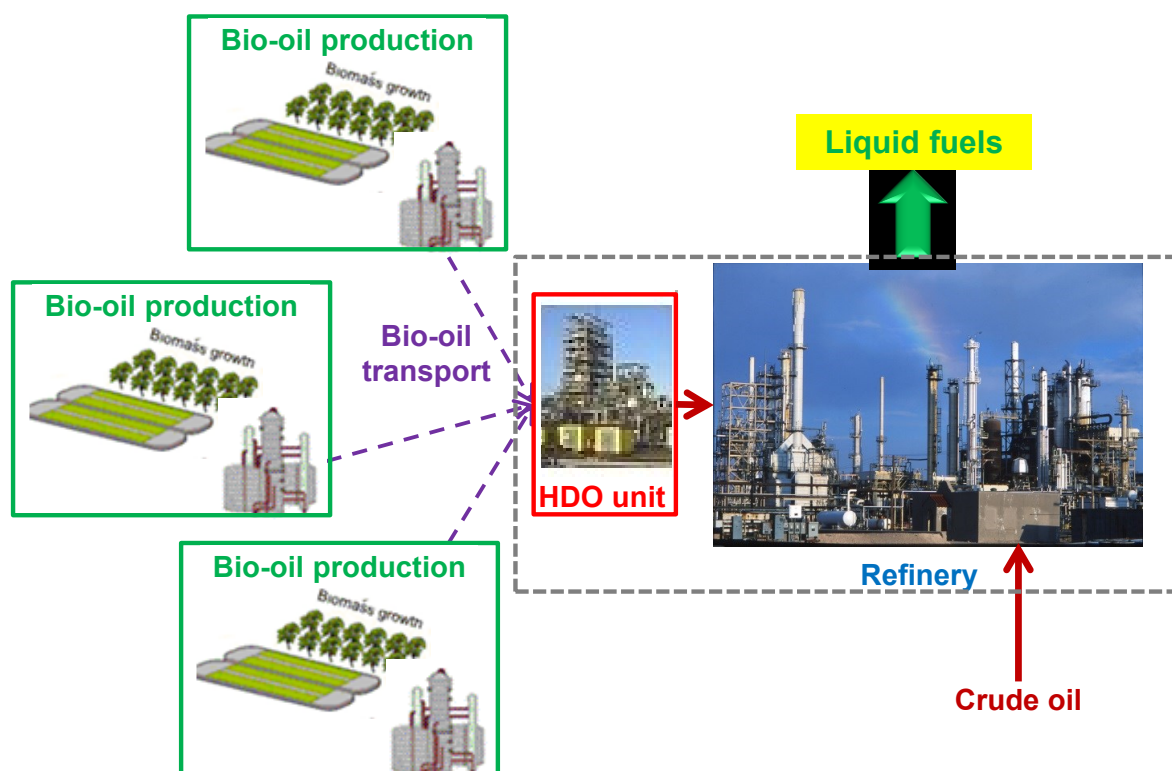
In addition, higher content of aromatics and lower amount of olefins are found in gasoline composition in co-feeding test, whereas the gas fraction contains a small amount of CO₂ and CO as compared to the conventional feed. The optimization step (blending) in refinery could help to adapt the final specification of these fractions. Coke formation is not significantly different in both feeds, further confirming the potential in such tests. Last but

not least, these results might give opportunities for the fast implementation of such renewable liquid fuels from bio-oil obtained from second generation biomass.

Chapter 7

Conclusions and Outlook

The main findings and contribution of this thesis with respect to potential and perspectives for the provision of renewable liquid fuels is summarized in this chapter. Some recommendations for further improvement is also given.



7.1 The role of second metal in bimetallic catalysts for bio-oil HDO

Developing highly active catalysts for hydrodeoxygenation (HDO) of bio-oil obtained from FP process is the biggest challenge up to now for researchers. Various catalyst systems have been tested for bio-oil HDO, e.g., supported noble metal (Pt, Pd, Ru, Rh,...), supported non-noble metal (Ni, Cu, Co, Fe, ...), HDS catalysts (CoMoS₂/Al₂O₃, NiMoS₂/Al₂O₃) and so on. Bimetallic catalysts often show different activity and selectivity compared to corresponding monometallic catalyst. In the present work, therefore, bimetallic Ni based catalysts have been developed for bio-oil HDO.

Ni/HZSM-5 catalyst has been modified with second metals Cu and Co. The first test series with phenol as a model compound for bio-oil in a batch reactor revealed that the presence of Ni is essential for high activity, most likely due to its outstanding capability of H₂ activation and dissociation. Nevertheless, modification with Cu deteriorated the catalytic performance significantly whereas substitution with Co not only increased the activity but also selectivity toward the target hydrocarbons cyclohexane and benzene. Characterization studies performed by using TEM, XPS, XRD, TPR, N₂ physisorption, py-IR and CHN analyzer elucidated detrimental effects of the second metals. Both Cu and Co form alloys with Ni; however, Cu caused a loss of active sites as well as tended to segregate at the near surface region, whereas Co strongly stabilized the active Ni sites and made the particles smaller, thus increasing the dispersion and accelerating the hydrogenation step in the reaction sequence and finally enhancing the activity. Moreover, the addition of Co suppresses the coke deposition as compared with monometallic catalyst.

Additional studies using individual intermediate products such as cyclohexanol, cyclohexanone, cyclohexene and benzene as feeds point out the impact of the catalyst composition on key reaction steps. A catalyst Ni-Co/HZSM-5 with 10 wt% of each metal showed almost 100% hydrocarbon selectivity at complete conversion. Hence, this Ni-Co/HZSM-5 with optimum mass Ni: Co ratio (= 1) together with the corresponding 21Ni/HZSM-5 (as a reference) should be used for further investigation.

7.2 The effect of supports in bimetallic catalysts

Two general pathways have been proposed for HDO of phenol such as: (i) direct deoxygenation or hydrogenolysis to benzene, (ii) hydrogenation of aromatic ring followed by dehydration and subsequent hydrogenation toward cyclohexane. Two types of active sites (metal and acid sites) are necessary for the consecutive reactions. The specific surface area of catalyst and acid sites usually is determined/introduced by supports. Thus,

different acidic materials (HZSM-5, HY, HBeta and ZrO₂) were selected to study the impact of support on catalyst performance. The testing with two series of monometallic (20Ni) and bimetallic (10Ni10Co) catalysts on these supports in a batch reactor revealed that the bimetallic catalysts outperform the monometallic catalysts. The tests also emphasized that the acidities of supports strongly affect the product distribution. In this respect, a higher acidity leads to higher selectivities toward deoxygenated products (benzene, cyclohexane, cyclohexene and MCP), whereas majority of oxygenated products (cyclohexanol, cyclohexanone) are found in catalysts with lower acidity. The combination of metal and acid sites is necessary for the effective elimination of oxygen from phenol, in which metal sites promote the hydrogenation reaction of phenol to cyclohexanone/cyclohexanol and benzene/cyclohexene to cyclohexane, whereas acid sites are needed for the dehydration reaction and to activate oxygenates. The impact of the supports was further confirmed with tests in a continuous fixed bed reactor and shows the same dependencies. The tests with the different modes of operation (batch and continuous runs) gave more detail in impact of supports, and the continuous runs extend the information on the reaction network with consecutive reactions due to the improved control of contact time.

In addition, the hydrothermal stability of the support should be considered in aqueous phase reaction. In fact, the HY and HBeta show a low resistance against aqueous environment as proved by XRD and N₂ physisorption method, bringing low activity and stability in a continuous flow reactor. Among the studied catalysts, HZSM-5 containing bimetallic domains is found as an excellent solid owing to its HDO performance and high acidity as well as high hydrothermal stability.

7.3 Performance of Ni-based catalysts in HDO of phenol

Apart from the support, various reaction conditions (temperature, pressure, reaction time, WHSV) affect the reaction pathways and catalyst performance in both batch experiments and continuous flow reactor. Of the investigated conditions, high H₂ pressure leads to an increase of saturated hydrocarbon fraction in the product mixture due to high H₂ solubility in the reaction mixture and provides more available H₂ on catalyst surface, which strongly promotes the hydrogen consuming reactions (e.g. hydrogenation). On the other side, the strong temperature-selectivity dependence causes a significant change in product distribution, e.g. the formation of benzene and MCP at high temperature and the formation of cyclohexane at low temperature. Decreasing the reaction time (batch) or contact time (flow reactor) finally lowers the conversion and selectivity toward hydrocarbons, which are formed in the last steps of the reaction network.

The prolonged tests at the given condition (250 °C, 60 bar, WHSV = 1.8 h⁻¹, H₂: phenol molar ratio = 28) show that 10Ni10Co/HZSM-5 is highly stable with almost 100% conversion and slight reduction (from 100% to 90%) in selectivity toward deoxygenated products after 24 h on-stream. In contrast, 21Ni/HZSM-5 shows a decline in both the phenol conversion (from 100 to 83%) and deoxygenated products selectivity (from 100 to 86%), which originate from the lower number of Brønsted acid sites and high coke formation, the fast Ni agglomeration and Ni leaching compared to bimetallic catalyst, which is confirmed by data of various characterization techniques for the spent catalysts.

7.4 HDO of bio-oil and subsequent co-processing in a standard refinery unit

The advantage of bimetallic catalysts is evident in the test series with bio-oil which reveals the outstanding performance of 10Ni10Co/HZSM-5 compared to 21Ni/HZSM-5 and other bimetallic catalysts in terms of DOD and oil yield. The catalyst shows an excellently balanced combination of metal and acid sites to accelerate all the elementary steps in the preferred deoxygenation pathway. In addition, the high hydrothermal stability and Ni-Co alloying are beneficial for the obtained high performance as well. These results further confirm the results from model reactions.

The bio-oil upgraded with the best performing catalyst (UBO) was ultimately used for a co-processing test with conventional feed (atmospheric distillation residue) in a commercial lab-scale FCC unit. A lower catalyst-to-oil (CTO) ratio (CTO = 2.5 g/g) slightly lowers both conversion and yield for desired products. With at higher CTO value (CTO = 3 g/g), the reduction of HCO yields leads to the slight raising of desired fraction (gasoline, gas and LCO) at a similar conversion. These results indicate that the FCC unit is rather insensitive to such UBO co-feeding.

In conclusion, the introduction of second metal (Co) into the Ni based catalyst not only improves the activity but also shifts selectivity towards highly stable deoxygenated products under mild conditions. The superior catalytic performance of bimetallic catalysts in both model reaction and bio-oil HDO originates from the high dispersion owing to alloying and a good combination of metal and acid sites, which enables the bimetallic catalyst to effectively promote the key steps in the reaction network. Upgraded bio-oil is successfully co-processed with a conventional feed using a commercial catalyst in FCC unit with high yield, which in turn shows the potential for renewable liquid fuels production from bio-oil.

7.5 Outlook

The results of the present work show opportunities to combine a mild HDO step and subsequent co-processing at FCC conditions. Future works should continue the tests in a continuous flow reactor with bio-oil or its aqueous fraction over the developed catalysts, which are not performed yet in this work due to the lack of a suitable equipment (e.g. special pump for feeding of high viscosity bio-oil, proper reactor). Additionally, further use and development of suitable techniques for bio-oil and UBO analysis and quantification would be attractive and supportive. All of this might give more insights in the bio-oil upgrading.

Future trials with different catalyst preparation techniques (e.g. sol-gel method) and optimization of the catalyst preparation parameters (e.g. calcination temperature, heating rates) are recommended that might further improve the catalyst performance and avoid the metal agglomeration during reaction. Additionally, trials with other supports based on micro-mesoporous composites might improve the hydrothermal stability and accessibility. Apart from that, the tests in a suitable setup for kinetic and mechanistic measurements would provide valuable knowledge and understanding of structure-reactivity relationship. Some of those have been now started via an international project in our department.

The co-processing should be more deeply investigated using standard conventional feeds and commercial FCC catalysts. With this database, further FCC catalyst modification and development (if any) can be made for fast implementation in standard refinery. As for the upstream FP process, which was not part of the present work, the greater the improvement of FP, the higher the quality of bio-oil during storage and transportation and the easier the upgrading steps.

Finally, these results show a potential pathway for utilization of fuels from renewable source (biomass) via the integration into the existing infrastructure of petroleum industry. Taking advantage of this mature technology assures that the chemical energy of biomass is fixed in fuels to the maximum possible extent. This will help to lower the costs of bringing a new technology to market, guarantee high product quality and promote the acceptance of bio-fuels in general. This could be beneficial for an emerging market like Vietnam and in particular for the development program of Vietnam Oil and Gas Group.

8. References

- [1] BP *Statistical Review of World Energy* June 2015, www.bp.com/en/global/corporate/about-bp/energy-economics/statistical-review-of-world-energy.html.
- [2] I. Dincer, *Renewable Sustainable Energy Rev.* **2000**, *4*, 157-175.
- [3] D. Carpenter, T.L. Westover, S. Czernik, W. Jablonski, *Green Chem.* **2014**, *16*, 384-406.
- [4] J.A. Melero, J. Iglesias, A. Garcia, *Energy Environ. Sci.* **2012**, *5*, 7393-7420.
- [5] G.W. Huber, J.A. Dumesic, *Catal. Today* **2006**, *111*, 119-132.
- [6] A.V. Bridgwater, G.V.C. Peacocke, *Renewable Sustainable Energy Rev.* **2000**, *4*, 1-73.
- [7] D. Meier, B. van de Beld, A.V. Bridgwater, D.C. Elliott, A. Oasmaa, F. Preto, *Renewable Sustainable Energy Rev.* **2013**, *20*, 619-641.
- [8] A.V. Bridgwater, *Biomass Bioenergy* **2012**, *38*, 68-94.
- [9] D.C. Elliott, P. Biller, A.B. Ross, A.J. Schmidt, S.B. Jones, *Bioresour. Technol.* **2015**, *178*, 147-156.
- [10] A. Hammerschmidt, N. Boukis, E. Hauer, U. Galla, E. Dinjus, B. Hitzmann, T. Larsen, S.D. Nygaard, *Fuel* **2011**, *90*, 555-562.
- [11] J. Akhtar, N.A.S. Amin, *Renewable Sustainable Energy Rev.* **2011**, *15*, 1615-1624.
- [12] G.W. Huber, S. Iborra, A. Corma, *Chem. Rev.* **2006**, *106*, 4044-4098.
- [13] A. Bridgwater, in *Thermal Biomass Conversion* (Eds.: A. Bridgwater, H. Hofbauer, S.v. Loo), CPL Press, Newbury, UK, **2009**, pp. 37-78.
- [14] A.V. Bridgwater, in *Biomass power for the world: Transformation to effective use*, (Eds.: W.v. Swaaij, S.R.A. Kersten, W. Palz), Pan Stanford Publishing Pte. Ltd., Great Britain, **2015**, pp. 473-513.
- [15] Y. Zhang, in *Biofuels from Agricultural Wastes and Byproducts*, (Eds.: H. P. Blaschek, T.C. Ezeji, J. Scheffran), Wiley-Blackwell, **2010**, pp. 201-232.
- [16] S.S. Toor, L. Rosendahl, A. Rudolf, *Energy* **2011**, *36*, 2328-2342.
- [17] D. Mohan, C.U. Pittman, P.H. Steele, *Energy Fuels* **2006**, *20*, 848-889.
- [18] P.M. Mortensen, J.D. Grunwaldt, P.A. Jensen, K.G. Knudsen, A.D. Jensen, *Appl. Catal. A* **2011**, *407*, 1-19.
- [19] N. Dahmen, E. Henrich, A. Kruse, K. Raffelt, in *Biomass to Biofuels: Strategies for Global Industries*, (Eds.: A.A. Vertès, N. Qureshi, H.P. Blaschek, H. Yukawa), Wiley, Chichester, UK, **2010**, pp. 89-122.
- [20] E. Furimsky, *Appl. Catal. A* **2000**, *199*, 147-190.

- [21] D.C. Elliott, *Energy Fuels* **2007**, *21*, 1792-1815.
- [22] I. Graça, J.M. Lopes, H.S. Cerqueira, M.F. Ribeiro, *Ind. Eng. Chem. Res.* **2013**, *52*, 275-287.
- [23] P.T. Patil, U. Armbruster, M. Richter, A. Martin, *Energy Fuels* **2011**, *25*, 4713-4722.
- [24] V.N. Bui, D. Laurenti, P. Afanasiev, C. Geantet, *Appl. Catal. B* **2011**, *101*, 239-245.
- [25] V.N. Bui, D. Laurenti, P. Delichère, C. Geantet, *Appl. Catal. B* **2011**, *101*, 246-255.
- [26] M.V. Bykova, D.Y. Ermakov, V.V. Kaichev, O.A. Bulavchenko, A.A. Saraev, M.Y. Lebedev, V.A. Yakovlev, *Appl. Catal. B* **2012**, *113-114*, 296-307.
- [27] X. Zhang, T. Wang, L. Ma, Q. Zhang, T. Jiang, *Bioresour. Technol.* **2013**, *127*, 306-311.
- [28] D.-Y. Hong, S.J. Miller, P.K. Agrawal, C.W. Jones, *Chem. Commun.* **2010**, *46*, 1038-1040.
- [29] F.E. Massoth, P. Politzer, M.C. Concha, J.S. Murray, J. Jakowski, J. Simons, *J. Phys. Chem. B* **2006**, *110*, 14283-14291.
- [30] Y. Romero, F. Richard, S. Brunet, *Appl. Catal. B* **2010**, *98*, 213-223.
- [31] M.J. Mendes, O.A.A. Santos, E. Jordão, A.M. Silva, *Appl. Catal. A* **2001**, *217*, 253-262.
- [32] A.Y. Stakheev, L.M. Kustov, *Appl. Catal. A* **1999**, *188*, 3-35.
- [33] H. Wan, R. Chaudhari, B. Subramaniam, *Top. Catal.* **2012**, *55*, 129-139.
- [34] M. Badawi, J.F. Paul, S. Cristol, E. Payen, Y. Romero, F. Richard, S. Brunet, D. Lambert, X. Portier, A. Popov, E. Kondratieva, J.M. Goupil, J. El Fallah, J.P. Gilson, L. Mariey, A. Traver, F. Maugé, *J. Catal.* **2011**, *282*, 155-164.
- [35] C. Newman, X. Zhou, B. Goundie, I.T. Ghampson, R.A. Pollock, Z. Ross, M.C. Wheeler, R.W. Meulenber, R.N. Austin, B.G. Frederick, *Appl. Catal. A* **2014**, *477*, 64-74.
- [36] P.M. Mortensen, J.-D. Grunwaldt, P.A. Jensen, A.D. Jensen, *ACS Catal.* **2013**, *3*, 1774-1785.
- [37] C. Zhao, J. He, A.A. Lemonidou, X. Li, J.A. Lercher, *J. Catal.* **2011**, *280*, 8-16.
- [38] C. Zhao, S. Kasakov, J. He, J.A. Lercher, *J. Catal.* **2012**, *296*, 12-23.
- [39] T.M. Huynh, U. Armbruster, A. Martin, in *Chemicals and Fuels from Bio-based Building Blocks*, (Eds.: F. Cavani, S. Albonetti, F. Basile, A.A. Gandini), Wiley, **2016**, pp. In press.
- [40] T.V. Choudhary, C.B. Phillips, *Appl. Catal. A* **2011**, *397*, 1-12.
- [41] Q. Bu, H. Lei, A.H. Zacher, L. Wang, S. Ren, J. Liang, Y. Wei, Y. Liu, J. Tang, Q. Zhang, R. Ruan, *Bioresour. Technol.* **2012**, *124*, 470-477.
- [42] H. Wang, J. Male, Y. Wang, *ACS Catal.* **2013**, *3*, 1047-1070.

- [43] M. Saidi, F. Samimi, D. Karimipourfard, T. Nimmanwudipong, B.C. Gates, M.R. Rahimpour, *Energy Environ. Sci.* **2014**, *7*, 103-129.
- [44] E.G. Baker, D.C. Elliott, in *Research in Thermochemical Biomass Conversion*, (Eds.: A.V. Bridgwater, J.L. Kuester), Springer Netherlands, **1988**, pp. 883-895.
- [45] D.C. Elliott, E.G. Baker, *US 4,795,841* **1989**, Patent.
- [46] G.B. Eddie, C.E. Douglas, in *Pyrolysis Oils from Biomass*, (Eds.: E.J. Soltes, T.A. Milne), American Chemical Society, **1988**, pp. 228-240.
- [47] D.C. Elliott, E.G. Baker, J. Piskorz, D.S. Scott, Y. Solantausta, *Energy Fuels* **1988**, *2*, 234-235.
- [48] W. Baldauf, U. Balfanz, M. Rupp, *Biomass Bioenergy* **1994**, *7*, 237-244.
- [49] B.S. Gevert, J.E. Otterstedt, *Biomass* **1987**, *13*, 105-115.
- [50] J. Wildschut, F.H. Mahfud, R.H. Venderbosch, H.J. Heeres, *Ind. Eng. Chem. Res.* **2009**, *48*, 10324-10334.
- [51] J. Wildschut, M. Iqbal, F.H. Mahfud, I.M. Cabrera, R.H. Venderbosch, H.J. Heeres, *Energy Environ. Sci.* **2010**, *3*, 962-970.
- [52] D.C. Elliott, T.R. Hart, *Energy Fuels* **2009**, *23*, 631-637.
- [53] D.C. Elliott, T.R. Hart, G.G. Neuenschwander, L.J. Rotness, A.H. Zacher, *Environ. Prog. Sustainable Energy* **2009**, *28*, 441-449.
- [54] R.H. Venderbosch, A.R. Ardiyanti, J. Wildschut, A. Oasmaa, H.J. Heeres, *J. Chem. Technol. Biotechnol.* **2010**, *85*, 674-686.
- [55] J. Wildschut, J. Arentz, C.B. Rasrendra, R.H. Venderbosch, H.J. Heeres, *Environ. Prog. Sustainable Energy* **2009**, *28*, 450-460.
- [56] D.C. Elliott, T.R. Hart, G.G. Neuenschwander, L.J. Rotness, M.V. Olarte, A.H. Zacher, Y. Solantausta, *Energy Fuels* **2012**, *26*, 3891-3896.
- [57] R.J. French, J. Stunkel, R.M. Baldwin, *Energy Fuels* **2011**, *25*, 3266-3274.
- [58] T.P. Vispute, G.W. Huber, *Green Chem.* **2009**, *11*, 1433-1445.
- [59] T.P. Vispute, H. Zhang, A. Sanna, R. Xiao, G.W. Huber, *Science* **2010**, *330*, 1222-1227.
- [60] A. Kruse, E. Dinjus, *J. Supercrit. Fluids* **2007**, *39*, 362-380.
- [61] A. Kruse, E. Dinjus, *J. Supercrit. Fluids* **2007**, *41*, 361-379.
- [62] P. Duan, P.E. Savage, *Bioresour. Technol.* **2011**, *102*, 1899-1906.
- [63] P. Duan, P.E. Savage, *Appl. Catal. B* **2011**, *104*, 136-143.
- [64] P. Duan, P.E. Savage, *Energy Environ. Sci.* **2011**, *4*, 1447-1456.
- [65] C. Zhao, J.A. Lercher, *Angew. Chem. Int. Ed.* **2012**, *51*, 5935-5940.
- [66] A. Oasmaa, E. Kuoppala, A. Ardiyanti, R.H. Venderbosch, H.J. Heeres, *Energy Fuels* **2010**, *24*, 5264-5272.

- [67] M.C. Samolada, W. Baldauf, I.A. Vasalos, *Fuel* **1998**, 77, 1667-1675.
- [68] M. Al-Sabawi, J. Chen, S. Ng, *Energy Fuels* **2012**, 26, 5355-5372.
- [69] S. Arbogast, D. Bellman, J.D. Paynter, J. Wykowski, *Fuel Process. Technol.* **2012**, 104, 121-127.
- [70] S. Arbogast, D. Bellman, J.D. Paynter, J. Wykowski, *Fuel Process. Technol.* **2013**, 106, 518-525.
- [71] Y. Zhang, T.R. Brown, G. Hu, R.C. Brown, *Chem. Eng. J.* **2013**, 225, 895-904.
- [72] M. Stöcker, *Angew. Chem. Int. Ed.* **2008**, 47, 9200-9211.
- [73] A. Corma, G.W. Huber, L. Sauvanaud, P. O'Connor, *J. Catal.* **2007**, 247, 307-327.
- [74] M.E. Domine, A.C. van Veen, Y. Schuurman, C. Mirodatos, *ChemSusChem* **2008**, 1, 179-181.
- [75] I. Graça, F.R. Ribeiro, H.S. Cerqueira, Y.L. Lam, M.B.B. de Almeida, *Appl. Catal. B* **2009**, 90, 556-563.
- [76] I. Graça, J.M. Lopes, M.F. Ribeiro, F. Ramôa Ribeiro, H.S. Cerqueira, M.B.B. de Almeida, *Appl. Catal. B* **2011**, 101, 613-621.
- [77] F. de Miguel Mercader, M.J. Groeneveld, S.R.A. Kersten, N.W.J. Way, C.J. Schaverien, J.A. Hogendoorn, *Appl. Catal. B* **2010**, 96, 57-66.
- [78] G. Fogassy, N. Thegarid, G. Toussaint, A.C. van Veen, Y. Schuurman, C. Mirodatos, *Appl. Catal. B* **2010**, 96, 476-485.
- [79] R.H. Venderbosch, H.J. Heeres, in *Biomass power for the world: Transformation to effective use*, (Eds.: W.v. Swaaij, S.R.A. Kersten, W. Palz), Pan Stanford Publishing Pte. Ltd., Great Britain, **2015**, pp. 515-540.
- [80] F. de Miguel Mercader, M.J. Groeneveld, S.R.A. Kersten, C. Geantet, G. Toussaint, N.W.J. Way, C.J. Schaverien, K.J.A. Hogendoorn, *Energy Environ. Sci.* **2011**, 4, 985-997.
- [81] F. De Miguel Mercader, P.J.J. Koehorst, H.J. Heeres, S.R.A. Kersten, J.A. Hogendoorn, *AIChE Journal* **2011**, 57, 3160-3170.
- [82] A. Gutierrez, R.K. Kaila, M.L. Honkela, R. Slioor, A.O.I. Krause, *Catal. Today* **2009**, 147, 239-246.
- [83] E. Laurent, B. Delmon, in *Studies in Surface Science and Catalysis*, (Eds.: B. Delmon, G.F. Froment), Elsevier, **1994**, pp. 459-466.
- [84] E. Laurent, B. Delmon, *J. Catal.* **1994**, 146, 281-291.
- [85] Y. Wang, Y. Fang, T. He, H. Hu, J. Wu, *Catal. Commun.* **2011**, 12, 1201-1205.
- [86] H. Ohta, H. Kobayashi, K. Hara, A. Fukuoka, *Chem. Commun.* **2011**, 47, 12209-12211.
- [87] N. Li, G.W. Huber, *J. Catal.* **2010**, 270, 48-59.

- [88] R. Runnebaum, T. Nimmanwudipong, D. Block, B. Gates, *Catal. Lett.* **2011**, *141*, 817-820.
- [89] S. Sitthisa, T. Pham, T. Prasomsri, T. Sooknoi, R.G. Mallinson, D.E. Resasco, *J. Catal.* **2011**, *280*, 17-27.
- [90] S. Sitthisa, D. Resasco, *Catal. Lett.* **2011**, *141*, 784-791.
- [91] X. Zhu, L.L. Lobban, R.G. Mallinson, D.E. Resasco, *J. Catal.* **2011**, *281*, 21-29.
- [92] A. Ausavasukhi, Y. Huang, A.T. To, T. Sooknoi, D.E. Resasco, *J. Catal.* **2012**, *290*, 90-100.
- [93] C. Zhao, Y. Kou, A.A. Lemonidou, X. Li, J.A. Lercher, *Angew. Chem. Int. Ed.* **2009**, *48*, 3987-3990.
- [94] C. Zhao, J.A. Lercher, *ChemCatChem* **2012**, *4*, 64-68.
- [95] C.R. Lee, J.S. Yoon, Y.-W. Suh, J.-W. Choi, J.-M. Ha, D.J. Suh, Y.-K. Park, *Catal. Commun.* **2012**, *17*, 54-58.
- [96] S. Sitthisa, T. Sooknoi, Y. Ma, P.B. Balbuena, D.E. Resasco, *J. Catal.* **2011**, *277*, 1-13.
- [97] R.N. Olcese, M. Bettahar, D. Petitjean, B. Malaman, F. Giovanella, A. Dufour, *Appl. Catal. B* **2012**, *115–116*, 63-73.
- [98] K.L. Deutsch, B.H. Shanks, *Appl. Catal. A* **2012**, *447–448*, 144-150.
- [99] P.T.M. Do, A.J. Foster, J. Chen, R.F. Lobo, *Green Chem.* **2012**, *14*, 1388-1397.
- [100] J. Sun, A.M. Karim, H. Zhang, L. Kovarik, X.S. Li, A.J. Hensley, J.-S. McEwen, Y. Wang, *J. Catal.* **2013**, *306*, 47-57.
- [101] Y. Hong, H. Zhang, J. Sun, K.M. Ayman, A.J.R. Hensley, M. Gu, M.H. Engelhard, J.-S. McEwen, Y. Wang, *ACS Catal.* **2014**, *4*, 3335-3345.
- [102] A.R. Ardiyanti, S.A. Khromova, R.H. Venderbosch, V.A. Yakovlev, H.J. Heeres, *Appl. Catal. B* **2012**, *117–118*, 105-117.
- [103] S. Leng, X. Wang, X. He, L. Liu, Y. Liu, X. Zhong, G. Zhuang, J.G. Wang, *Catal. Commun.* **2013**, *41*, 34-37.
- [104] L. Nie, P.M. de Souza, F.B. Noronha, W. An, T. Sooknoi, D.E. Resasco, *J. Mol. Catal. A: Chem.* **2014**, *388–389*, 47-55.
- [105] S. Boullosa-Eiras, R. Lødeng, H. Bergem, M. Stöcker, L. Hannevold, E.A. Blekkan, *Catal. Today* **2014**, *223*, 44-53.
- [106] D.M. Alonso, S.G. Wettstein, J.A. Dumesic, *Chem. Soc. Rev.* **2012**.
- [107] X.H. Yang, Z. Li, C. Sun, H.G. Yang, C. Li, *Chem. Mater.* **2011**, *23*, 3486-3494.
- [108] D.L. Hoang, T.T.H. Dang, J. Engeldinger, M. Schneider, J. Radnik, M. Richter, A. Martin, *J. Sol. State Chem.* **2011**, *184*, 1915-1923.
- [109] D.L. Hoang, H. Lieske, *Thermochim. Acta* **2000**, *345*, 93-99.

- [110] D.A.M. Monti, A. Baiker, *J. Catal.* **1983**, *83*, 323-335.
- [111] C.A. Emeis, *J. Catal.* **1993**, *141*, 347-354.
- [112] B. Scholze, D. Meier, *J. Anal. Appl. Pyrol.* **2001**, *60*, 41-54.
- [113] A.G. Gayubo, A. Alonso, B. Valle, A.T. Aguayo, M. Olazar, J. Bilbao, *Fuel* **2010**, *89*, 3365-3372.
- [114] J.H. Sinfelt, *Acc. Chem. Res.* **1977**, *10*, 15-20.
- [115] K. Hadjiivanov, H. Knözinger, M. Mihaylov, *J. Phys. Chem. B* **2002**, *106*, 2618-2624.
- [116] M. Mihaylov, K. Hadjiivanov, *Langmuir* **2002**, *18*, 4376-4383.
- [117] A.J. Maia, B. Louis, Y.L. Lam, M.M. Pereira, *J. Catal.* **2010**, *269*, 103-109.
- [118] L. De Rogatis, T. Montini, A. Cognigni, L. Olivi, P. Fornasiero, *Catal. Today* **2009**, *145*, 176-185.
- [119] A. Carrero, J.A. Calles, A.J. Vizcaíno, *Appl. Catal. A* **2007**, *327*, 82-94.
- [120] X. Wang, H.-Y. Chen, W.M.H. Sachtler, *Appl. Catal. B* **2000**, *26*, L227-L239.
- [121] M. Zhao, N.H. Florin, A.T. Harris, *Appl. Catal. B* **2010**, *97*, 142-150.
- [122] K.M. Hardiman, C.G. Cooper, A.A. Adesina, *Ind. Eng. Chem. Res.* **2004**, *43*, 6006-6013.
- [123] K.M. Hardiman, T.T. Ying, A.A. Adesina, E.M. Kennedy, B.Z. Dlugogorski, *Chem. Eng. J.* **2004**, *102*, 119-130.
- [124] K.E. Sedor, M.M. Hossain, H.I. de Lasa, *Chem. Eng. Sci.* **2008**, *63*, 2994-3007.
- [125] W. Qiwu, Y. Jianlong, R. Jingfang, H. Minming, Y. Chunhua, *Catal. Lett.* **1990**, *4*, 63-74.
- [126] A. Jentys, J.A. Lercher, in *Studies in Surface Science and Catalysis*, (Eds.: H. van Bekkum, E. M. Flanigen, P. A. Jacobs, J.C. Jansen), Elsevier, **2001**, pp. 345-386.
- [127] I. Gandarias, V.L. Barrio, J. Requies, P.L. Arias, J.F. Cambra, M.B. Güemez, *Int. J. Hydrogen Energy* **2008**, *33*, 3485-3488.
- [128] C. Zhao, D.M. Camaioni, J.A. Lercher, *J. Catal.* **2012**, *288*, 92-103.
- [129] J.H. Sinfelt, J.L. Carter, D.J.C. Yates, *J. Catal.* **1972**, *24*, 283-296.
- [130] A.B. Ene, T. Archipov, E. Roduner, *J. Phys. Chem. C* **2011**, *115*, 3688-3694.
- [131] J. Xu, W. Zhou, Z. Li, J. Wang, J. Ma, *Int. J. Hydrogen Energy* **2009**, *34*, 6646-6654.
- [132] J. Zhang, H. Wang, A.K. Dalai, *J. Catal.* **2007**, *249*, 300-310.
- [133] E. Furimsky, F.E. Massoth, *Catal. Today* **1999**, *52*, 381-495.
- [134] Z. Xue, T. Zhang, J. Ma, H. Miao, W. Fan, Y. Zhang, R. Li, *Micropor. Mesopor. Mater.* **2012**, *151*, 271-276.
- [135] P. Morales-Pacheco, J.M. Domínguez, L. Bucio, F. Alvarez, U. Sedran, M. Falco, *Catal. Today* **2011**, *166*, 25-38.

- [136] T.M. Huynh, U. Armbruster, L.H. Nguyen, D.A. Nguyen, A. Martin, *JSBS* **2015**, *5*, 151-160.
- [137] T.M. Huynh, U. Armbruster, M.-M. Pohl, M. Schneider, J. Radnik, D.-L. Hoang, B.M.Q. Phan, D.A. Nguyen, A. Martin, *ChemCatChem* **2014**, *6*, 1940-1951.
- [138] T.M. Huynh, U. Armbruster, B.M.Q. Phan, D.A. Nguyen, A. Martin, *Chim. Oggi* **2014**, *32* (2), 40-44.
- [139] R.M. Ravenelle, F. Schüßler, A. D'Amico, N. Danilina, J.A. van Bokhoven, J.A. Lercher, C.W. Jones, C. Sievers, *J. Phys. Chem. C* **2010**, *114*, 19582-19595.
- [140] J.E. Germain, *Catalytic Conversion of Hydrocarbons*, Vol., ed., Acad. Press, London, UK, **1969**.
- [141] S. Echeandia, B. Pawelec, V.L. Barrio, P.L. Arias, J.F. Cambra, C.V. Loricera, J.L.G. Fierro, *Fuel* **2014**, *117*, Part B, 1061-1073.
- [142] S. van Donk, A.H. Janssen, J.H. Bitter, K.P. de Jong, *Catal. Reviews* **2003**, *45*, 297-319.
- [143] J.C. Groen, L.A.A. Peffer, J.A. Moulijn, J. Pérez-Ramírez, *Chem. Eur. J.* **2005**, *11*, 4983-4994.
- [144] S. Abelló, A. Bonilla, J. Pérez-Ramírez, *Appl. Catal. A* **2009**, *364*, 191-198.
- [145] P.M. Mortensen, *Thesis, Technical University of Denmark* **2013**.
- [146] X. Hu, R.J.M. Westerhof, L. Wu, D. Dong, C.-Z. Li, *Green Chem.* **2015**.
- [147] http://www.pytecsite.de/pytec_eng/flash_pyrolyse_2.htm, accessed date 08/14/2015.
- [148] http://www.bsr.com.vn/read/119_thong-tin-ve-du-an.aspx, accessed date 4/16/2013.
- [149] R. Sadeghbeigi, *Fluid Catalytic Cracking Handbook: Design, Operation and Troubleshooting of FCC Facilities*, Vol., 2nd ed., Gulf Professional Publishing, Houston, US, **2000**.
- [150] D. Wallenstein, M. Seese, X. Zhao, *Appl. Catal. A* **2002**, *231*, 227-242.
- [151] G.W. Huber, A. Corma, *Angew. Chem. Int. Ed.* **2007**, *46*, 7184-7201.
- [152] A.T. To, D.E. Resasco, *J. Catal.* **2015**, *329*, 57-68.
- [153] S. Vitolo, M. Seggiani, P. Frediani, G. Ambrosini, L. Politi, *Fuel* **1999**, *78*, 1147-1159.
- [154] S. Vitolo, B. Bresci, M. Seggiani, M.G. Gallo, *Fuel* **2001**, *80*, 17-26.
- [155] M. Ibáñez, B. Valle, J. Bilbao, A.G. Gayubo, P. Castaño, *Catal. Today* **2012**, *195*, 106-113.
- [156] S. Li, S. Zhang, Z. Feng, Y. Yan, *Environ. Prog. Sustainable Energy* **2015**, *34*, 240-247.

9. Appendices

Appendix A: List of supporting figures and tables



Figure A1. Experimental set up (autoclave) of HDO of phenol (left) and bio-oil (right).

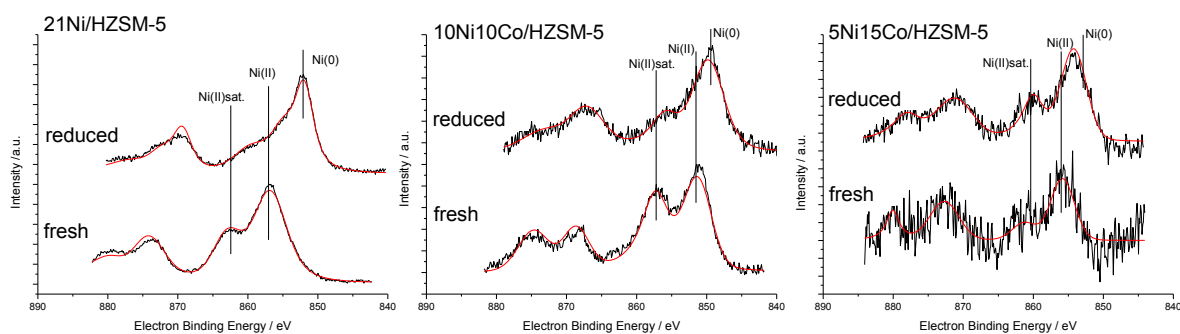


Figure A2. XPS spectra (Ni_{2p}) of fresh and pre-reduced Ni/HZSM-5 and Ni-Co/HZSM-5.

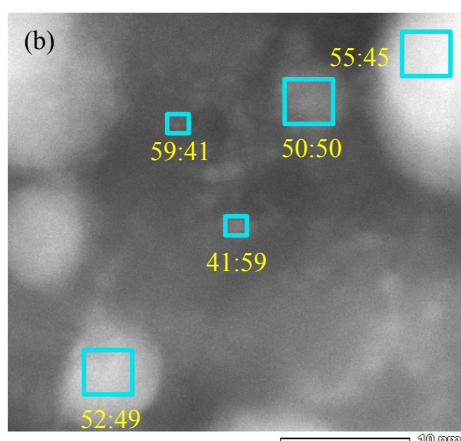


Figure A3. EDXS measurements of pre-reduced 10Ni10Co/HZSM-5 catalyst. The numbers represent Ni: Co atomic ratio in metal particle of different sizes.

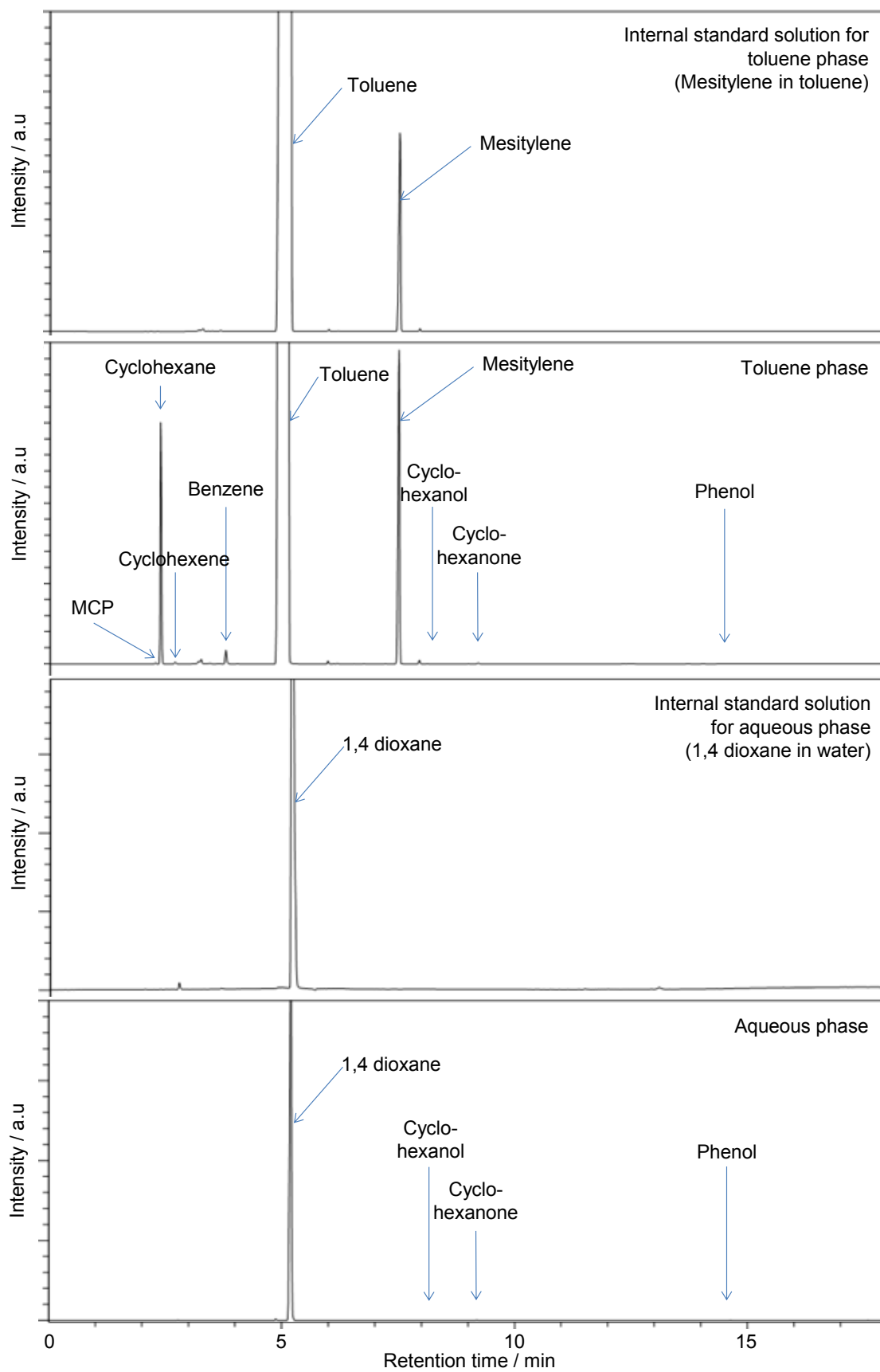


Figure A4. Typical gas chromatograms of organic (toluene) and aqueous phases.

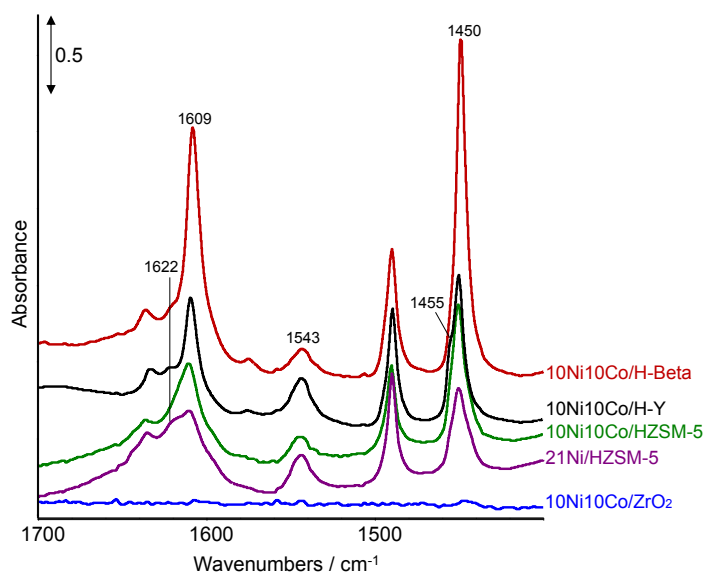


Figure A5. Py-IR spectra of the bimetallic Ni-Co catalysts (at 150 °C) supported on various zeolites and ZrO₂.

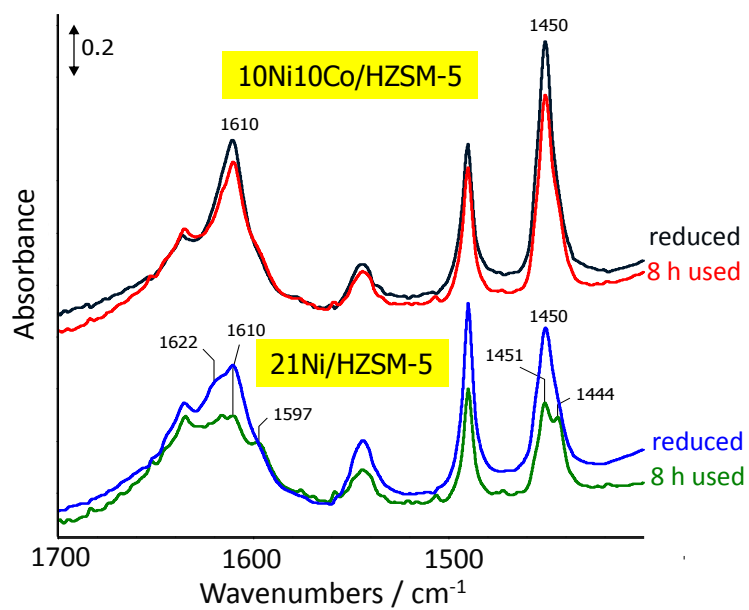


Figure A6. Py- IR spectra of selected reduced and spent catalysts.

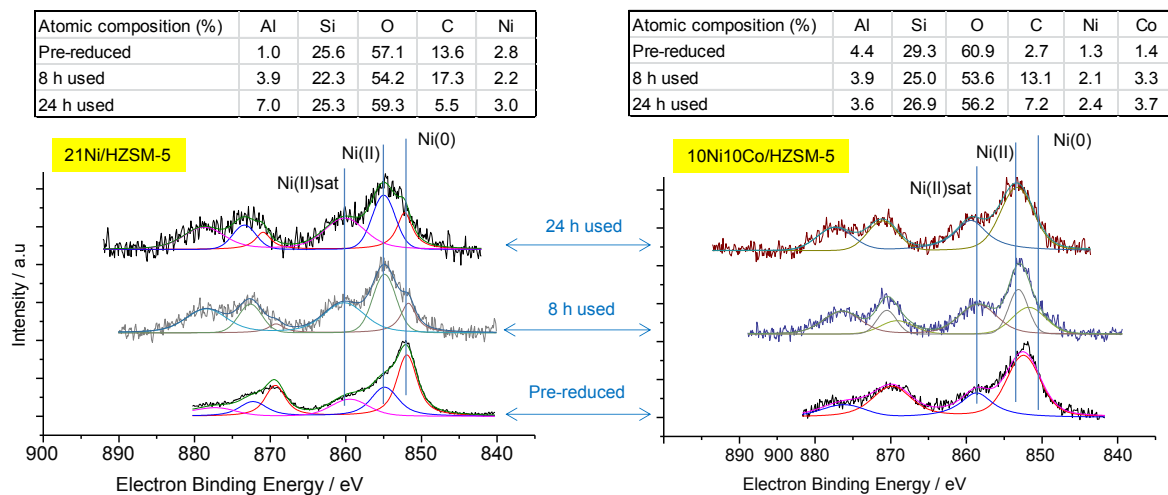


Figure A7. XPS spectra (Ni2p) of pre-reduced and spent catalysts.

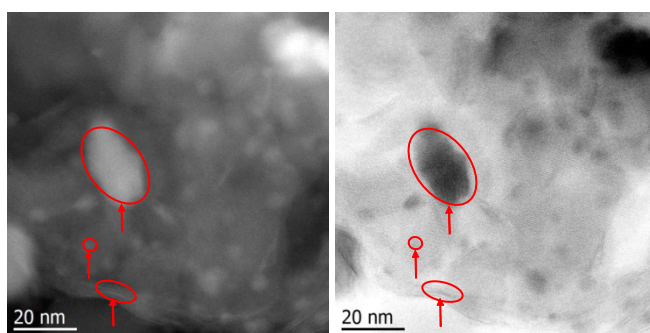


Figure A8. TEM images of spent 10Ni10Co/HZSM-5 after 8 h on-stream. The arrows indicates different particle sizes and new domain/crystallite species of metal.

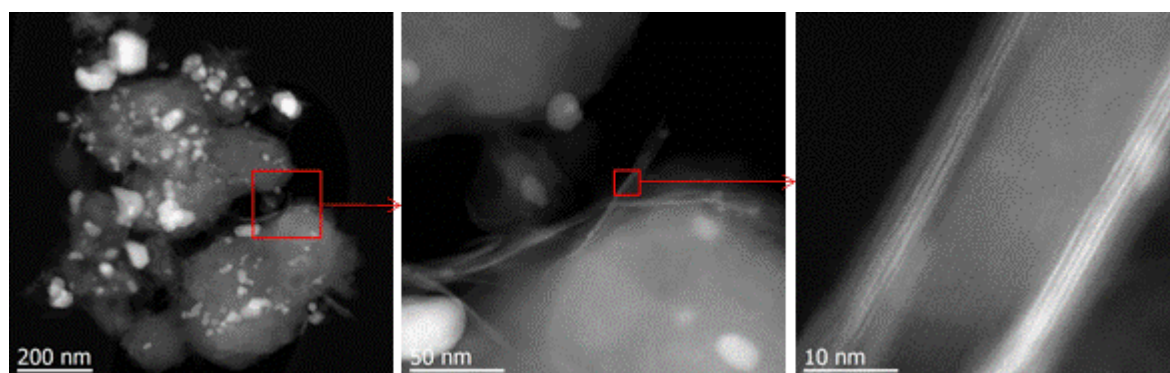


Figure A9. 21Ni/HZSM-5 spent catalyst after 24 h on-stream. The arrows shows the more detailed view of the specific region in sample.

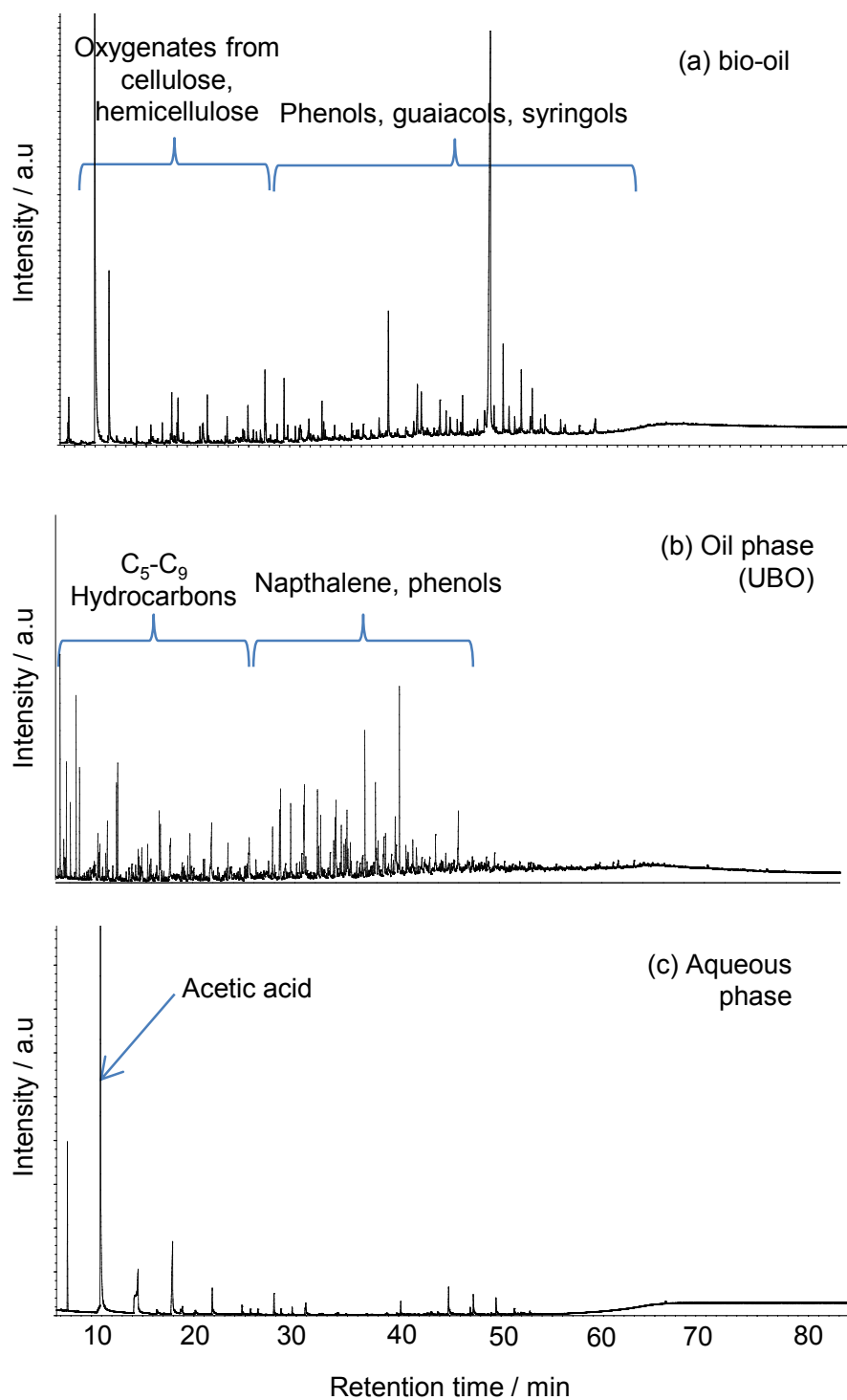


Figure A10. GC-MS results for original bio-oil (a), UBO (b) and aqueous phase (c)

Table A1. Change of metal contents after reaction based on ICP-OES and AAS results.

Catalysts	% loss (wt%)			
	Ni	Co	Si	Al
10Ni10Co/HZSM-5	1.9	1.8	4.7	0.7
21Ni/HZSM-5	6.5	-	5.0	0.9

Table A2. Effect of CTO ratios and fraction of UBO on the gas composition.

Samples	0UBO	5UBO	10UBO	20UBO	0UBO	5UBO	10UBO	20UBO
	2.5				3			
CTO ratio (g/g)								
H ₂	0.73	0.55	0.48	0.65	0.78	0.52	0.61	0.47
CH ₄	1.95	2.43	3.14	2.70	2.48	2.34	2.39	2.90
Ethane	1.35	1.45	2.09	1.70	1.71	1.60	1.60	1.98
Ethene	1.61	1.84	2.63	2.13	1.81	1.96	2.02	2.53
Propane	3.36	3.83	4.24	4.02	4.38	4.20	4.16	4.32
Propylene	26.34	25.70	25.84	24.88	26.55	26.26	25.29	25.04
i-Butane	12.41	13.39	13.19	13.30	14.78	14.42	14.35	13.71
n-Butane	3.86	4.23	4.28	4.23	4.58	4.55	4.46	4.36
t-2-Butene	13.58	12.70	12.08	11.50	12.40	12.52	12.03	11.39
1-Butene	9.64	9.03	8.59	8.25	8.89	8.90	8.51	8.05
i-Butene	15.16	13.55	11.48	11.77	12.53	12.41	11.51	10.16
c-2-Butene	10.00	9.36	8.90	8.45	9.09	9.20	8.85	8.36
CO ₂	-	1.69	1.80	5.21	-	1.12	3.34	5.04
CO	-	0.23	1.26	1.21	-	-	0.89	1.69

Appendix B: List of Publications

Book Chapter

T. M. Huynh, U. Armbruster, A. Martin, "Deoxygenation of Liquid and Liquified Biomass", in *Chemicals and Fuels from Bio-Based Building Blocks*, WILEY VCH, 2016, in press. ISBN: 978-3-527-33897-9

Journal

T.M. Huynh, U. Armbruster, M.M. Pohl, M. Schneider, J. Radnik, D. L. Hoang, B.M.Q. Phan, D.A. Nguyen, A. Martin, "Hydrodeoxygenation of Phenol as a Model Compound for Bio-oil on Non-noble Bimetallic Nickel-based Catalysts", *ChemCatChem* 2014, 6, 1940 – 1951.

T.M. Huynh, U. Armbruster, B. M. Q. Phan, D. A. Nguyen, A. Martin, "The influence of cobalt in bimetallic Ni-Co catalyst supported on HBeta for phenol hydrodeoxygenation", *Chemistry Today* 2014, 32(2), 40-44.

T.M. Huynh, U. Armbruster, L. H. Nguyen, D. A. Nguyen, A. Martin, "Hydrodeoxygenation of bio-oil on bimetallic catalysts: from model compound to real feed", *JSBS*, 2015, 5, 151-160.

T.M. Huynh, U. Armbruster, H. Atia, U. Bentrup, B. M. Q. Phan, R. Eckelt, L. H. Nguyen, D. A. Nguyen, A. Martin, "Upgrading of bio-oil and subsequent co-processing at FCC conditions for fuel production", *React. Chem. Eng.*, 2015, Accepted.

T.M. Huynh, U. Armbruster, C. R. Kreyenschulte, L. H. Nguyen, B. M. Q. Phan, D. A. Nguyen, A. Martin, "Understanding the catalytic performance of supported Ni-Co based catalysts in phenol HDO in batch and continuous-flow modes", *App. Cat. A*, 2015, submitted.

T.M. Huynh, U. Armbruster, B. M. Q. Phan, D. A. Nguyen, A. Martin, "Hydrodeoxygenation of pyrolysis oil and subsequent co-processing at FCC conditions for fuel production", *Papers of the 23rd European Biomass Conference*, 2015, 1257-1262, ISBN 978-88-89407-516 (proceedings).

T.M. Huynh, U. Armbruster, B.M.Q. Phan, D.A. Nguyen, A. Martin, "Impact of second metal (Cu, Co) on catalytic performance of bimetallic Ni-Based Catalyst for Phenol HDO", *Chem. Ing. Tech.* 2014, 86, 1354. (proceedings)

Conference Contribution

23rd European Biomass Conference and Exhibition, June 1 – 4, Vienna, Austria

T.M. Huynh, U. Armbruster, B. M. Q. Phan, D. A. Nguyen, A. Martin, “Hydrodeoxygenation of pyrolysis oil and subsequent co-processing at FCC conditions for fuel production” (Poster Presentation)

Energy Science Technology – An International Conference and Exhibition, May 20 – 22, 2015, Karlsruhe, Germany

T.M. Huynh, U. Armbruster, A. Martin, “Development of bimetallic catalysts for bio-oil upgrading” (Poster Presentation).

ProcessNet-Jahrestagung und 31.DECHEMA-Jahrestagung der Biotechnologen, Sep 30 – Oct 02, 2014, Aachen, Germany.

T.M. Huynh, U. Armbruster, B. M. Q. Phan, D. A. Nguyen, A. Martin, “The impact of second metal (Cu, Co) on catalytic performance of bimetallic Ni-based catalyst for Phenol HDO” (Oral presentation)

Southeast Asia Refinery & Petrochemicals 2014 Conference, May 07-09, 2014, Ho Chi Minh City, Vietnam

T.M. Huynh, U. Armbruster, A. Martin, “Biorefineries – current status, opportunities and challenges for application in Vietnam” (Oral presentation).

46. Jahrestreffen Deutscher Katalytiker, Weimar, Germany, March 13-15, 2014,

T.M. Huynh, U. Armbruster, U. Bentrup, B. M. Q. Phan, D. A. Nguyen, A. Martin, “The effect of support on bimetallic Ni-Co catalysts for phenol hydrodeoxygenation” (Poster Presentation)

10th Green Chemistry Conference - An international event, Barcelona, Spain, November 05-07, 2013,

T.M. Huynh, U. Armbruster, B. M. Q. Phan, D. A. Nguyen, A. Martin, “Effect of second metal (Cu, Co) on catalytic performance of bimetallic Ni-based catalyst for phenol HDO” (Oral Presentation)

LIKAT/CaSuS Workshop, Rostock, Germany, September 16-18, 2013

T.M. Huynh, U. Armbruster, B. M. Q. Phan, D. A. Nguyen, A. Martin, “Improved catalytic performance of Ni-Co alloy supported on HZSM-5 for HDO of phenol as a model compound of bio-oil” (Poster Presentation)

Appendix C: Curriculum Vitae

Personal information

Full name	Huynh, Minh Thuan
Date of birth	19.05.1981
Gender	Male
Nationality	Vietnam
Email	thuan.huynh@catalysis.de ; thuanhm@pvpro.com.vn

Academic Education

2.2012-present	Leibniz Institute for Catalysis at University of Rostock, Germany PhD student at the Department of Heterogeneous Catalytic Processes Supervisors: PD Dr. Andreas Martin, Dr. Ing. Udo Armbruster
9.2005-7.2008:	Ho Chi Minh City University of Technology, Vietnam Master of Engineering, Chemical Engineering, majoring in refinery and gas processing. Supervisor: Dr. Trinh Van Than
9.1999-8.2004	Hanoi University of Science and Technology, Vietnam Bachelor of Science, Chemical Engineering, majoring in petrochemical and organic processing. Supervisors: Prof. Dr. Dinh Thi Ngo, Prof. Dr. Pham Van Thiem

Profession

9.2004-1.2012:	Research and Development Center for Petroleum Processing, Vietnam Petroleum Institute, Vietnam Oil and Gas Group (Petrovietnam)
7.2011-1.2012	Manager of Biofuels Department
5.2009-6.2011	Manager of Petrochemical Technology Department
7.2008-4.2009	Deputy Manager of Petrochemical Technology Department
9.2004-6.2008	Project engineer in Project Department.

